AD-A032 018 TEXAS UNIV AT AUSTIN APPLIED RESEARCH LABS F/G 17/1
TARGET CLASSIFICATION USING LIKELIHOOD RATIOS AND QUADRATURE CO--ETC(U)
JUN 69 J F HOFFMAN N00024-69-C-1129
UNCLASSIFIED ARL-TM-69-11 NL

1 OF 2
AD
A032 018

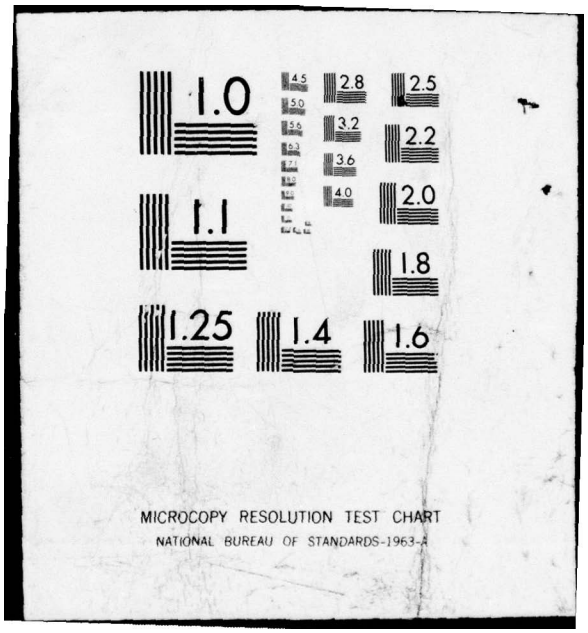
1.0
1.1
1.25
1.4
1.6
1.8
2.0
2.2
2.5
2.8
3.2
3.6
4.0
4.5
5.0
5.6
6.3
MICROCOPY RESOLUTION TEST CHART
NATIONAL BUREAU OF STANDARDS-1963-A

APPLIED RESEARCH LABORATORIES
THE UNIVERSITY OF TEXAS AT AUSTIN

ARL-TM-69-11

Copy No. 1

TARGET CLASSIFICATION USING LIKELIHOOD RATIOS AND QUADRATURE COMPONENTS

J. F. Hoffman

NAVAL SHIP SYSTEMS COMMAND
CONTRACT N00024-69-C-1129

DISSERTATION

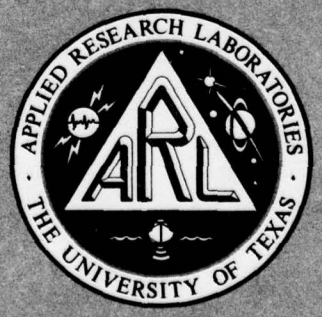

TARGET CLASSIFICATION USING LIKELIHOOD RATIOS

AND QUADRATURE COMPONENTS

APPROVED BY SUPERVISORY COMMITTEE:

C. W. Horton

F. W. de Wolfe

H. E. Millett

A. W. Holle

(6) TARGET CLASSIFICATION USING LIKELIHOOD RATIOS AND QUADRATURE COMPONENTS.

(9) by Doctoral thesis,

(10) JEROME FRANCIS HOFFMAN, B.S. in Physics, M.A. (Physics)

(14) ARL-TM-69-11

DISSERTATION

Presented to the Faculty of the Graduate School of

The University of Texas at Austin

in Partial Fulfillment

of the Requirements

for the Degree of

DOCTOR OF PHILOSOPHY

(15) N00024-69-C-1129

(12) 126 P.

THE UNIVERSITY OF TEXAS AT AUSTIN

(11) June, 1969

ABSTRACT

This dissertation presents the quantitative determination of the applicability of a likelihood ratio processor in the classification of sonar returns. The ability of a likelihood ratio processor to classify simple, similar targets was measured under highly controlled conditions. The five targets used were 7 in. diam, 5 in. diam, and 3 in. diam solid aluminum spheres, a 5 in. diam styrofoam sphere, and a 5 in. diam hollow aluminum sphere. The two transmissions used were:

(1) a sinusoidal pulse with a frequency of 70 kHz and a pulse length of 80 μsec, and
(2) a linear FM of bandwidth 12.5 kHz with a center frequency of 63.75 kHz and a pulse length of 3 msec.

Since the S/N ratios of the recorded echoes were large, Gaussian noise from a random noise generator was added to the echoes in order to simulate a more realistic problem in target classification. In classifying messages (echo-noise combinations) from two target classes, the performance of the likelihood ratio processor was measured by means of ROC curves. The classification was based on the quadrature components of the messages. For the sinusoidal pulse, the likelihood ratio processor performed satisfactorily in classifying the messages for a majority of the target pairs when the S/N ratio of the messages was 0 dB or larger.

For the sinusoidal pulse, the effect of variations in the S/N ratio of the messages on the performance of the likelihood ratio processor was measured. The S/N ratio was found to be a sensitive parameter that influenced the performance. Also for the sinusoidal pulse, the likelihood ratio processor was able to classify target classes using only the in-phase or out-of-phase components of the messages.

The effect on performance of an uncertainty in epoch over a cycle of the carrier was measured for the sinusoidal pulse. The uncertainty in epoch brought about the same change in performance as a 6 dB drop in the S/N ratio of the messages.

Since the reciprocal of the pulse length of the sinusoidal pulse was equal to the bandwidth of the linear FM, it was asserted and found that equivalent performances could be obtained with either of the two transmissions if the following equation were true:

$$\left(\frac{E}{\langle N^2 \rangle}\right)_{sp} = \left(\frac{E}{\langle N^2 \rangle}\right)_{FM},$$

where

E is the signal energy in an echo,
$< N^2 >$ is the mean square of the added Gaussian noise,
sp denotes a sinusoidal pulse, and
FM denotes a linear FM.

The dependence of performance on $\frac{E}{< N^2 >}$ implies that a linear FM has more potential for improvement in the performance of a likelihood ratio processor than a sinusoidal pulse, since the energy in a sinusoidal pulse is restricted by the effects of cavitation.

ACKNOWLEDGMENTS

I wish to express my sincere appreciation to Dr. Loyd Hampton, Dr. Claude Horton, and Mr. Pat Pitt for their support and patience during the course of this study. Special thanks are due Dr. Claude Horton for his constructive criticisms, encouragement, and time.

Appreciation is expressed to the members of the Signal Physics Group at the Applied Research Laboratories of the University of Texas at Austin. In particular, I extend thanks to Ken Vaughan for the digitization of data, to Don Grace for his assistance in the use of sampling techniques, and to Steve Mitchell for many helpful discussions.

My appreciation is expressed to Barbara Schulze and her competent staff in the Technical Reports Office of Applied Research Laboratories for preparing the final draft of the dissertation.

I express my appreciation to the U. S. Naval Ship Systems Command for financial support.

Jerome Francis Hoffman

Austin, Texas

April, 1969

TABLE OF CONTENTS

TABLE OF CONTENTS

LIST OF TABLES

LIST OF FIGURES

LIST OF FIGURES (Cont'd)

CHAPTER I

INTRODUCTION

The objective of this investigation is to determine quantitatively the applicability of a likelihood ratio processor in the classification of sonar returns from targets.

The likelihood ratio processor implements the Bayes' decision rule in the classification of targets. The Bayes' decision rule is optimum in the sense that no other rule will yield a smaller average risk to the observer.

The ability of a likelihood ratio processor to classify correctly sonar returns from similar, simple targets was measured for both a sinusoidal pulse and a linear FM transmission. The classification of the targets was based on the in-phase and out-of-phase quadrature components of sonar returns. Measurements were made on the ability of the likelihood ratio processor to classify correctly sonar returns using the in-phase components and the out-of-phase components separately. In addition, the effects of variations in the average S/N ratio and the epoch (or reference time) of the sonar returns on the ability of the likelihood ratio processor to classify correctly were measured.

A discussion of the statistical decision theory and the application of theory in psychophysical experiments is presented in Signal Detection Theory and Psychophysics by David Green and John Swets. The techniques of specification of an optimal detection process and of the use of ROC curves as a measure of experimental

observations are similar to those implemented in target classification. In the classification of similar, simple targets, a metric is applied as a geometrical description of target echoes. A discussion of a measurement of the similarity of points in a multidimensional vector space expressed by a metric is found in Decision-Making Processes in Pattern Recognition by George Sebestyen.

The problem of target classification is important in many areas of information processing. The use of a likelihood ratio processor in target classification is applicable to sonar and radar surveillance, to geophysical prospecting, to classification of magnetic spin echoes, and to radio astronomy.

CHAPTER II

THEORY

A. Likelihood Ratio

The following discussion concerning likelihood ratio assumes that an active source transmits a bandlimited signal directed at one of two possible targets present in a propagating medium.

The signals from the targets are defined as

$$S^j(t;\varphi_o),\ j = A \text{ or } B \quad ,$$

where

j = A refers to a signal from target A, and

j = B refers to a signal from target B.

The starting phase of a signal is φ_o and it is contained within the interval $-\pi < \varphi_o < \pi$. The assumed density function for φ_o is $P(\varphi_o) = \frac{1}{2\pi}$. This assumption is made since the epoch of a signal at the receiver is not known. The receiver output is defined as V(t), the echo,

where

$$V(t) = N(t) + S^j(t;\varphi_o) \quad . \tag{2.1}$$

The echo V(t) is bandlimited to a bandwidth W with a center frequency f_o. The additive noise, N(t), is composed of ambient noise in the medium and in the receiver; i.e., reverberation is not considered.

Since the echo V(t) is an analog signal, it must be digitized by an analog-to-digital converter before it is used in any digital computations. After V(t) is sampled and digitized, it is expressed as $\vec{V} = (V(\ell\Delta t)) = (V_\ell)$. The time interval between the samples is Δt, and $\ell = 1, 2, \ldots .$ TF, where TF is the total number of samples of V(t) that are sufficient to reconstruct V(t) from a specified interpolation formula. F is the sampling rate used to obtain samples of V(t), and T is the pulse length of V(t). The sampled vector $\vec{V}$ defines a point in a TF-dimensional observation space Γ.

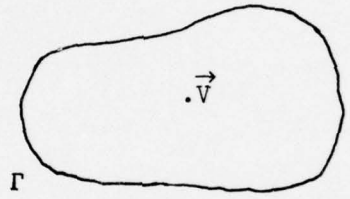

In this study the noise $\vec{N}$ is restricted to a stationary Gaussian process of zero mean. Also, $\vec{N}$ is bandlimited to a bandwidth W with center frequency f_o. The multivariate probability density function describing TF discrete samples of the noise is

$$P(\vec{N}) = \frac{|a^F_{mn}|^{1/2}}{(2\pi)^{TF/2}} e^{-1/2 \sum_{m,n=1}^{TF} a^F_{mn} N_m N_n} . \qquad (2.2)$$

For a stationary Gaussian process a^F_{mn} is a function of τ where

$$\tau = t_m - t_n \quad ,$$

$$t_m = \frac{m}{F} \quad , \text{ and}$$

$$t_n = \frac{n}{F} \quad .$$

The coefficients a^F_{mn} form a matrix a^F that is the inverse of the autocovariance matrix C^F computed from $\vec{N}$. $|a^F_{mn}|^{1/2}$ is the square root of the determinant of a^F. The elements of the matrix C^F are computed with the formula

$$C^F(\tau) = \frac{1}{P-\tau} \sum_{\sigma=1}^{P-\tau} N_\sigma N_{\sigma+\tau} \qquad (2.3)$$

where

$$P \geqq 10\ TF^{[1]} \text{ and } N_\sigma = N(\tfrac{\sigma}{F}) \quad .$$

A problem in hypothesis testing is formulated by defining two hypotheses:

$$H_1 : \vec{V} = \vec{N} + \vec{S}^A(\varphi_o) \quad , \text{ and} \qquad (2.4)$$

$$H_2 : \vec{V} = \vec{N} + \vec{S}^B(\varphi_o) \quad . \qquad (2.5)$$

In order to obtain a Bayes' solution to the problem of hypothesis testing, it is necessary to assign a priori probabilities for the two hypotheses H_1 and H_2. Namely, H_1 is assigned an a priori

---

[1] J. S. Bendat, and A. G. Piersol, Measurement and Analysis of Random Data, John Wiley and Sons, Inc., New York, N. Y., (1966) p. 290.

probability of q_1, and H_2 an *a priori* probability of q_2 where $q_1 + q_2 = 1$. If the *a priori* probabilities q_1 and q_2 are not known, it is necessary to train the observer with a representative sample set in order to obtain values for q_1 and q_2. The hypothesis H_1 is tested by observing an echo $\vec{V}$. After observing $\vec{V}$, H_1 is either accepted or rejected. A decision rule, which is needed to make one of the two possible decisions, will be formulated by dividing the observation space Γ into two disjoint subspaces Γ_1 and Γ_2, where $\Gamma = \Gamma_1 U \Gamma_2$. A decision is made to accept H_1 if $\vec{V}$ is contained in Γ_1, or reject H_1 if $\vec{V}$ falls into Γ_2.

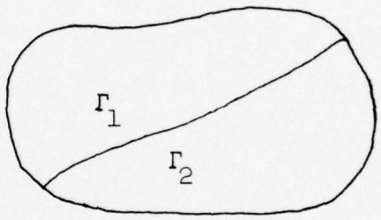

$$\Gamma = \Gamma_1 U \Gamma_2$$

$$\Gamma_1 \cap \Gamma_2 = 0 \quad .$$

Since many choices for the boundary are possible, a method is needed for determining an optimum decision boundary. In determining an optimum decision boundary, it is possible to make two kinds of errors:

(1) rejection of H_1 when it is true, and

(2) acceptance of H_1 when it is false.

A choice of a boundary determines the probability of making an error of each type as follows:

$$\alpha(\varphi_o) = \int_{\Gamma_2} P(\vec{V}|H_1;\varphi_o)d\vec{V} = \text{probability of error No. 1 as a function of } \varphi_o, \text{ where } \varphi_o \text{ is the starting phase, and} \quad (2.6)$$

$$P(\vec{V}|H_1;\varphi_o) = \frac{|a^F_{mn}|^{1/2}}{(2\pi)^{TF/2}} e^{-1/2 \sum_{m,n=1}^{TF} a^F_{mn}\left(V_m - S^A_m(\varphi_o)\right)\left(V_n - S^A_n(\varphi_o)\right)} \quad ;(2.7)$$

also

$$\beta(\varphi_o) = \int_{\Gamma_1} P(\vec{V}|H_2;\varphi_o)d\vec{V} = \text{probability of error No. 2 as a function of } \varphi_o \quad , \quad (2.8)$$

where

$$P(\vec{V}|H_2;\varphi_o) = \frac{|a^F_{mn}|^{1/2}}{(2\pi)^{TF/2}} e^{-1/2 \sum_{m,n=1}^{TF} a^F_{mn}\left(V_m - S^B_m(\varphi_o)\right)\left(V_n - S^B_n(\varphi_o)\right)} \quad .(2.9)$$

It is possible to make either $\alpha(\varphi_o)$ or $\beta(\varphi_o)$ arbitrarily small by adjusting the boundary to decrease the number of elements in either Γ_1 or Γ_2, but it is not possible to make $\alpha(\varphi_o)$ and $\beta(\varphi_o)$ both arbitrarily small.[2]

A general solution to the hypothesis testing problem known as the Bayes' solution is possible if a set of cost functions (C_{ij}),

---

[2] J. C. Hancock and P. A. Wirtz, Signal Detection Theory, McGraw-Hill Book Co., New York, N. Y., (1966), p. 35.

which describe the consequences of deciding that hypothesis H_i is true when H_j is true $(i,j=1,2)$, is available. In this study, the four cost functions are predetermined as follows:

$C_{11} = 0$ = cost to the observer if he decides H_1 is true when it is true,

C_{12} = cost to the observer if he decides H_1 is true when H_2 is true,

C_{21} = cost to the observer if he decides H_2 is true when H_1 is true,

$C_{22} = 0$ = cost to the observer if he decides H_2 is true when it is true.

The Bayes' decision rule, which results in the minimum average risk to the observer and establishes a boundary between Γ_1 and Γ_2, is formulated by defining two conditional expected risk functions as follows:

$$r_{H_1}(\varphi_o) = \text{expected risk given } H_1 \text{ is true} \quad , \text{ or}$$

$$r_{H_1}(\varphi_o) = C_{21}\alpha(\varphi_o) \quad , \text{ and} \tag{2.10}$$

$$r_{H_2}(\varphi_o) = \text{expected risk given } H_2 \text{ is true} \quad , \text{ or}$$

$$r_{H_2}(\varphi_o) = C_{12}\beta(\varphi_o) \quad . \tag{2.11}$$

The average risk is given by

$$R = \int_{-\pi}^{\pi} \left[q_1 r_{H_1}(\varphi_o) + q_2 r_{H_2}(\varphi_o) \right] P(\varphi_o) d\varphi_o \quad , \text{ or} \tag{2.12}$$

$$R = q_1 C_{21} \int_{\Gamma_2} \int_{-\pi}^{\pi} P(\vec{V}|H_1;\varphi_o)\ P(\varphi_o) d\varphi_o d\vec{V}$$

$$+ q_2 C_{12} \int_{\Gamma_1} \int_{-\pi}^{\pi} P(\vec{V}|H_2;\varphi_o)\ P(\varphi_o) d\varphi_o d\vec{V} \quad . \tag{2.13}$$

From the result that

$$1 = \int_{\Gamma} \int_{-\pi}^{\pi} P(\vec{V}|H_1;\varphi_o)\ P(\varphi_o) d\varphi_o d\vec{V} \quad , \text{ or}$$

$$1 = \int_{\Gamma_2} \int_{-\pi}^{\pi} P(\vec{V}|H_1;\varphi_o)\ P(\varphi_o) d\varphi_o d\vec{V}$$

$$+ \int_{\Gamma_1} \int_{-\pi}^{\pi} P(\vec{V}|H_1;\varphi_o)\ P(\varphi_o) d\varphi_o d\vec{V} \quad , \tag{2.14}$$

Eq. (2.13) becomes

$$R = q_1 C_{21} + \int_{\Gamma_1} \int_{-\pi}^{\pi} \left[q_2 C_{12}\ P(\vec{V}|H_2;\varphi_o) - q_1 C_{21}\ P(\vec{V}|H_1;\varphi_o) \right] P(\varphi_o) d\varphi_o d\vec{V} \quad . \tag{2.15}$$

Since the first term in Eq. (2.15) is a constant, the average risk is a minimum when the integral over Γ_1 is a minimum. Since the integrand consists of two non-negative terms, the integral attains its minimum value if the following two conditions are satisfied:

1) The subspace Γ_1 consists of those values of $\vec{V}$ for which

$$q_1 C_{21} \int_{-\pi}^{\pi} P(\vec{V}|H_1;\varphi_o)\ P(\varphi_o) d\varphi_o > q_2 C_{12} \int_{-\pi}^{\pi} P(\vec{V}|H_2;\varphi_o)\ P(\varphi_o) d\varphi_o \quad ; \tag{2.16}$$

2) The subspace Γ_2 consists of those values of $\vec{V}$ for which

$$q_1 C_{21} \int_{-\pi}^{\pi} P(\vec{V}|H_1;\varphi_o)\ P(\varphi_o)d\varphi_o < q_2 C_{12} \int_{-\pi}^{\pi} P(\vec{V}|H_2;\varphi_o)\ P(\varphi_o)d\varphi_o \quad . \quad (2.17)$$

The generalized likelihood ratio[3], $\Lambda(\vec{V})$, is defined as

$$\Lambda(\vec{V}) = \frac{\int_{-\pi}^{\pi} P(\vec{V}|H_2;\varphi_o)\ P(\varphi_o)d\varphi_o}{\int_{-\pi}^{\pi} P(\vec{V}|H_1;\varphi_o)\ P(\varphi_o)d\varphi_o} \quad . \quad (2.18)$$

In summary, the Bayes' decision rule assigns to Γ_1 those $\vec{V}$ for which $\Lambda(\vec{V}) < \frac{q_1 C_{21}}{q_2 C_{12}}$, and assigns to Γ_2 those $\vec{V}$ for which $\Lambda(\vec{V}) > \frac{q_1 C_{21}}{q_2 C_{12}}$. The number $\frac{q_1 C_{21}}{q_2 C_{12}}$ is interpreted as a threshold. A device that implements the generalized likelihood ratio calculations in hypothesis testing is referred to as a generalized likelihood ratio processor.

If the epoch of the echoes were known, the probability density function for the starting phase would become $P(\varphi_o) = \delta(\varphi_o)$, a Dirac delta function, and the generalized likelihood ratio would reduce to the likelihood ratio[4], which is defined as

$$\ell(\vec{V}) = \frac{P(\vec{V}|H_2)}{P(\vec{V}|H_1)} \quad . \quad (2.19)$$

---

[3] Ibid., p. 58.

[4] Ibid., p. 39.

Similarly, a device that implements likelihood ratio calculations in hypothesis testing is called a likelihood ratio processor. The threshold used in likelihood ratio calculations is $\frac{q_1 C_{21}}{q_2 C_{12}}$.

Upon the substitution of Eq. (2.7) and Eq. (2.9) into Eq. (2.18), the generalized likelihood ratio becomes

$$\Lambda(\vec{V}) = \frac{\frac{1}{2\pi}\int_{-\pi}^{\pi} \frac{|a^F_{mn}|^{1/2}}{(2\pi)^{TF/2}} e^{-1/2 \sum_{m,n=1}^{TF} a^F_{mn}\left(V_m - S^B_m(\varphi)\right)\left(V_n - S^B_n(\varphi)\right)} d\varphi}{\frac{1}{2\pi}\int_{-\pi}^{\pi} \frac{|a^F_{mn}|^{1/2}}{(2\pi)^{TF/2}} e^{-1/2 \sum_{m,n=1}^{TF} a^F_{mn}\left(V_m - S^A_m(\varphi)\right)\left(V_n - S^A_n(\varphi)\right)} d\varphi} \quad . \quad (2.20)$$

Upon the simplification of Eq. (2.20), $\Lambda(\vec{V})$ becomes

$$\Lambda(\vec{V}) = \frac{\int_{-\pi}^{\pi} e^{+\sum_{m,n=1}^{TF} a^F_{mn}\left[V_m S^B_n(\varphi) - 1/2\, S^B_m(\varphi) S^B_n(\varphi)\right]} d\varphi}{\int_{-\pi}^{\pi} e^{+\sum_{m,n=1}^{TF} a^F_{mn}\left[V_m S^A_n(\varphi) - 1/2\, S^A_m(\varphi) S^A_n(\varphi)\right]} d\varphi} \quad . \quad (2.21)$$

Upon the substitution of Eq. (2.7) and Eq. (2.9) into Eq. (2.19) and simplification, the likelihood ratio $\ell(\vec{V})$ for $\varphi_o = 0$ becomes

$$\ell(\vec{V}) = \frac{e^{+\sum_{m,n=1}^{TF} a^F_{mn}\left[V_m S^B_n - 1/2\ S^B_m S^B_n\right]}}{e^{+\sum_{m,n=1}^{TF} a^F_{mn}\left[V_m S^A_n - 1/2\ S^A_m S^A_n\right]}} \qquad (2.22)$$

where

$$S^B(t_m;\varphi_o = 0) = S^B(t_m) = S^B_m \quad , \text{ and}$$

$$S^A(t_m;\varphi_o = 0) = S^A(t_m) = S^A_m \quad .$$

B. Narrow Band Signals

Many signals used in physical applications are bandlimited to a frequency interval $\left(f_o - \frac{W}{2}\right) < |f| < \left(f_o + \frac{W}{2}\right)$ where W is small compared to f_o. Signals of this type are referred to as narrow band signals. A representation for these narrow band signals is

$$S(t) = S_1(t) \cos 2\pi f_o t + S_2(t) \sin 2\pi f_o t \qquad (2.23)$$

where

$$S_1(t) = A(t) \cos \varphi(t) \quad , \text{ and}$$

$$S_2(t) = -A(t) \sin \varphi(t) \quad .$$

$S_1(t)$ and $S_2(t)$ are bandlimited to the frequency interval $|f| < \frac{W}{2}$.

$A(t)$ is the envelope,

$\varphi(t)$ is the phase, and

f_o is the carrier frequency of $S(t)$.

For the present $S_1(t)$ and $S_2(t)$ are assumed to be of infinite duration.

$S_1(t)$ and $S_2(t)$ are called the quadrature components of the signal $S(t)$. These functions contain both the envelope and phase information of $S(t)$, and are of lower frequency than the signal $S(t)$. $S_1(t)$ is referred to as the in-phase component and $S_2(t)$ is referred to as the out-of-phase component.

It is assumed that $S(t)$, $S_1(t)$, and $S_2(t)$ have Fourier transforms. The Fourier transforms of $S(t)$, $S_1(t)$, and $S_2(t)$ are denoted as $\hat{S}(f)$, $\hat{S}_1(f)$, and $\hat{S}_2(f)$. Graphically, $\hat{S}(f)$, $\hat{S}_1(f)$, and $\hat{S}_2(f)$ can be depicted in the frequency domain as shown in Fig. 2.1.

The frequency domain occupied by $\hat{S}_1(f)$ and $\hat{S}_2(f)$ is constructed by heterodyning $\hat{S}(f)$ to a center frequency of 0.

The function $\hat{S}_1(f)$ can be represented over the frequency range $-W/2 < f < W/2$ by the complex Fourier series

$$\hat{S}_1(f) = \sum_{n=-\infty}^{n=+\infty} C_n \, e^{-\frac{i2\pi nf}{W}} \quad , \tag{2.24}$$

where

$$C_n = \frac{1}{W}\int_{-W/2}^{W/2} \hat{S}_1(f) \, e^{+\frac{i2\pi nf}{W}} \, df \tag{2.25}$$

$n = 0, \pm 1, \pm 2, \ldots.$

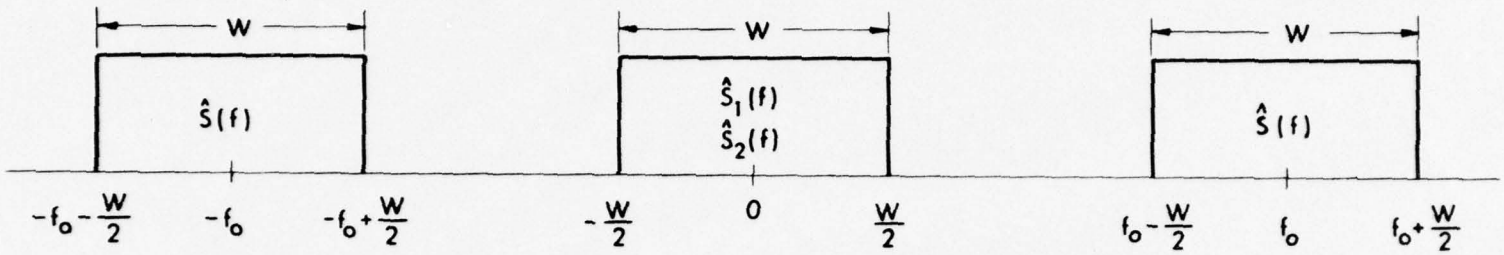

FIGURE 2.1

FREQUENCY DOMAINS OCCUPIED BY $\hat{S}(f)$, $\hat{S}_1(f)$ AND $\hat{S}_2(f)$

The infinite set of coefficients C_n determine $\hat{S}_1(f)$ uniquely. The Fourier transform of $\hat{S}_1(f)$ can be written as

$$S_1(t) = \int_{-W/2}^{W/2} \hat{S}_1(f)\, e^{+i2\pi ft}\, df \quad . \tag{2.26}$$

Comparison of Eq. (2.25) and Eq. (2.26) yields

$$C_n = \frac{1}{W}\, S_1\left(\frac{n}{W}\right) \tag{2.27}$$

Therefore the in-phase component $S_1(t)$ and the out-of-phase component $S_2(t)$ must be sampled at a minimum rate of $W \frac{\text{samples}}{\text{sec}}$ in order to extract all of the information contained in $S_1(t)$ and $S_2(t)$. Samples of $S_1(t)$ obtained at the minimum rate of $W \frac{\text{samples}}{\text{sec}}$ will be independent of each other. Namely, a change in one or more of the sampled values $S_1(n/W)$, $n = 0, \pm 1, \pm 2, \ldots$, does not alter the rest.[5] Samples of $S_2(t)$ obtained at the minimum rate of $W \frac{\text{samples}}{\text{sec}}$ also will be independent of each other.

It was assumed that $S(t)$ was of infinite duration. However, if the duration of a signal is not infinite, but is long compared to its fluctuation time $(1/2W)$, an interpolation formula can represent the signal from its samples in the interval $(-T/2, T/2)$ to within an error that is of the order $1/T$.[6]

If the pulse length T of the quadrature components is finite, a minimum of TW samples of each quadrature component is required for digital processing of the quadrature components.

---

[5] David Middleton, An Introduction To Statistical Communication Theory, McGraw-Hill Book Co., New York, N. Y., 1960, p. 209.

[6] Ibid., p. 211.

C. Quadrature Sampling

The technique of quadrature sampling[7] is used to obtain the quadrature components of a narrow band signal. The use of quadrature sampling to obtain the quadrature components eliminates the need to heterodyne a signal.

The in-phase component $S_1(t)$ of $S(t)$ is obtained by sampling $S(t)$ at times $t = nK/f_o$, $n = 1, 2, \ldots TW_Q$. TW_Q is the number of samples of $S_1(t)$ where $W_Q = f_o/K$. The sampling parameter, K, is a positive integer that determines the time interval between samples of $S_1(t)$ in multiples of $1/f_o$. The sampling parameter, K, is equal to $[f_o/W]$ where $[f_o/W]$ denotes the largest integer $K \leq f_o/W$.

To obtain the out-of-phase components, $S_2(t)$, $S(t)$ is sampled at times $t = nK/f_o + 1/4f_o$, $n = 1, 2, \ldots TW_Q$. If W is small compared to f_o, the approximation $S_2(nK/f_o + 1/4f_o) \cong S_2(nK/f_o)$ can be made. Otherwise $S_2(nK/f_o)$ may be computed from $S_2(nK/f_o + 1/4f_o)$ by using an interpolation formula.

From the samples of $S_1(t)$ and $S_2(t)$, the envelope and phase of $S(t)$ can be computed at a time nK/f_o as follows:

$$A\left(\frac{nK}{f_o}\right) = \sqrt{S_1^2\left(\frac{nK}{f_o}\right) + S_2^2\left(\frac{nK}{f_o}\right)} \quad , \text{ and} \tag{2.28}$$

$$\varphi\left(\frac{nK}{f_o}\right) = -\tan^{-1} \frac{S_2\left(\frac{nK}{f_o}\right)}{S_1\left(\frac{nK}{f_o}\right)} \quad . \tag{2.29}$$

---

[7] O. D. Grace and S. P. Pitt, "Quadrature Sampling of High Frequency Waveforms," J. Acoust. Soc. Am. 24, (1968) pp. 1453-1454.

Each sample of the in-phase component will be independent of other samples of the in-phase component when $W_Q = W$. Each sample of the out-of-phase component will be independent of other samples of the out-of-phase component for this same condition. Also the quadrature components resolved from a signal are dependent on the choice of origin for the time scale.

If samples of S(t) cannot be obtained at the times nK/f_o, $nK/f_o + 1/4f_o$, n=1, 2, ... TW_Q because of physical limitations on the analog-to-digital converter, but can be obtained at times nK/f'_o, $nK/f'_o + 1/4f'_o$, n = 1, 2, ... TW'_Q, it is permissible to redefine the center frequency (f_o) as f'_o and the bandwidth (W) as W'. The redefined center frequency f'_o is as near the value of f_o as the limitations on the analog-to-digital converter allow, $W' = W + 2\,|f_o - f'_o|$ and $W'_Q = f'_o/[f'_o/W']$. The equation for S(t) then becomes

$$S(t) = S'_1(t) \cos \omega'_o t + S'_2(t) \sin \omega'_o t$$

where $\omega'_o = 2\pi f'_o$. If W is small compared to f_o and $|f_o - f'_o| \ll f_o$, the approximation $S'_2(nK/f'_o + 1/4f'_o) \cong S'_2(nK/f'_o)$ can be made.

The maximum error (e_A) made in the approximation $S_2(nK/f_o + 1/4f_o) \cong S_2(nK/f_o)$ is proportional to W/f_o[8]. The

---

[8] Athanasious Papoulis, "Limits on Band-limited Signals," Proc. IEEE 55, No. 10, (October 1967), p. 1680.

increase in error (Δe_A), resulting from redefining the bandwidth as W' and the center frequency as f'_o, is proportional to $(W'/f'_o - W/f_o)$. And

$$\frac{\Delta e_A}{e_A} = \frac{\frac{W'}{f'_o} - \frac{W}{f_o}}{\frac{W}{f_o}} \quad , \text{ or}$$

$$\Delta e_A = e_A \left[\frac{f_o W'}{f'_o W} - 1 \right] \quad .$$

The echoes discussed in Chapter IV were bandlimited to a bandwidth of 20 kHz with a center frequency of 70 kHz. The echoes were digitized at a rate of 300 kHz instead of the desired rate of 280 kHz. Physical limitations on the analog-to-digital converter necessitated the use of this rate. The bandwidth was redefined as 30 kHz with a center frequency of 75 kHz. The increase in error (Δe_A) resulting from redefining the bandwidth and the center frequency was $0.4\ e_A$.

In Fig. 2.2, the in-phase component $S'_1(t)$ and the out-of-phase component $S'_2(t)$ of a narrow band echo are plotted.

In Fig. 2.3, the envelope computed from the quadrature components $S'_1(t)$ and $S'_2(t)$ of a narrow band echo is plotted. The

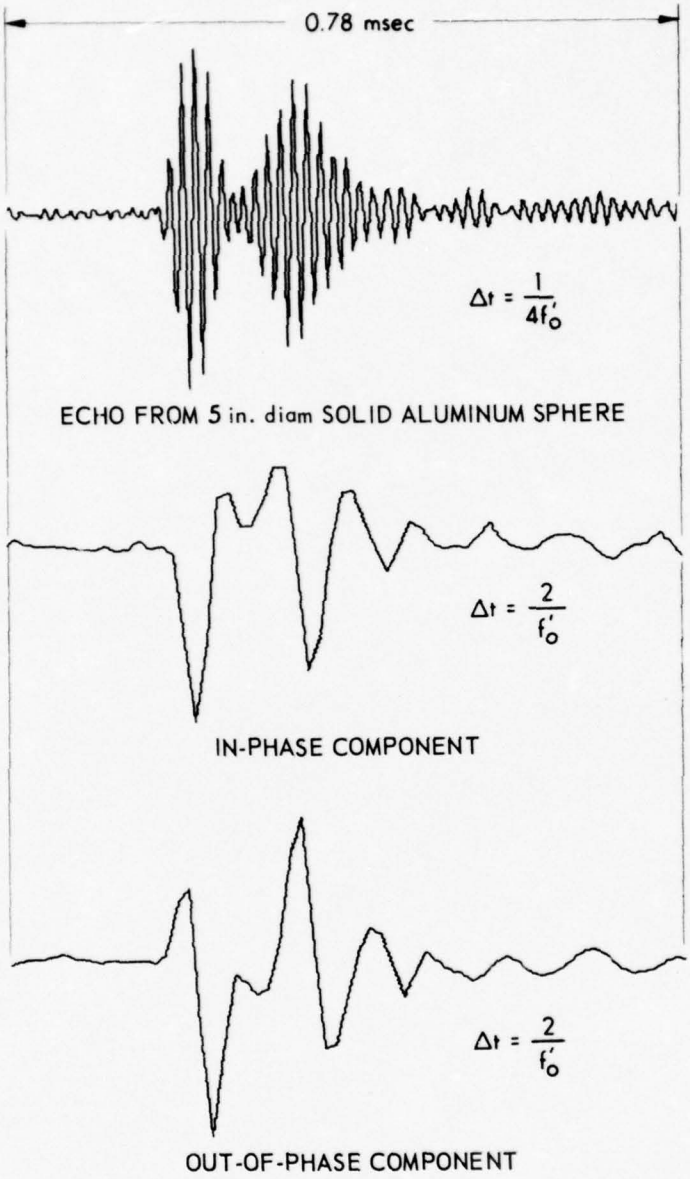

FIGURE 2.2
ECHO FROM 5 in. diam SOLID ALUMINUM SPHERE
AND ITS IN-PHASE AND OUT-OF-PHASE COMPONENTS
f_o' = 75 kHz W' = 30 kHz
TRANSMITTING WAVEFORM WAS A SINUSOIDAL PULSE
f_o = 70 kHz T = 80 μsec PEAK |AMPLITUDE| = 1.0 in.

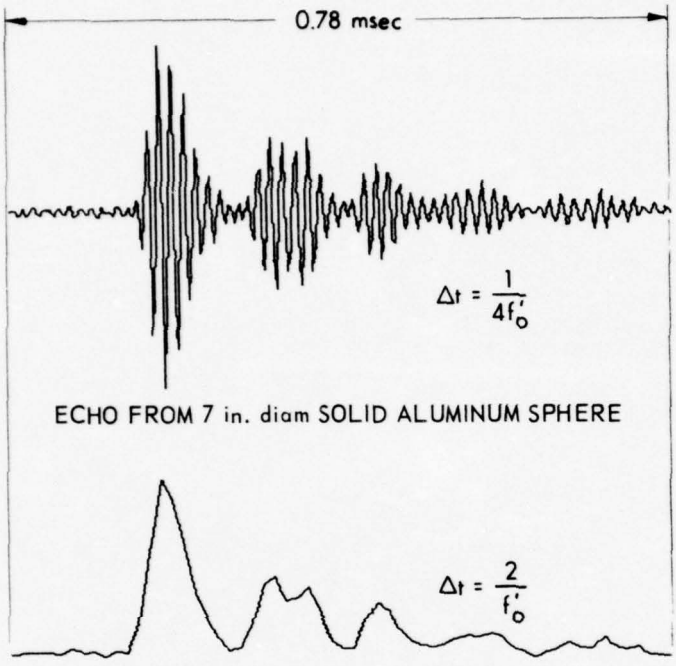

FIGURE 2.3
ECHO FROM 7 in. diam SOLID ALUMINUM
SPHERE AND ITS ENVELOPE
f_o' = 75 kHz W' = 30 kHz
TRANSMITTING WAVEFORM WAS A SINUSOIDAL PULSE
f_o = 70 kHz T = 80 μsec PEAK |AMPLITUDE| = 1.0 in.

total error ($1.4\ e_A$) made in the approximation

$$S_2'\left(\frac{nK}{f_o'} + \frac{1}{4f_o'}\right) \cong S_2'\left(\frac{nK}{f_o'}\right)$$

is considered to be small since the envelope plotted in Fig. 2.3 would closely correspond to a plot of the actual envelope of the echo if the actual envelope were plotted.

D. Implementation of Likelihood Ratio Calculations Using Quadrature Components Obtained by Quadrature Sampling

The quadrature components obtained by quadrature sampling can be used in a generalized likelihood ratio calculation. Pertinent to the justification of the use of quadrature sampling is a generalized crosscorrelation, such as

$$\int_{-\infty}^{\infty}\int_{-\infty}^{\infty} a(t-u)\ V(u)\ S^B(t;\varphi_o)\ du\,dt \quad .$$

The functions $S^B(t;\varphi_o)$ and $V(u)$ are narrow band signals of bandwidth W with center frequency f_o, where W is small compared to f_o, and $a(t-u)$ is a kernel that is a symmetric function of $t-u$. The result of integrating over u is a crosscorrelation

$$\int_{-\infty}^{\infty} X(t)\ S^B(t;\varphi_o)\ dt \quad ,$$

where

$$X(t) = \int_{-\infty}^{\infty} a(t-u)\ V(u)\ du \quad . \qquad (2.30)$$

Since $X(t)$ is equal to a convolution of two functions in the time domain, $\hat{X}(\omega)$ can be described as

$$\hat{X}(\omega) = \hat{a}(\omega)\ \hat{V}(\omega) \tag{2.31}$$

in the frequency domain,

where

$\hat{X}(\omega)$ is the Fourier transform of $X(t)$, etc.

Since $\hat{V}(\omega)$ is narrow band, it follows that $\hat{X}(\omega)$ is narrow band.

The aim of the following arguments is to show that the generalized crosscorrelation in integral form is approximately equal to each of the two following operations:

(1) $$\frac{1}{F^2} \sum_{m,n=1}^{TF} a^F_{mn} V_m S^B_n(\varphi_o)$$

where

a^F_{mn} is a sample of the kernel $a(t-u)$ at the times $t_m = m/F$,

$u_n = n/F$, and

V_m is a sample of $V(t)$ at the time $t_m = m/F$, etc., and

(2) $$\frac{1}{2W_Q^2} \sum_{p,q=1}^{TW_Q} a^{W_Q}_{pq} [V_{1p} S^B_{1q}(\varphi) + V_{2p} S^B_{2q}(\varphi)]$$

where

$$\frac{1}{W_Q} = \frac{\left[\frac{f_o}{W}\right]}{f_o}, \text{ and}$$

$\left[\frac{f_o}{W}\right]$ is the largest integer $K \leq \frac{f_o}{W}$,

$a^{W_Q}_{pq}$ is a sample of the kernel $a(t-u)$ at the times

$$t_p = \frac{p}{W_Q} \quad ,$$

$$u_q = \frac{q}{W_Q} \quad ,$$

V_{1p} is a sample of $V_1(t)$ at the time

$$t_p = \frac{p}{W_Q} \quad , \text{ etc.}$$

After it has been demonstrated that the two operations defined in the last statement are equivalent to the same generalized cross-correlation, the two operations can be set equal to each other.

Thus

$$\frac{1}{F^2} \sum_{m,n=1}^{TF} a^F_{mn} V_m S^B_n(\varphi_o) = \frac{1}{2W_Q^2} \sum_{p,q=1}^{TW_Q} a^{W_Q}_{pq} \left[V_{1p} S^B_{1q}(\varphi_o) + V_{2p} S^B_{2q}(\varphi_o) \right] \quad .$$

This demonstration is important since it shows how the summations in the generalized likelihood ratio defined by Eq. (2.21) can be replaced by summations involving quadrature components.

A bandpass signal such as $X(t)$ is determined by taking W $\frac{\text{samples}}{\text{sec}}$ of the signal $X(t)$ and W $\frac{\text{samples}}{\text{sec}}$ of the corresponding signal $\tilde{X}(t)$, where $\tilde{X}(t)$ is the Hilbert transform of $X(t)$.

In terms of samples of $X(t)$ and of $\tilde{X}(t)$, $X(t)$ may be written[9] as

---

[9] C. Van Schooneveld, "Some Remarks on Sampling Methods for a Band Pass Signal," Signal Processing, NATO Advanced Study Institute, (September, 1964), p. 412.

$$X(t) = \sum_{q=-\infty}^{\infty} X(\tfrac{q}{W}) \frac{\sin \pi(Wt-q)}{\pi(Wt-q)} \cos 2\pi f_o(t-\tfrac{q}{W}) + \sum_{q=-\infty}^{\infty} \tilde{X}(\tfrac{q}{W}) \frac{\sin \pi(Wt-q)}{\pi(Wt-q)} \sin 2\pi f_o(t-\tfrac{q}{W}) \quad . \tag{2.32}$$

The functions $b(t-\frac{q}{W})$ and $d(t-\frac{q}{W})$,

where

$$b(t-\tfrac{q}{W}) = \frac{\sin \pi(Wt-q)}{\pi(Wt-q)} \cos 2\pi f_o(t-\tfrac{q}{W}) \quad , \text{ and}$$

$$d(t-\tfrac{q}{W}) = \frac{\sin \pi(Wt-q)}{\pi(Wt-q)} \sin 2\pi f_o(t-\tfrac{q}{W})$$

are mutually orthogonal[10], that is

$$\int_{-\infty}^{\infty} b(t-\tfrac{p}{W})\, b(t-\tfrac{q}{W})dt = \frac{1}{2W} \delta pq \tag{2.33}$$

$$\int_{-\infty}^{\infty} d(t-\tfrac{p}{W})\, d(t-\tfrac{q}{W})dt = \frac{1}{2W} \delta pq \quad , \text{ and} \tag{2.34}$$

$$\int_{-\infty}^{\infty} b(t-\tfrac{p}{W})\, d(t-\tfrac{q}{W})dt = 0 \text{ for all } p,q \quad . \tag{2.35}$$

The application of the orthogonal relations defined by Eq. (2.33), Eq. (2.34), and Eq. (2.35) to the right side of the following equation,

---

[10] Ibid., p. 412.

$$\int_{-\infty}^{\infty} X(t)S^B(t;\varphi_o)dt = \int_{-\infty}^{\infty} \sum_{q=-\infty}^{\infty} \left[X(\tfrac{q}{W}) \frac{\sin \pi(Wt-q)}{\pi(Wt-q)} \cos 2\pi f_o(t-\tfrac{q}{W}) \right.$$

$$\left. + \tilde{X}(\tfrac{q}{W}) \frac{\sin \pi(Wt-q)}{\pi(Wt-q)} \sin 2\pi f_o(t-\tfrac{q}{W}) \right]$$

$$\sum_{p=-\infty}^{\infty} \left[S^B(\tfrac{p}{W};\varphi_o) \frac{\sin \pi(Wt-p)}{\pi(Wt-p)} \cos 2\pi f_o(t-\tfrac{p}{W}) \right. \qquad (2.36)$$

$$\left. + \tilde{S}^B(\tfrac{p}{W};\varphi_o) \frac{\sin \pi(Wt-p)}{\pi(Wt-p)} \sin 2\pi f_o(t-\tfrac{p}{W}) \right] dt \quad ,$$

results in Eq. (2.37),

$$\int_{-\infty}^{\infty} X(t)S^B(t;\varphi_o)dt = \frac{1}{2W} \sum_{q=-\infty}^{\infty} \left[X_q S_q^B(\varphi_o) + \tilde{X}_q \tilde{S}_q^B(\varphi_o) \right] \qquad (2.37)$$

where

$$X(\tfrac{q}{W}) = X_q \quad ,$$

$$S^B(\tfrac{p}{W};\varphi_o) = S_p^B(\varphi_o) \quad , \text{ etc.}$$

Thus the crosscorrelation, $\int_{-\infty}^{\infty} X(t)S^B(t;\varphi_o)dt$, is equivalent to an operation on the evenly spaced samples of $X(t)$, $\tilde{X}(t)$ and $S^B(t;\varphi_o)$, $\tilde{S}^B(t;\varphi_o)$ obtained at the minimum rate $W \frac{\text{samples}}{\text{sec}}$.

In Chapter II, Sec. B, $X(t)$ is written as

$$X(t) = A(t) \cos (\varphi(t) + \omega_o t) = X_1(t) \cos \omega_o t + X_2(t) \sin \omega_o t$$

where

$$X_1(t) = A(t) \cos \varphi(t) \quad , \text{ and}$$

$$X_2(t) = -A(t) \sin \varphi(t) \quad .$$

$X_1(t)$ is called the in-phase component of $X(t)$ and $X_2(t)$ is called the out-of-phase component of $X(t)$.

The Hilbert transform of $X(t)$ can be obtained by shifting the phase $\varphi(t)$ of $X(t)$ by a quarter of a cycle of the carrier f_o. Thus $\tilde{X}(t)$ becomes

$$\tilde{X}(t) = A(t) \cos\left(\varphi(t) + \omega_o t + \frac{1}{4f_o}\right)$$

$$= A(t)\left[\cos\varphi(t)\cos\left(\omega_o t + \frac{1}{4f_o}\right) - \sin\varphi(t)\sin\left(\omega_o t + \frac{1}{4f_o}\right)\right]$$

$$= X_2(t)\cos\omega_o t - X_1(t)\sin\omega_o t \quad .$$

If $X(t)$ is sampled at the times $t_n = nK/f_o$, $n = 0, \pm1, \pm2, \ldots$ where $K = [f_o/W]$, the result is samples of $X_1(nK/f_o)$. If $X(t)$ is sampled at the times $t_n = nK/f_o + 1/4f_o$, $n = 0, \pm1, \pm2, \ldots$ the result is samples of $X_2(nK/f_o + 1/4f_o)$. If W is small compared to f_o, then the approximation $X_2(nK/f_o + 1/4f_o) \cong X_2(nK/f_o)$ can be made, and the samples $X_2(nK/f_o)$, $n = 0, \pm1, \pm2, \ldots$ can be interpreted as samples of $\tilde{X}(nK/f_o)$, $n = 0, \pm1, \pm2, \ldots$.

If samples of $X_1(t)$, $X_2(t)$, and $S_1^B(t;\varphi_o)$, $S_2^B(t;\varphi_o)$ are obtained at the rate W_Q, where $W_Q = f_o/K$, then Eq. (2.37) can be written as

$$\int_{-\infty}^{\infty} X(t)S^B(t;\varphi_o)dt = \frac{1}{2W_Q}\sum_{q=-\infty}^{\infty}\left[X_{1q}S_{1q}^B(\varphi_o) + X_{2q}S_{2q}^B(\varphi_o)\right] \quad , \tag{2.38}$$

where

$$X_1\left(\frac{q}{W_Q}\right) = X_{1q}, \text{ etc.}$$

In terms of quadrature components, Eq. (2.30) can be written as

$$X_1(t) \cos \omega_o t + X_2(t) \sin \omega_o t = \int_{-\infty}^{\infty} a(t-u)\left[V_1(u) \cos \omega_o u + V_2(u) \sin \omega_o u\right] du \quad , \tag{2.39}$$

where

$$X(t) = X_1(t) \cos \omega_o t + X_2(t) \sin \omega_o t \quad ,$$

$$a(t-u)V(u) = a(t-u)\left[V_1(u) \cos \omega_o u + V_2(u) \sin \omega_o u\right]$$

and $X_1(t)$, $X_2(t)$, $a(t-u)V_1(u)$, and $a(t-u)V_2(u)$ are of bandwidth W with center frequency $f_o = 0$.

If $X(t)$ is sampled at the times t_q,

where

$t_q = qK/f_o$, $q = 0, \pm 1, \pm 2, \ldots$ and $a(t_q-u)V(u)$ is sampled at the times

$u_p = pK/f_o$, $p = 0, \pm 1, \pm 2, \ldots$,

then

$$X_1(t_q) = \frac{1}{W_Q} \sum_{p=-\infty}^{\infty} a^{W_Q}(t_q-u_p)V_1(u_p) \quad , \text{ or} \tag{2.40}$$

$$X_{1q} = \frac{1}{W_Q} \sum_{p=-\infty}^{\infty} a_{pq}^{W_Q} V_{1p} \quad , \tag{2.41}$$

where

$$a^{W_Q}(t_q-u_p) = a_{qp}^{W_Q} = a_{pq}^{W_Q} \quad .$$

If $X(t)$ is sampled at the times $t_q + 1/4f_o$,

where

$t_q = qK/f_o$, $q = 0, \pm1, \pm2, \ldots$ and $a(qK/f_o + 1/4f_o, u)\, V(u)$ is sampled at the times $u_p + 1/4f_o$, where $u_p = pK/f_o$, $p = 0, \pm1, \pm2, \ldots$, then

$$X_2(t_q + \tfrac{1}{4f_o}) = \frac{1}{W_Q} \sum_{p=-\infty}^{\infty} a^{W_Q}(t_q + \tfrac{1}{4f_o} - u_p - \tfrac{1}{4f_o}) V_2(u_p + \tfrac{1}{4f_o}) \quad . \tag{2.42}$$

If W_Q is small compared to f_o, then

$$X_2(t_q + 1/4f_o) \cong X_2(t_q) = X_{2q} \quad ,$$

$$V_2(u_p + 1/4f_o) \cong V_2(u_p) = V_{2p} \quad ,$$

and Eq. (2.42) becomes

$$X_{2q} = \frac{1}{W_Q} \sum_{p=-\infty}^{\infty} a_{pq}^{W_Q} V_{2p} \quad , \tag{2.43}$$

where

$$a^{W_Q}(qK/f_o + 1/4f_o - pK/f_o - 1/4f_o) = a^{W_Q}(t_q - u_p) = a_{qp}^{W_Q} = a_{pq}^{W_Q} \quad .$$

Substitution of Eq. (2.41) and Eq. (2.43) into Eq. (2.38) results in

$$\int_{-\infty}^{\infty} X(t) S^B(t;\varphi_o)\, dt = \frac{1}{2W_Q^2} \sum_{p,q=-\infty}^{\infty} a_{pq}^{W_Q} \left[V_{1p} S_{1q}^B(\varphi_o) + V_{2p} S_{2q}^B(\varphi_o) \right] \quad . \tag{2.44}$$

In the previous equations, the sums on p and q are from $-\infty$ to $+\infty$. This assumes that the signals $V_1(t)$, $V_2(t)$, and $S_1^B(t;\varphi_o)$, $S_2^B(t;\varphi_o)$ are of infinite duration. However, if the duration of a signal such as $V_1(t)$ is not infinite, but is long compared to its fluctuation time $(1/2W)$, an interpolation formula can represent the signal from its samples in the interval $(-T/2, T/2)$ to within an error that is of the order $1/T$.[11]

A representation of a signal such as $V_1(t)$ in the interval $(-T/2, T/2)$ by an interpolation formula is

$$V_1(t) = \sum_{q=-\frac{TW_Q}{2}}^{\frac{TW_Q}{2}} V_1\left(\frac{q}{W_Q}\right) \frac{\sin \pi(W_Q t-q)}{\pi(W_Q t-q)} \quad . \tag{2.45}$$

Upon a translation of the time coordinate, namely, $t = t + T/2 + 1/W_Q$, the interpolation formula becomes

$$V_1(t) = \sum_{q=1}^{TW_Q} V_1\left(\frac{q}{W_Q}\right) \frac{\sin \pi(W_Q t-q)}{\pi(W_Q t-q)} \quad , \tag{2.46}$$

where

$$TW_Q + 1 \cong TW_Q \quad .$$

---

[11] David Middleton, An Introduction to Statistical Communication Theory. McGraw-Hill Book Co., New York, N. Y., (1960), p. 211.

Therefore, if the signals $V_1(t)$, $V_2(t)$, and $S_1^B(t;\varphi_o)$, $S_2^B(t;\varphi_o)$ are long compared to $(1/2W)$, the generalized crosscorrelation in integral form can be written as follows:

$$\int_{-\infty}^{\infty}\int_{-\infty}^{\infty} a(t-u)V(u)S^B(t;\varphi_o)\,dudt = \frac{1}{2W_Q^2}\sum_{p,q=1}^{TW_Q} a_{pq}^{W_Q}\left[V_{1p}S_{1q}^B(\varphi_o) + V_{2p}S_{2q}^B(\varphi_o)\right] . \tag{2.47}$$

The next step is to obtain the generalized crosscorrelation in the form

$$\frac{1}{F^2}\sum_{m,n=1}^{TF} a_{mn}^F V_m S_n^B(\varphi_o) \quad ,$$

where

a_{mn}^F is a sample of the kernel $a(t-u)$ at the times $t_m = m/F$, $u_n = n/F$, and

V_m is a sample of $V(u)$ at the time $u_m = m/F$, etc.

The crosscorrelation $\int_{-\infty}^{\infty} X(t)S^B(t;\varphi_o)\,dt$, where $X(t)$ is defined by Eq. (2.30), is also equivalent to an operation on the evenly spaced samples of $X(t)$ and $S^B(t;\varphi_o)$ obtained at a sampling rate[12] of F; namely,

$$\int_{-\infty}^{\infty} X(t)S^B(t;\varphi_o)\,dt = \frac{1}{F}\sum_{n=-\infty}^{\infty} X_n S_n^B(\varphi_o) \quad , \tag{2.48}$$

---

[12] C. Van Schooneveld, "Some Remarks on Sampling Methods for a Band Pass Signal," Signal Processing, NATO Advanced Study Institute, (September 1964), p. 413.

where

$t_n = n/F$, $n = 0, \pm 1, \pm 2, \ldots$ and $X(t_n) = X_n$, etc. The sampling rate F is sufficiently high such that $X(t)$ and $S^B(t;\varphi_o)$ can be reconstructed by an interpolation formula from their respective samples.

The sample $X(t_n)$, defined by Eq. (2.30), can also be written in terms of evenly spaced samples of $a(t_n - u)\, V(u)$ obtained at the rate F; namely,

$$X(t_n) = X_n = \frac{1}{F} \sum_{m=-\infty}^{\infty} a^F(t_n - \frac{m}{F})\, V(\frac{m}{F}) = \frac{1}{F} \sum_{m=-\infty}^{\infty} a^F_{mn} V_m \quad , \qquad (2.49)$$

where

$$a^F_{nm} = a^F_{mn} \text{ and } V(\frac{m}{F}) \approx V_m \quad , \text{ etc.}$$

Substitution of Eq. (2.49) into Eq. (2.48) results in

$$\int_{-\infty}^{\infty} X(t) S^B(t;\varphi_o)dt = \frac{1}{F^2} \sum_{m,n=-\infty}^{\infty} a^F_{mn}\, V_m S^B_n(\varphi_o) \quad . \qquad (2.50)$$

Upon the application of similar arguments that showed the generalized crosscorrelation is approximately equal to an operation on TW_Q samples of each quadrature component, the generalized crosscorrelation is also approximatley equal to an operation on TF samples each of $V(u)$ and $S^B(t;\varphi_o)$; namely,

$$\int_{-\infty}^{\infty}\int_{-\infty}^{\infty} a(t - u)\, V(u) S^B(t;\varphi_o)dudt = \frac{1}{F^2} \sum_{m,n=1}^{TF} a^F_{mn}\, V_m S^B_n(\varphi_o) \quad . \qquad (2.51)$$

The substitution of Eq. (2.47) into Eq. (2.51) results in

$$\frac{1}{F^2}\sum_{m,n=1}^{TF} a^{F}_{mn}\, V_m S^{B}_{n}(\varphi_o) = \frac{1}{2W_Q^2}\sum_{p,q=1}^{TW_Q} a^{W_Q}_{pq}\left[V_{1p}S^{B}_{1q}(\varphi_o) + V_{2p}S^{B}_{2q}(\varphi_o)\right] \quad , \tag{2.52}$$

where

a^{F}_{mn} is a sample of the kernel $a(t-u)$ at the times $t_m = \frac{m}{F}$, $u_n = \frac{n}{F}$, and

$a^{W_Q}_{pq}$ is a sample of the kernel $a(t-u)$ at the times $t_p = \frac{p}{W_Q}$,

$u_q = \frac{q}{W_Q}$, etc.

The function $S^{B}(t;\varphi_o)$ can be written as

$$S^{B}(t;\varphi_o) = S^{B}_{1}(t;\varphi_o)\cos\omega_o t + S^{B}_{2}(t;\varphi_o)\sin\omega_o t, \text{ or}$$

$$S^{B}(t;\varphi_o) = S^{B}_{1}(t+\epsilon_o)\cos\omega_o(t+\epsilon_o) + S^{B}_{2}(t+\epsilon_o)\sin\omega_o(t+\epsilon_o) \quad ,$$

where

$$\epsilon_o = \frac{\varphi_o}{\omega_o} \, .$$

If $-\pi < \varphi_o < \pi$, then it is possible to make the approximations $S^{B}_{1}(t+\epsilon_o) \cong S^{B}_{1}(t)$ and $S^{B}_{2}(t+\epsilon_o) \cong S^{B}_{2}(t)$, and $S(t;\varphi_o)$ becomes

$$S^{B}(t;\varphi_o) = S^{B}_{1}(t)\left[\cos\omega_o t\cos\varphi_o - \sin\omega_o t\sin\varphi_o\right]$$

$$+ S^{B}_{2}(t)\left[\sin\omega_o t\cos\varphi_o + \cos\omega_o t\sin\varphi_o\right] \quad .$$

If $S^{B}(t;\varphi_o)$ is sampled at the times $t_q = \frac{qK}{f_o}$, $q = 0, \pm1, \pm2, \ldots$, then

$$S^{B}\left(\frac{qK}{f_o};\varphi_o\right) = S^{B}_{1}\left(\frac{qK}{f_o};\varphi_o\right) = S^{B}_{1}\left(\frac{qK}{f_o}\right)\cos\varphi_o + S^{B}_{2}\left(\frac{qK}{f_o}\right)\sin\varphi_o \quad , \text{ or}$$

$$S^{B}_{1q}(\varphi_o) = S^{B}_{1q}\cos\varphi_o + S^{B}_{2q}\sin\varphi_o \quad . \tag{2.53}$$

If $S^B(t;\varphi_o)$ is sampled at the times $t_q = \frac{qK}{f_o} + \frac{1}{4f_o}$, $q = 0, \pm 1, \pm 2, \ldots$, then

$$S^B\left(\frac{qK}{f_o} + \frac{1}{4f_o};\varphi_o\right) = S_2^B\left(\frac{qK}{f_o} + \frac{1}{4f_o};\varphi_o\right) \cong S_2^B\left(\frac{qK}{f_o};\varphi_o\right) \quad , \text{ or}$$

$$S_{2q}^B(\varphi_o) = -S_{1q}^B \sin\varphi_o + S_{2q}^B \cos\varphi_o \quad . \tag{2.54}$$

Substitution of Eq. (2.53) and Eq. (2.54) into Eq. (2.52) results in

$$\frac{1}{F^2}\sum_{m,n=1}^{TF} a_{mn}^F V_m S_n^B(\varphi) = \frac{1}{2W_Q^2}\sum_{p,q=1}^{TW_Q} a_{pq}^{W_Q}\Big[V_{1p}\left(S_{1q}^B \cos\varphi_o + S_{2q}^B \sin\varphi_o\right)$$

$$+ V_{2p}\left(-S_{1q}^B \sin\varphi_o + S_{2q}^B \cos\varphi_o\right)\Big] \quad , \text{ or}$$

$$\sum_{m,n=1}^{TF} a_{mn}^F V_m S_n^B(\varphi) = \frac{F^2}{2W_Q^2}\sum_{p,q=1}^{TW_Q} a_{pq}^{W_Q}\Big[V_{1p}S_{1q}^B + V_{2p}S_{2q}^B\Big]\cos\varphi_o$$

$$+ \frac{F^2}{2W_Q^2}\sum_{p,q=1}^{TW_Q} a_{pq}^{W_Q}\Big[V_{1p}S_{2q}^B - V_{2p}S_{1q}^B\Big]\sin\varphi_o \quad . \tag{2.55}$$

Upon the application of similar arguments that resulted in Eq. (2.55), it follows that

$$\sum_{m,n=1}^{TF} a_{mn}^F S_m^B(\varphi_o) S_n^B(\varphi_o) = \frac{F^2}{2W_Q^2}\sum_{p,q=1}^{TW_Q} a_{pq}^{W_Q}\Big[S_{1m}^B S_{1n}^B + S_{2m}^B S_{2n}^B\Big] \quad , \tag{2.56}$$

$$\sum_{m,n=1}^{TF} a^F_{mn} V_m S^A_n(\varphi_o) = \frac{F^2}{2W_Q^2} \sum_{p,q=1}^{TW_Q} a^{W_Q}_{pq}\left[V_{1p} S^A_{1q} + V_{2p} S^A_{2q}\right]\cos\varphi_o + \frac{F^2}{2W_Q^2} \sum_{p,q=1}^{TW_Q} a^{W_Q}_{pq}\left[V_{1p} S^A_{2q} - V_{2p} S^A_{1q}\right]\sin\varphi_o \quad , \text{ and} \tag{2.57}$$

$$\sum_{m,n=1}^{TF} a^F_{mn} S^A_m(\varphi_o) S^A_n(\varphi_o) = \frac{F^2}{2W_Q^2} \sum_{p,q=1}^{TW_Q} a^{W_Q}_{pq}\left[S^A_{1m} S^A_{1n} + S^A_{2m} S^A_{2n}\right] \quad . \tag{2.58}$$

In order to shorten the equation describing $\Lambda(\vec{V})$ in terms of quadrature components, the following substitutions are made:

$$\alpha^A = \frac{F^2}{4W_Q^2} \sum_{p,q=1}^{TW_Q} a^{W_Q}_{pq}\left[S^A_{1p} S^A_{1q} + S^A_{2p} S^A_{2q}\right] \quad , \tag{2.59}$$

$$\alpha^B = \frac{F^2}{4W_Q^2} \sum_{p,q=1}^{TW_Q} a^{W_Q}_{pq}\left[S^B_{1p} S^B_{1q} + S^B_{2p} S^B_{2q}\right] \quad , \tag{2.60}$$

$$\lambda^A = \frac{F^2}{2W_Q^2} \sum_{p,q=1}^{TW_Q} a^{W_Q}_{pq}\left[V_{1p} S^A_{1q} + V_{2p} S^A_{2q}\right] \quad , \tag{2.61}$$

$$\lambda^B = \frac{F^2}{2W_Q^2} \sum_{p,q=1}^{TW_Q} a^{W_Q}_{pq}\left[V_{1p} S^B_{1q} + V_{2p} S^B_{2q}\right] \quad , \tag{2.62}$$

$$\nu^A = \frac{F^2}{2W_Q^2} \sum_{p,q=1}^{TW_Q} a^{W_Q}_{pq}\left[V_{1p} S^A_{2q} - V_{2p} S^A_{1q}\right] \quad , \tag{2.63}$$

$$\nu^B = \frac{F^2}{2W_Q^2} \sum_{p,q=1}^{TW_Q} a^{W_Q}_{pq}\left[V_{1p} S^B_{2q} - V_{2p} S^B_{1q}\right] \quad . \tag{2.64}$$

The equation for $\Lambda(\vec{V})$ then becomes

$$\Lambda(\vec{V}) = e^{\alpha^A - \alpha^B} \frac{\int_{-\pi}^{\pi} e^{\lambda^B \cos \varphi_o + \nu^B \sin \varphi_o} d\varphi_o}{\int_{-\pi}^{\pi} e^{\lambda^A \cos \varphi_o + \nu^A \sin \varphi_o} d\varphi_o} \quad . \tag{2.65}$$

If the following change of variables is made, $\varphi_o' = \varphi_o + \pi$, the result is

$$\Lambda(\vec{V}) = e^{\alpha^A - \alpha^B} \frac{\int_{o}^{2\pi} e^{-\lambda^B \cos \varphi_o' - \nu^B \sin \varphi_o'} d\varphi_o'}{\int_{o}^{2\pi} e^{-\lambda^A \cos \varphi_o' - \nu^A \sin \varphi_o'} d\varphi_o'} \quad . \tag{2.66}$$

The integrals can be integrated directly to give

$$\Lambda(\vec{V}) = e^{\alpha^A - \alpha^B} \frac{I_o\left[\left(\lambda^{B^2} + \nu^{B^2}\right)^{1/2}\right]}{I_o\left[\left(\lambda^{A^2} + \nu^{A^2}\right)^{1/2}\right]} \quad , \tag{2.67}$$

where

I_o represents the modified Bessel function of the first kind of order zero.

The equation for $\ell(\vec{V})$, from Eq. (2.22), is

$$\ell(\vec{V}) = e^{-\sum_{m,n=1}^{TF} a_{mn}^F \left[V_m S_n^A - V_m S_n^B - \frac{1}{2} S_m^A S_n^A + \frac{1}{2} S_m^B S_n^B\right]} \quad . \tag{2.68}$$

Written in terms of quadrature components, Eq. (2.68) becomes

$$\ell(\vec{V}) = e^{-\frac{F^2}{2W_Q^2} \sum_{p,q=1}^{TW_Q} a_{pq}^{W_Q} \left[V_{1p} S_{1q}^A + V_{2p} S_{2q}^A - V_{1p} S_{1q}^B - V_{2p} S_{2q}^B\right.} \tag{2.69}$$

$$\left. - \frac{1}{2} S_{1p}^A S_{1q}^A - \frac{1}{2} S_{2p}^A S_{2q}^A + \frac{1}{2} S_{1p}^B S_{1q}^B + \frac{1}{2} S_{2p}^B S_{2q}^B\right] \quad .$$

One advantage in using quadrature components for likelihood ratio calculations is that the dimensions of the square matrix $\left(a_{pq}^{W_Q}\right)$ are smaller than the dimensions of the square matrix $\left(a_{mn}^{F}\right)$. A second advantage is that the statistics of the in-phase components and the out-of-phase components of Gaussian noise remain Gaussian.

CHAPTER III

DATA USED FOR LIKELIHOOD RATIO PROCESSING

A. Arrangement of Apparatus

The data were taken at the Lake Travis Test Facility of the Applied Research Laboratories of The University of Texas at Austin. The source transducer, target, and receiving hydrophone were suspended in a line beneath a barge at a depth of 16 feet, as indicated in Fig. 3.1. The source transducer (Edo 327) was in effect a "piston" transmitter with a resonant frequency of 70 kHz.

The output $Y(t)$ of a transducer, given the input $X(t)$ and the impulse response $H(t)$ of the transducer, is

$$Y(t) = \int_{-\infty}^{\infty} X(t-\tau)\, H(\tau)\, d\tau \quad . \tag{3.1}$$

For an input signal bandlimited to the frequency interval $f_o - W/2 < |f| < f_o + W/2$, $Y(t)$ can be written as

$$Y(t) = \int_{-f_o-\frac{W}{2}}^{-f_o+\frac{W}{2}} \hat{X}(f)\hat{H}(f)\, e^{i2\pi ft} df + \int_{f_o-\frac{W}{2}}^{f_o+\frac{W}{2}} \hat{X}(f)\hat{H}(f)\, e^{i2\pi ft} df \quad . \tag{3.2}$$

$\hat{H}(f)$ in general is a complex function, and it can be written as

$$\hat{H}(f) = A(f)\, e^{i\varphi(f)} \quad , \tag{3.3}$$

where $A(f)$ is the amplitude distortion and $\varphi(f)$ is the phase distortion of the transducer.

For the system composed of the source and receiving transducers, $A(f)$ was "flat" in the frequency interval of 60 kHz to 80 kHz,

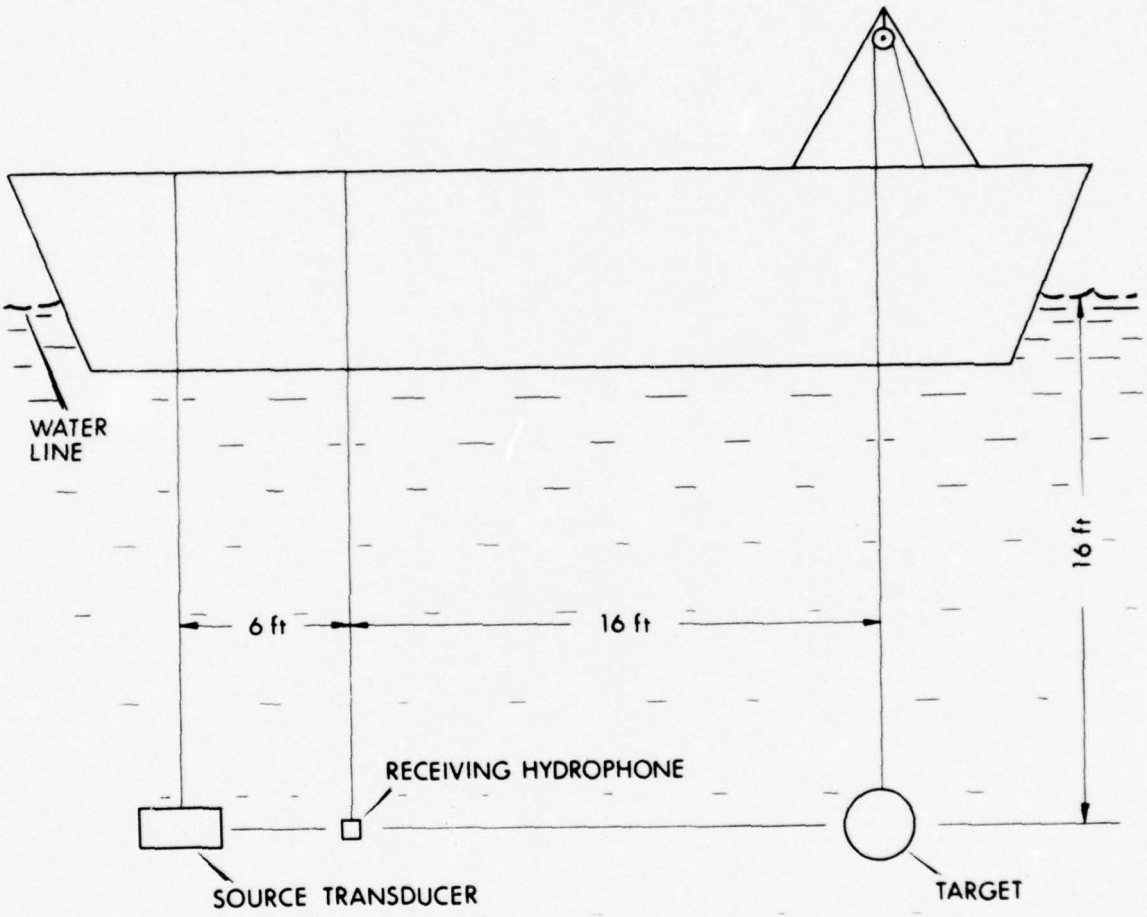

FIGURE 3.1
DIAGRAM OF THE EXPERIMENTAL ARRANGEMENT

even though the source transducer had a resonant frequency at 70 kHz. (The amplitude distortion is considered "flat" in a frequency interval if there is less than a 3 dB change in the magnitude of the amplitude distortion in the frequency interval.) Since the source transducer had a resonant frequency at 70 kHz, optimum use was made of this sensitivity. For the system, $\varphi(f)$ was linear in the frequency interval of 60 kHz to 80 kHz. (The linearity of $\varphi(f)$ in a frequency interval results only in a time delay of a signal in the time domain.)

The targets were suspended from the barge by 0.015 in. diam stainless steel wire, 22 feet from the source transducer. The receiving hydrophone was located between the source and the target, 16 feet from the target.

B. Targets

The five targets used were

(1) a 7 in. diam solid aluminum sphere,

(2) a 5 in. diam solid aluminum sphere,

(3) a 3 in. diam solid aluminum sphere,

(4) a 5 in. diam styrofoam sphere, and

(5) a 5 in. diam hollow aluminum sphere with a b/a of 0.975. (b is the inner diameter of the hollow sphere and a is the outer diameter.) The region inside the hollow sphere contained air at a pressure of one atmosphere.

The two signal transmissions used were

(1) a sinusoidal pulse of frequency 70 kHz with a pulse length of 80 μsec, and

(2) a linear FM of bandwidth 12.5 kHz with a center frequency of 63.75 kHz and a pulse length of 3 msec.

Plots of the two signal transmissions are shown in Fig. 3.2. In Table 3.1, ka values for a 3 in. diam, a 5 in. diam, and a 7 in. diam sphere for the 2 different transmissions are listed.

C. Echoes from the Targets

"The echoes from a rigid, freely movable sphere differ significantly from those from an immovable sphere only for values of ka less than five."[13] For values of ka less than two, the echoes from the rigid, freely movable sphere are similar to those from the solid elastic sphere for corresponding values of the densities of the two spheres.[14] "Presumably, beyond this stage, elastic vibrations have an increasing effect until they become the dominant factor in determining the very marked frequency dependence of echoes from solid, elastic materials in water."[15]

For the ka range of 10.5 to 26.9, an echo from a completely rigid sphere is similar to that of the incident pulse, and the arrival time of the echo shows that it was reflected from the portion of the the sphere closest to the source.[16] The echoes from elastic spheres, such as the solid aluminum spheres, are longer and more complicated.

---

[13] Robert Hickling and N. M. Wang, "Scattering of Sound by a Rigid Movable Sphere," J. Acoust. Soc. Am. 39, No. 2 (1966) p. 276.

[14] Ibid., p. 276.

[15] Ibid., p. 276.

[16] K. Jerome Dierks and R. Hickling, "Echoes from Hollow Aluminum Spheres in Water," J. Acoust. Soc. Am. 41, No. 2 (1967) p. 380.

TABLE 3.1

ka VALUES FOR 3 IN. DIAM, 5 IN. DIAM, AND 7 IN. DIAM SPHERES FOR THE TWO TRANSMISSION MODES

	Sinusoidal Pulse f_o = 70 kHz	Linear FM f_o = 63.75 kHz
3 in. diam Sphere	11.5	10.5
5 in. diam Sphere	19.2	17.4
7 in. diam Sphere	26.9	24.4

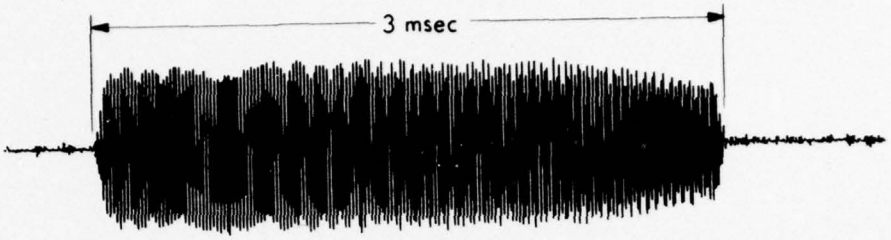

LINEAR FM TRANSMISSION

f_o = 63.75 kHz W = 12.5 kHz

T = 3 msec Δt = 1/300 msec

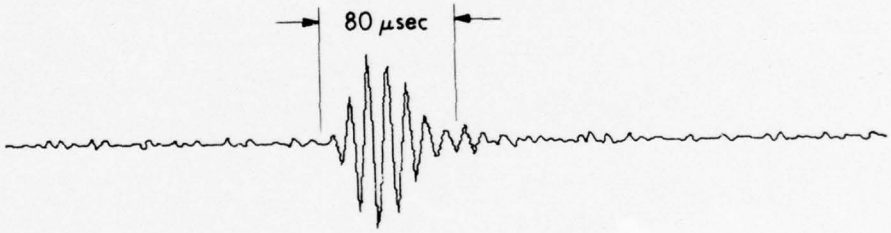

SINUSOIDAL PULSE TRANSMISSION

f_o = 70 kHz T = 80 μsec

Δt = 1/300 msec

FIGURE 3.2
TRANSMISSION WAVEFORMS
PEAK |AMPLITUDE| = 0.5 in.

The first portions of the echoes still retain the characteristics of the rigid sphere echoes, indicating that there are primary reflections from the outer surface, similar to those from a rigid body, followed by additional echoes caused by the elastic reaction of the sphere.[17] When the length of the incident pulse is less than the diameter of the sphere, the primary echo is separated in time from the secondary elastic echoes.[18] As the incident pulse length becomes shorter (or as the diameter of the sphere increases), each of the component parts of the echo contract and separate.[19] As the incident pulse grows longer (or as the diameter of the sphere decreases), the secondary echoes, due to the elastic vibrations in the sphere, begin to overlap with the primary reflection and with each other, and the interactions interfere constructively or destructively, depending on the particular value of the dominant frequency.[20]

The first highlights of the echoes from a 5 in. diam hollow aluminum sphere with b/a = 0.975 correspond to rigid body reflections. The remaining portions of the echoes are a result of the vibrations induced within the sphere.[21] For short incident pulses, these secondary echoes are separated from the primary echoes. For long pulses, the secondary echoes overlap and interfere with the

---

[17] Ibid., p. 381.

[18] Ibid., p. 381.

[19] Ibid., p. 381.

[20] Ibid., p. 381.

[21] Robert Hickling, "Analysis of Echoes from a Hollow Metallic Sphere in Water," J. Acoust. Soc. Am. 36, No. 6 (1964) p. 1133.

primary echo. For b/a = 0.975, the waves that occur in the solid material of the shell are mainly of a flexural type.[22] These waves travel around the shell with a velocity the same as or slightly less than the velocity of shear waves in the material.[23]

The 5 in. diam styrofoam sphere can be approximated as a 5 in. diam sphere with a pressure release surface. For a ka of about 20, the reflected pulse has the same wave shape as the emitted pulse, but the reflected pulse is inverted.[24]

The echoes for the sinusoidal pulse transmission were passed through a bandpass filter of bandwidth (W) equal to 20 kHz and a center frequency (f_o) equal to 70 kHz. The filter was designed to eliminate frequencies outside the 20 kHz bandwidth without the distortion of frequencies within the 12.5 kHz bandwidth. The echoes for the linear FM transmission were passed through a bandpass filter of bandwidth (W) equal to 20 kHz with a center frequency (f_o) equal to 65 kHz. Again the filter was designed to eliminate frequencies outside the 20 kHz bandwidth without the distortion of frequencies within the 12.5 kHz bandwidth. The following data were recorded on magnetic tape. On one channel of the tape, the transmitted signal was recorded. On a second channel, a 300 kHz continuous reference

---

[22] Ibid., p. 1133.

[23] Ibid., p. 1133.

[24] Robert Hickling, "Analysis of Echoes from a Solid Elastic Sphere in Water," J. Acoust. Soc. Am. 34, No. 10 (1962) p. 1584.

tone was recorded, and on the third channel, the echoes from the spheres were recorded. The 300 kHz reference tone was used in the digitizing process to eliminate the "wow and flutter" of the tape recorder. The transmitted signal was used as a trigger for the analog-to-digital converter to begin the analog-to-digital conversion of an echo.

The echoes were digitized at a rate of 300 kHz and recorded in digital form on magnetic tape. The gain settings of the amplifiers used in the digitizing process were set so that the amplitudes of the analog echoes had a possible maximum absolute value of 10 volts. In the analog-to-digital conversion, the amplitudes of the digitized echoes were scaled so that 10 volts were equal to 2047. The number 2047, $(2^{11} - 1)$, resulted from digitizing the amplitudes of the echoes into 12 bit words with the first bit of each word used as a sign bit (12 bit quantization).

In Fig. 3.3 an echo from each target for a sinusoidal pulse transmission is shown. The leading edge of the envelope for each echo in Fig. 3.3 is characterized by a steep, positive slope.

In Fig. 3.4 an echo for a linear FM transmission from each target is shown. The echoes for a linear FM transmission were passed through a "gate" for a duration of 5 msec. The gate was used to minimize the surface and volume reverberation in the recorded returns.

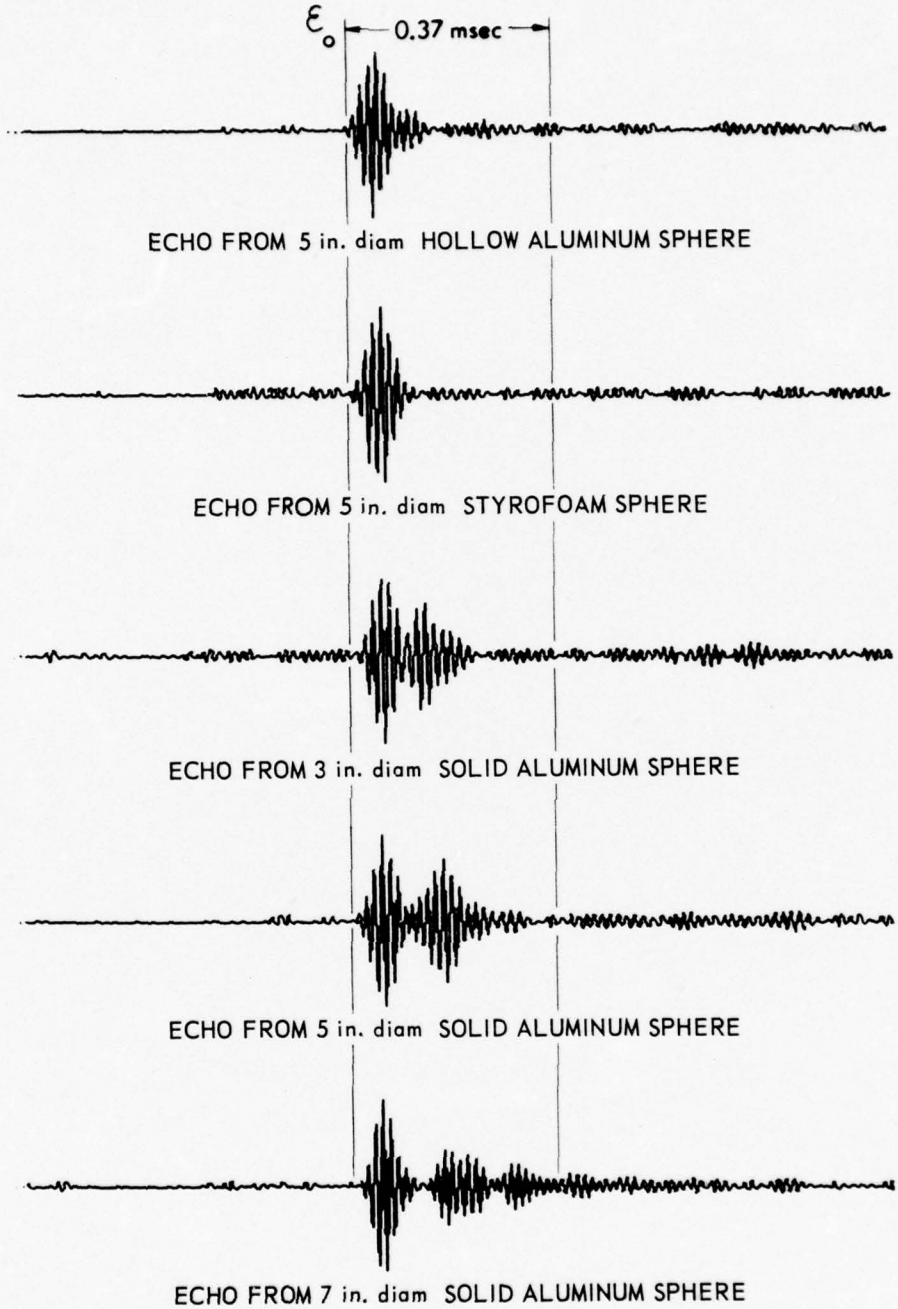

FIGURE 3.3
SONAR RETURNS FOR A SINUSOIDAL PULSE TRANSMISSION
PULSE LENGTH = 0.37 msec EPOCH = $\mathcal{E}_o$ Δt = 1/300 msec
f_o = 70 kHz W = 20 kHz PEAK |AMPLITUDE| = 0.5 in.

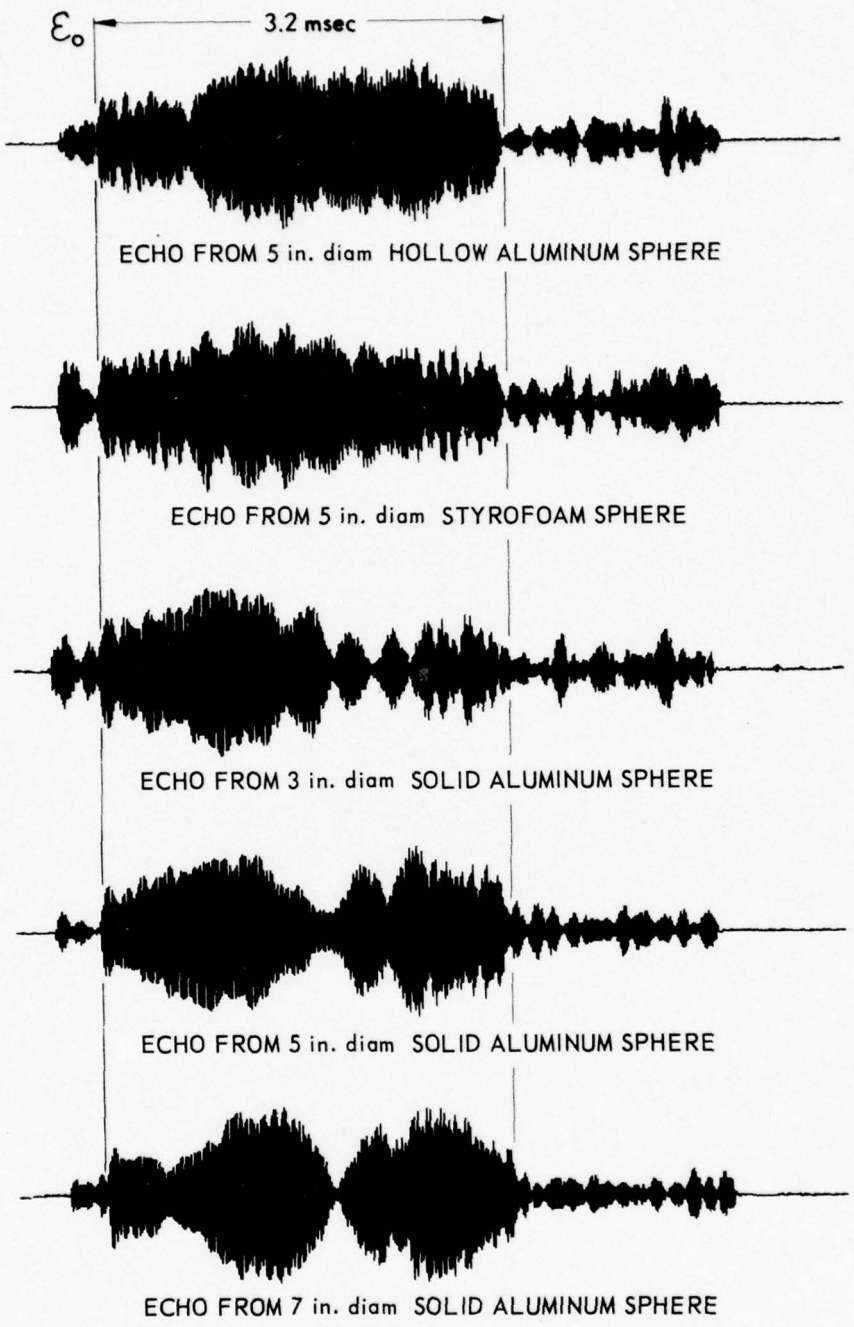

FIGURE 3.4
SONAR RETURNS FOR A LINEAR FM TRANSMISSION
PULSE LENGTH = 3.2 msec EPOCH = $\mathcal{E}_o$ Δt = 1/300 msec
f_o = 65 kHz W = 20 kHz PEAK |AMPLITUDE| = 0.5 in.
DURATION OF GATE = 5 msec

CHAPTER IV

TARGET CLASSIFICATION USING A SINUSOIDAL PULSE TRANSMISSION

A. Classification of Similar Targets

1. Signal-to-Noise Ratio

The ability of the likelihood ratio processor to classify sonar returns from similar targets for a sinusoidal pulse transmission was investigated. The five targets used were the 7 in. diam, 5 in. diam, and 3 in. diam solid aluminum spheres, the 5 in. diam styrofoam sphere, and the 5 in. diam hollow aluminum sphere. The sinusoidal pulse transmission and the echoes from the targets were described in Chapter III.

The S/N (signal-to-noise) ratio of an echo was defined as $\frac{\text{peak amplitude of signal}}{\text{rms of noise amplitude}}$. In units of decibels (dB), the S/N ratio was expressed as $20 \log_{10} \left(\frac{\text{peak amplitude of signal}}{\text{rms of noise amplitude}} \right)$ dB.

The S/N ratios of the digitized echoes from the five targets were large, ranging from an average S/N ratio of 34 dB for the echoes from the 3 in. diam solid aluminum sphere to an average S/N ratio of 41 dB for the echoes from the 5 in. diam hollow aluminum sphere.

2. Epoch

The use of a threshold technique to determine the epoch $\left(\epsilon_o = \frac{\varphi_o}{\omega_o} \right)$ of the digitized echoes from the five targets was possible since

(1) the S/N ratios of the echoes were large,

(2) the variations in A(t) and $\varphi(t)$ from echo to echo among the echoes from the same target were small, and

(3) the leading edge of the envelope for each echo was characterized by a steep positive slope.

This steepness in the slope was an important factor in the determination of epoch. The epoch (ϵ_o') for an echo was defined as the time at which the amplitude of an echo reached 20% of its peak amplitude.

After epoch (ϵ_o') was established, a new epoch (ϵ_o) was defined in order to include in a likelihood ratio calculation the portion of an echo occurring before the threshold. The new epoch (ϵ_o) was defined as occurring 0.027 msec (or 8 samples) before the threshold. The pulse lengths of the echoes were defined to be 0.37 msec, as indicated in Fig. 3.3.

In Fig. 4.1, the success of a threshold technique in determining epoch (ϵ_o) is demonstrated. Seven echoes from a 5 in. diam solid aluminum sphere are shown. Each echo is plotted along a different time axis. The distance from the beginning of a time axis to the epoch is the same for each echo.

The amplitudes of each echo from each target were scaled so that the peak amplitude of each echo from each target was equal to 1400. The purpose of this scaling was to be able to base the classification of targets on the differences in waveform of the echoes. The number of echoes available from each target varied from 12 to 14. A reference echo for a target was computed by taking an ensemble average of all the echoes from the target. The reference echo for target A was defined as $\vec{S}_R^A = \langle \vec{S}^A \rangle$, and the reference echo for target B was defined as $\vec{S}_R^B = \langle \vec{S}^B \rangle$. (The brackets denote an ensemble average over the available set of target echoes.)

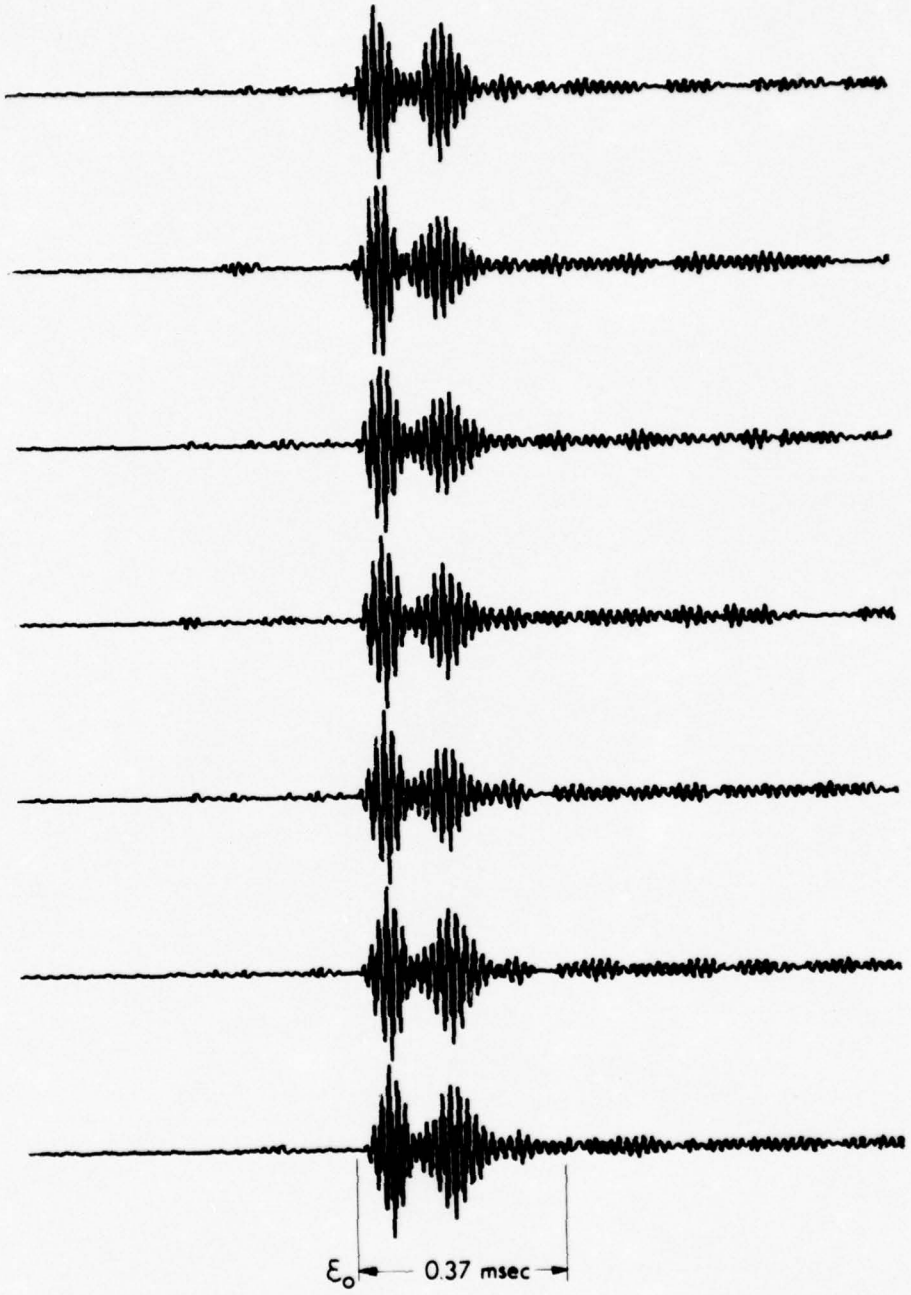

FIGURE 4.1
ECHOES FROM A 5 in. diam SOLID ALUMINUM SPHERE
PULSE LENGTH = 0.37 msec EPOCH = $\mathcal{E}_o$
Δt = 1/300 msec f_o = 70 kHz W = 20 kHz
S/N = 38.8 dB PEAK |AMPLITUDE| = 0.5 in.

3. Addition of Gaussian Noise to Echoes

Samples of stationary Gaussian noise of mean zero from a random noise generator were added to all the echoes for two purposes:

(1) to make the simulation of target classification more realistic;

(2) to increase the number of messages (echo-noise combinations) from each target class. (The members of a target class are characterized by the same Gaussian noise statistics and the same reference echo.)

The bandwidth of the Gaussian noise was 20 kHz with a center frequency of 70 kHz. A power spectrum computed from samples of the Gaussian noise is plotted in Fig. 4.2. The confidence interval[25] used in plotting the power spectrum was 80%. The random noise generator is further discussed in Appendix A.

The problem of classification was made more realistic by decreasing the S/N ratios of the echoes from a target to a prescribed lower value by specifying the rms of the amplitude of the Gaussian noise to be added to the echoes from the target. The desired S/N ratio of the echoes from a target was described as follows:

$$R_{SN} = \frac{P_A}{\sqrt{< N_A^2 > + < N^2 >}} \quad , \qquad (4.1)$$

[25] R. B. Blackman, and J. W. Tukey, The Measurement of Power Spectra, Dover Publications, Inc., New York, N. Y., (1958), p. 23.

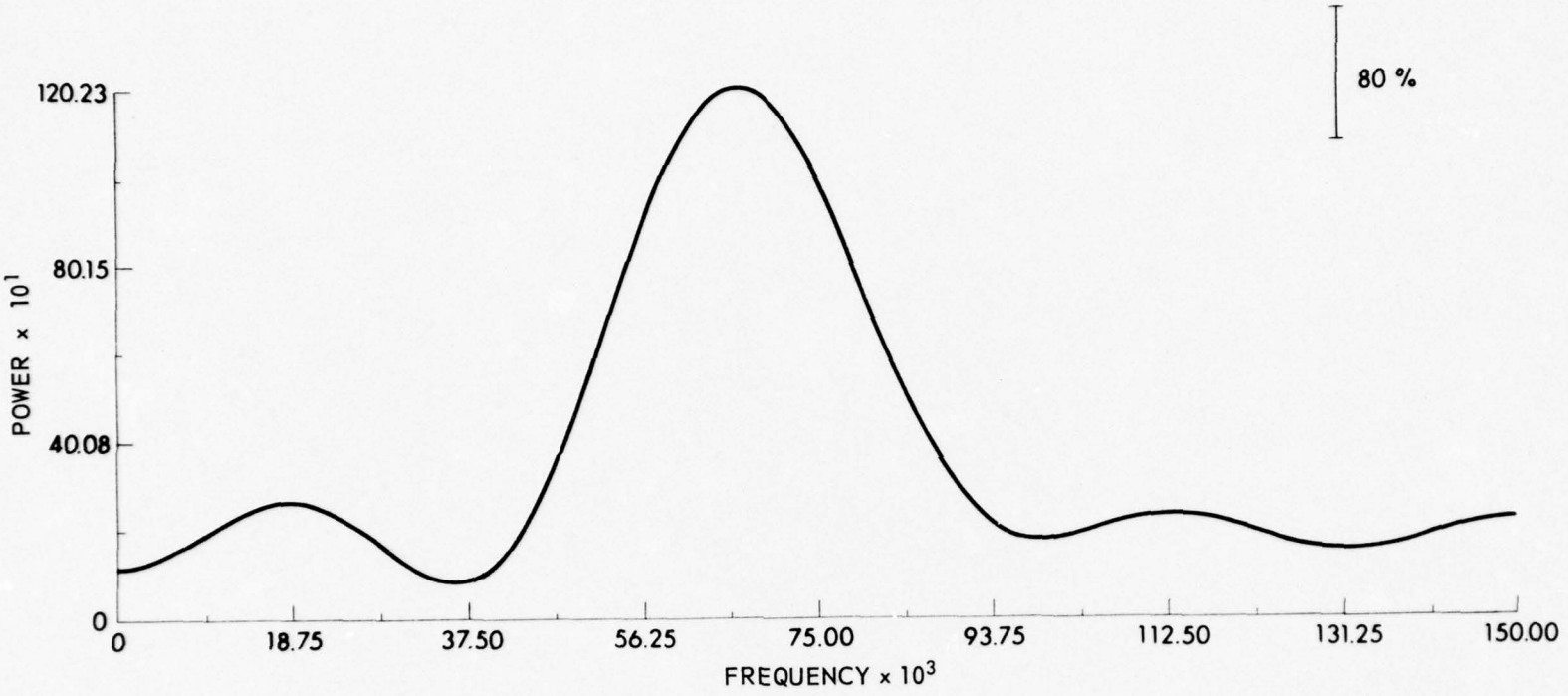

FIGURE 4.2
POWER SPECTRUM COMPUTED FROM SAMPLES
OF GAUSSIAN NOISE FROM RANDOM NOISE GENERATOR
W = 20 kHz f_o = 70 kHz SAMPLING RATE = 300 kHz

DENOTES SPREAD FOR 80% CONFIDENCE INTERVAL

where

$P_A = 1400$ = peak amplitude of each echo from a target,

$< N_A^2 >$ = mean square of ambient noise present in the echoes,

$< N^2 >$ = mean square of noise from the random noise generator, and

R_{SN} = desired S/N ratio of each echo from a target.

The ambient noise in an echo was independent of the additive Gaussian noise from the random noise generator. For R_{SN} of the order 1, the rms of the amplitude of the ambient noise in an echo was much less than the rms of the amplitude of the Gaussian noise from the random noise generator. From Eq. (4.1) the rms of the amplitude of the noise from the random noise generator was specified as follows:

$$< N^2 >^{1/2} = \left[\frac{P_A^2}{R_{SN}^2} - < N_A^2 > \right]^{1/2} . \qquad (4.2)$$

For R_{SN} of the order 1, the rms of the amplitude of the ambient noise was neglected in the computation of $< N^2 >^{1/2}$.

In the investigation of the ability of the likelihood ratio processor to classify similar targets, R_{SN} was set equal to one (0 dB). In Fig. 4.3, a message with a S/N ratio of 0 dB from each target class is shown. In Fig. 4.3, the distorted echoes of pulse length 0.37 msec are located between the two vertical lines.

The number of messages from each target class was increased by the addition of 10 separate noise signals from the random noise generator to each echo so that the total number of messages from each target class varied from 120 to 140. No noise signal was duplicated

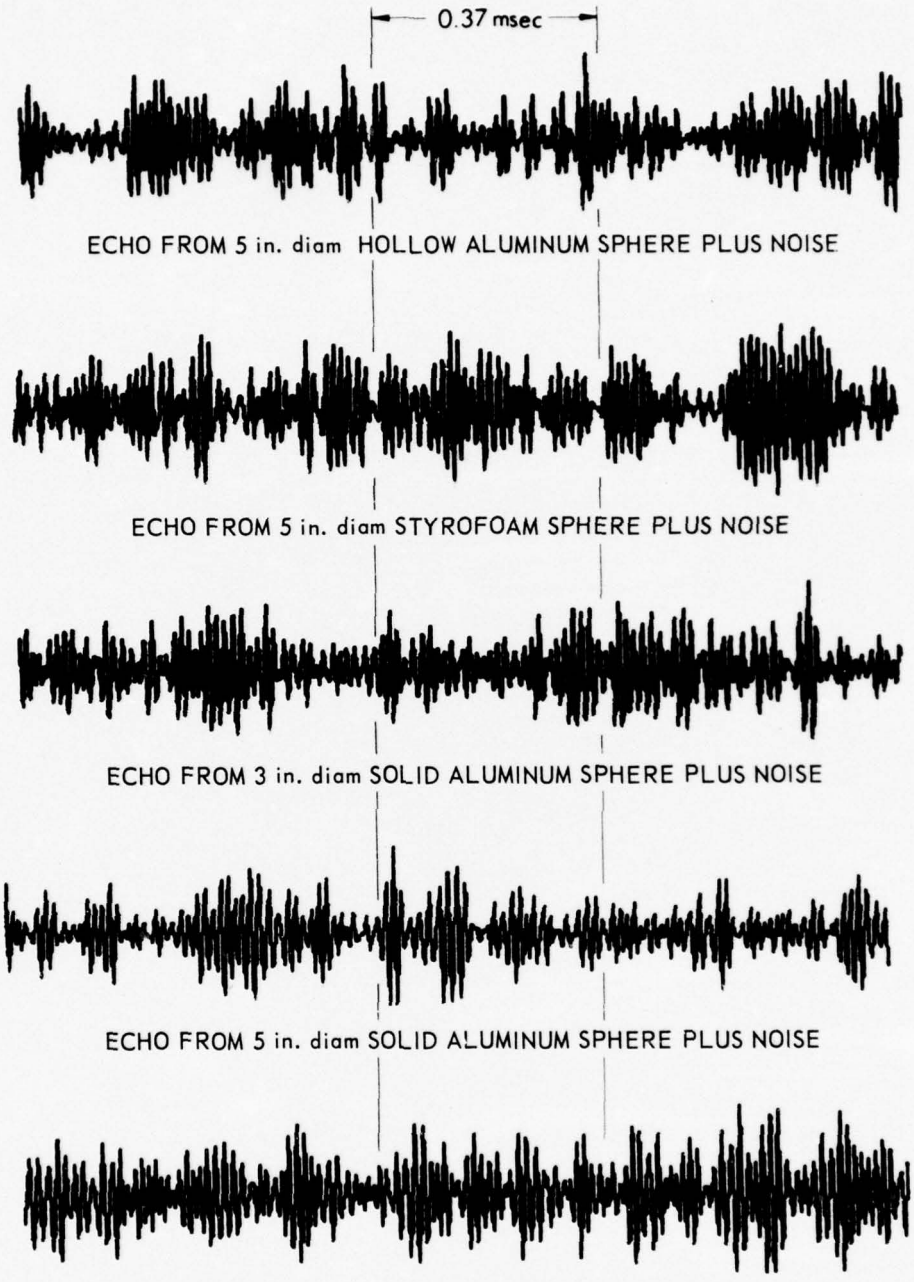

FIGURE 4.3
MESSAGES FOR SINUSOIDAL PULSE
POSITION OF 0.37 msec TIME INTERVAL INDICATES LOCATION OF EMBEDDED ECHO
PULSE LENGTH = 0.37 msec Δt = 1/300 msec f_o = 70 kHz
W = 20 kHz S/N = 0 dB PEAK |AMPLITUDE| = 0.5 in.

throughout this procedure. In the classification of the messages from two target classes, the same number of messages from each target class was used. Therefore, the a priori probability (q_1) for the messages from target class A was equal to the a priori probability (q_2) for the messages from target class B.

The knowledge of epoch was retained during the addition of Gaussian noise to the echoes so that the likelihood ratio processor described by Eq. (2.69) could be used to classify the messages.

In obtaining the quadrature components of the messages by quadrature sampling, a sampling parameter of K = 2 was used. This sampling parameter gave the minimum number of samples (TW'_Q) greater than TW' of the in-phase component $\left(W' = 30 \text{ kHz}, f'_o = 75 \text{ kHz}, \text{ and } W'_Q = \frac{f'_o}{\left[\frac{f'_o}{W'}\right]}\right)$ and the minimum number of samples (TW'_Q) greater than TW' of the out-of-phase component. This sampling parameter was used in the computation of the envelope plotted in Fig. 2.3.

4. Computation of Autocovariance Matrix for Noise

An autocovariance matrix $C^{W'_Q}$ of order $TW'_Q \times TW'_Q$ was computed from a discrete noise signal using the following formula:

$$C^{W'_Q}(\tau) = \frac{1}{P-\tau} \sum_{\sigma=1}^{P-\tau} N_\sigma N_{\sigma+\tau} \quad , \tag{4.3}$$

where

$P \geq 10\ TW'_Q$ [26], and

$N_\sigma = N\left(\frac{\sigma}{W'_Q}\right)$.

[26] Julius S. Bendat, and A. G. Piersol, Measurement and Analysis of Random Data, John Wiley and Sons, Inc., New York, N. Y., (1966), p. 290.

The noise signal consisted of samples of stationary Gaussian noise from the random noise generator. The rms of the noise signal amplitude was

$$< N^2 >^{1/2} = \frac{P_A}{R_{SN}} \tag{4.4}$$

where

R_{SN} = desired S/N ratio of each message, and

P_A = 1400 = peak amplitude of each echo.

The bandwidth of the noise signal was 20 kHz with a center frequency of 70 kHz. The matrix $a^{W'_Q}$ of order TW'_Q x TW'_Q where $a^{W'_Q} C^{W'_Q} = 1$, was computed by taking the inverse of the autocovariance matrix $C^{W'_Q}$.

5. Geometrical Description of Target Classes

A measure of the ability of the likelihood ratio processor to classify messages for a fixed threshold can be determined geometrically as follows: *The message vectors from target class A are* labeled as $\vec{V}^A$, and the message vectors from target class B are labeled as $\vec{V}^B$. The vectors $\vec{V}^A$, $\vec{V}^B$, $\vec{S}^A_R$, and $\vec{S}^B_R$ are located in a $2TW'_Q$-dimensional vector space and are depicted as located in a 3-dimensional vector space in Fig. 4.4.

The geometrical representation in Fig. 4.4 is based on the assumption that $(a_{mn}) = (a_o \delta_{mn})$ where a_o is a constant. In Fig. 4.4, the average radius of the sphere generated by the vectors $\vec{V}^A$ is $< |\vec{V}^A - \vec{S}^A_R| >$, and the average radius of the sphere generated by the vectors $\vec{V}^B$ is $< |\vec{V}^B - \vec{S}^B_R| >$. The deviation of $|\vec{V}^A - \vec{S}^A_R|$ from $< |\vec{V}^A - \vec{S}^A_R| >$ is $< \left(< |\vec{V}^A - \vec{S}^A_R| > - |\vec{V}^A - \vec{S}^A_R| \right)^2 >^{1/2}$, and the deviation

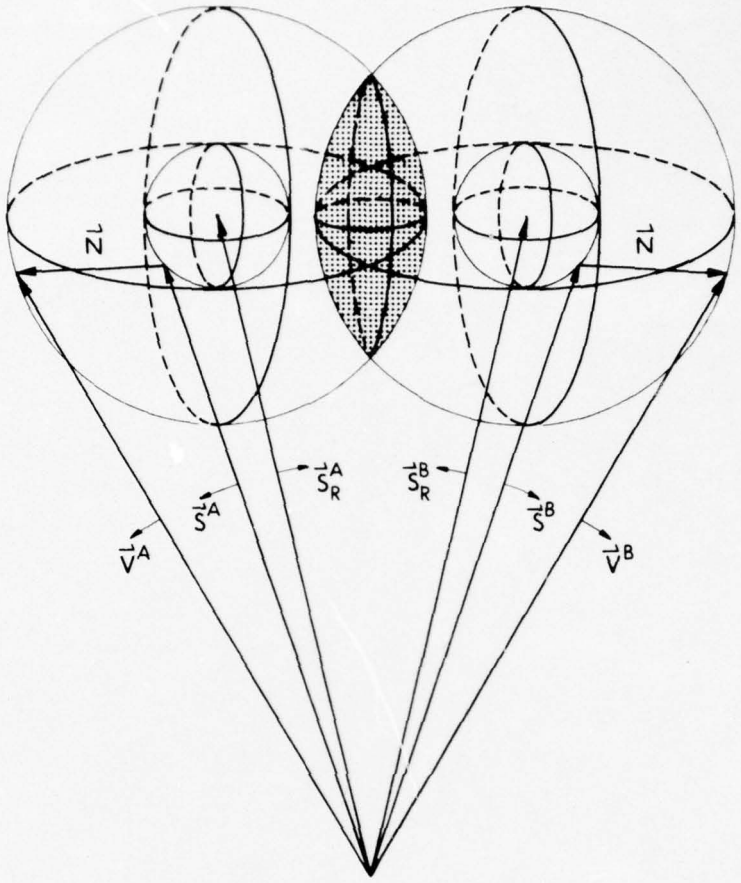

$$\langle \vec{S}^A \rangle = \vec{S}_R^A \qquad \vec{V}^A = \vec{S}^A + \vec{N}$$

$$\langle \vec{S}^B \rangle = \vec{S}_R^B \qquad \vec{V}^B = \vec{S}^B + \vec{N}$$

$$\langle \vec{N} \rangle = 0$$

FIGURE 4.4
REPRESENTATION OF $\vec{V}^A$ AND $\vec{V}^B$ IN
A 3-DIMENSIONAL VECTOR SPACE

of $|\vec{V}^B - \vec{S}_R^B|$ from $< |\vec{V}^B - \vec{S}_R^B| >$ is $< \left(< |\vec{V}^B - \vec{S}_R^B| > - |\vec{V}^B - \vec{S}_R^B| \right)^2 >^{1/2}$. The distance between the centers of the two spheres is $|\vec{S}_R^A - \vec{S}_R^B|$. The shaded portion indicates the overlapping volume of the two spheres. For $(a_{mn}) \neq (a_o \delta_{mn})$, the spheres are distorted into ellipsoids.

A hyperplane was constructed to intersect the centers of the two hyperspheres. A schematic projection of the hyperspheres onto the hyperplane is depicted in Fig. 4.5.

In Fig. 4.5, the short lines perpendicular to the perimeters of the two circles indicate the deviation of the radii of each circle from the average radius. If $|r_A - r_B|$ and $|d_A - d_B|$ are small compared to r_A and d_A respectively, the geometric threshold for equal costs for wrong decisions and equal a priori probabilities would be a line that perpendicularly bisects $|\vec{S}_R^A - \vec{S}_R^B|$. On consideration of the restrictions in the last statement, a geometric measure of the ability to classify two targets is $\frac{D_T}{D_o}$, where

$$\frac{D_T}{D_o} = \frac{< |\vec{V}^A - \vec{S}_R^A| > + < |\vec{V}^B - \vec{S}_R^B| > + |\vec{S}_R^A - \vec{S}_R^B|}{< |\vec{V}^A - \vec{S}_R^A| > + < |\vec{V}^B - \vec{S}_R^B| > - |\vec{S}_R^A - \vec{S}_R^B|} \quad . \qquad (4.5)$$

It is possible for D_o to go to zero without the attainment of perfect classification. An error in classification can still occur since the radii of each sphere deviate from an average radius. The angle between the two reference vectors $\vec{S}_R^A$ and $\vec{S}_R^B$ would be an unsatisfactory measure of the ability of the likelihood ratio processor to classify targets, because it does not indicate the values $|\vec{S}_R^A|$ and $|\vec{S}_R^B|$.

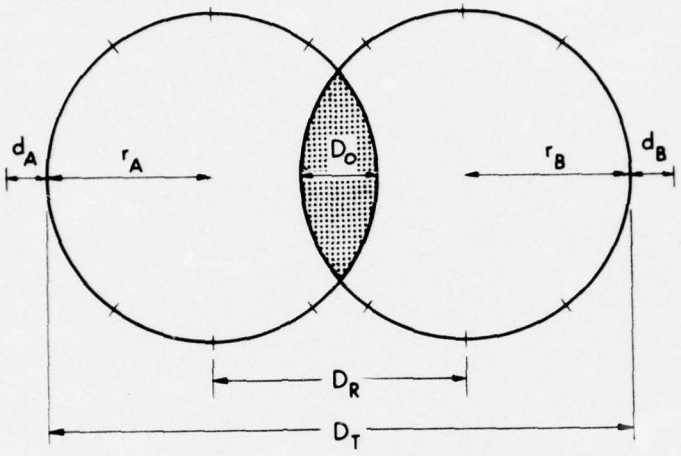

$$D_R = \left|\vec{S}_R^A - \vec{S}_R^B\right| \qquad r_A = \left\langle\left|\vec{V}^A - \vec{S}_R^A\right|\right\rangle$$

$$r_B = \left\langle\left|\vec{V}^B - \vec{S}_R^B\right|\right\rangle \qquad d_A = \left\langle\left(\left\langle\left|\vec{V}^A - \vec{S}_R^A\right|\right\rangle - \left|\vec{V}^A - \vec{S}_R^A\right|\right)^2\right\rangle^{\frac{1}{2}}$$

$$d_B = \left\langle\left(\left\langle\left|\vec{V}^B - \vec{S}_R^B\right|\right\rangle - \left|\vec{V}^B - \vec{S}_R^B\right|\right)^2\right\rangle^{\frac{1}{2}} \qquad D_T = 2r_A + 2r_B - D_o$$

FIGURE 4.5
INTERSECTION OF THE CENTERS OF THE HYPERSPHERES
WITH A HYPERPLANE REPRESENTED
IN A 2-DIMENSIONAL SPACE

6. ROC Curves

Another measure of the ability of the likelihood ratio processor to classify two targets is an ROC curve. (ROC is an acronym for Receiver Operator Characteristic.) An ROC curve gives the probability of correctly classifying target A and the probability of incorrectly classifying target B for any threshold.

An ROC curve is generated as follows: A threshold is specified. The number of likelihood ratios computed for the messages from target class A that are less than the threshold are counted. This number is normalized by dividing it by the total number of likelihood ratios computed for the messages from target class A. The resulting number is the probability of correctly classifying target A for the specified threshold. Next, the number of likelihood ratios computed for the messages from target class B that are less than the threshold are counted. This number is normalized by dividing it by the total number of likelihood ratios computed for the messages from target class B. The resulting number is the probability of incorrectly classifying target B for the specified threshold. The above procedure is repeated until all possible values of the threshold are used. For zero costs for right decisions, the optimum threshold is $\frac{q_1 C_{21}}{q_2 C_{12}}$, as discussed in Chapter II, Section A. The area under an ROC curve gives a measure of the performance of the likelihood ratio processor integrated over all values of the threshold. The area times 100 is equal to the expected percentage of correct decisions.[27]

---

[27] David M. Green, and John A. Swets, Signal Detection and Psychophysics, John Wiley and Sons, Inc., New York, N. Y., (1966), p. 217.

The ROC curves will be plotted within a square frame and the diagonal that bisects the lower left corner of the frame represents a performance equal to chance.

The ROC curves in Figs. 4.6 through 4.10 were computed using the techniques described in this chapter and the test function

$$\sum_{m,n=1}^{TW'_Q} a_{pq}^{W'_Q}\left[V_{1p}\, S_{1q}^{B} + V_{2p}\, S_{2q}^{B} - V_{1p}\, S_{1q}^{A} - V_{2p}\, S_{2q}^{A}\right] \quad .$$

The calculation of the test function instead of the likelihood ratio $\ell(\vec{V})$ described in Eq. (2.69) does not change the optimum character of an ROC curve since the test function is a monotonically increasing function of the likelihood ratio.[28] The areas under the ROC curves, along with $\frac{|r_A - r_B|}{r_A}$, $\frac{|d_A - d_B|}{d_A}$, and $\frac{D_T}{D_o}$, are listed in Tables 4.1 through 4.5.

7. Geometrical Interpretation of Results

The quantities r_A and r_B are dependent on the number of samples used to describe an echo and on the magnitude of the scaling of amplitudes of the echoes.

A change in r_A with each target B is a result of the random nature of the amplitude of the noise from the random noise generator. A change in r_B with each target B is a result of the random nature of the amplitude of the noise from the random noise generator, plus the use of a different target.

---

[28] David Middleton, Topics in Communication Theory, McGraw-Hill Book Company, New York, N. Y., (1965), p. 25.

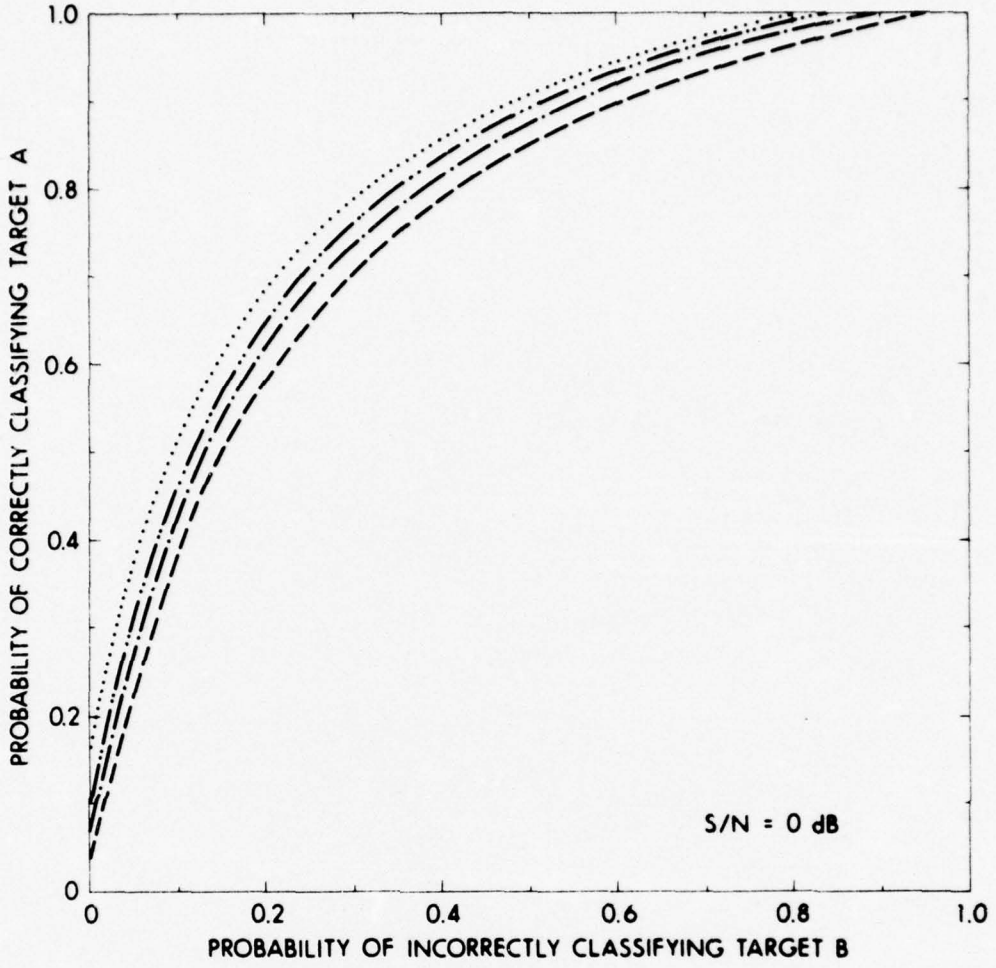

CODE FOR TARGET B

- — — — 5 in. diam SOLID ALUMINUM SPHERE
- —·— 3 in. diam SOLID ALUMINUM SPHERE
- ····· 5 in. diam STYROFOAM SPHERE
- —··— 5 in. diam HOLLOW ALUMINUM SPHERE

FIGURE 4.6
RECEIVER OPERATING CHARACTERISTIC CURVES FOR SIMILAR TARGETS
TARGET A = 7 in. diam SOLID ALUMINUM SPHERE

TABLE 4.1

TARGET A = 7 IN. DIAM SOLID ALUMINUM SPHERE, S/N = 0 dB

Target B	5 in. diam Solid Aluminum Sphere	3 in. diam Solid Aluminum Sphere	5 in. diam Styrofoam Sphere	5 in. diam Hollow Aluminum Sphere
$\left\lvert\frac{r_A - r_B}{r_A}\right\rvert$	0.009	0.001	0.001	0.004
$\left\lvert\frac{d_A - d_B}{d_A}\right\rvert$	0.06	0.05	0.02	0.07
$\frac{D_T}{D_o}$	1.29	1.30	1.43	1.38
Area under ROC Curve	0.760	0.782	0.816	0.789

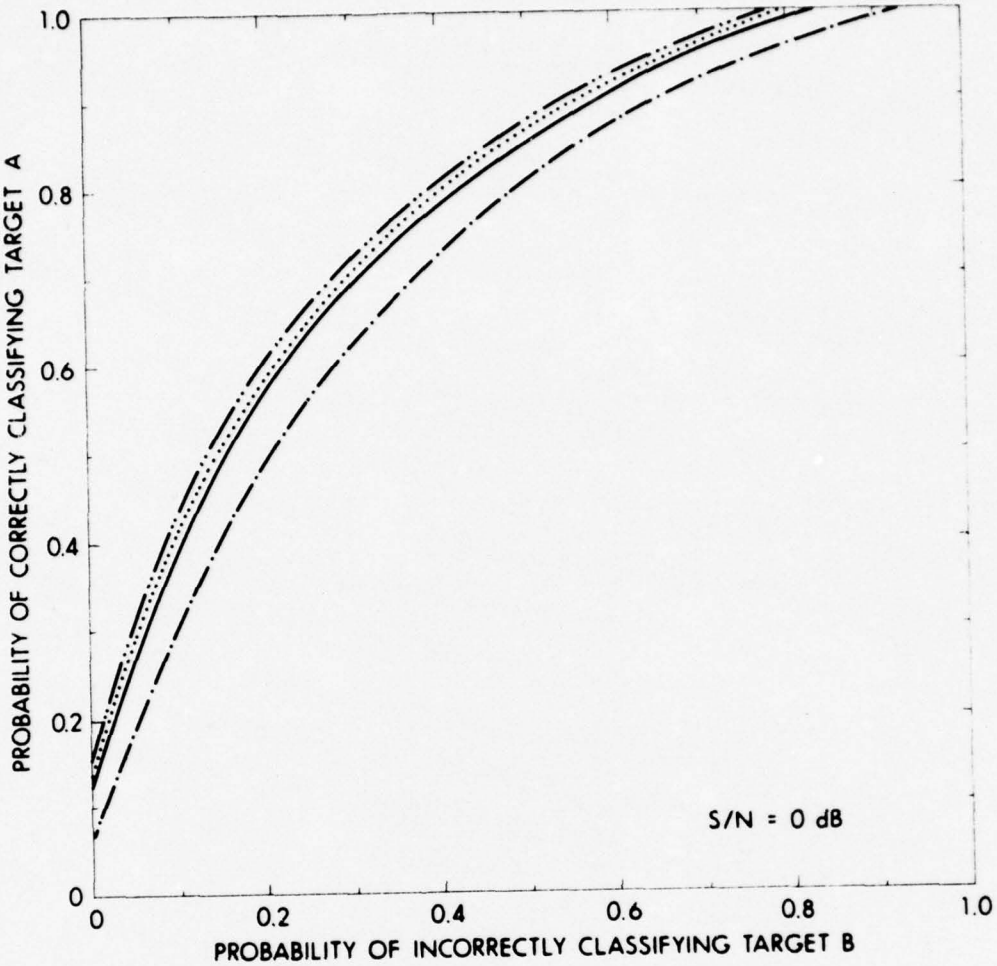

CODE FOR TARGET B

——— 7 in. diam SOLID ALUMINUM SPHERE
—·— 3 in. diam SOLID ALUMINUM SPHERE
····· 5 in. diam STYROFOAM SPHERE
—··— 5 in. diam HOLLOW ALUMINUM SPHERE

FIGURE 4.7
RECEIVER OPERATING CHARACTERISTIC CURVES FOR SIMILAR TARGETS
TARGET A = 5 in. diam SOLID ALUMINUM SPHERE

TABLE 4.2

TARGET A = 5 IN. DIAM SOLID ALUMINUM SPHERE, S/N = 0 dB

Target B	7 in. diam Solid Aluminum Sphere	3 in. diam Solid Aluminum Sphere	5 in. diam Styrofoam Sphere	5 in. diam Hollow Aluminum Sphere
$\left\lvert\frac{r_A - r_B}{r_A}\right\rvert$	0.009	0.004	0.004	0.003
$\left\lvert\frac{d_A - d_B}{d_A}\right\rvert$	0.06	0.02	0.04	0.05
$\frac{D_T}{D_o}$	1.29	1.23	1.30	1.32
Area under ROC Curve	0.760	0.719	0.763	0.773

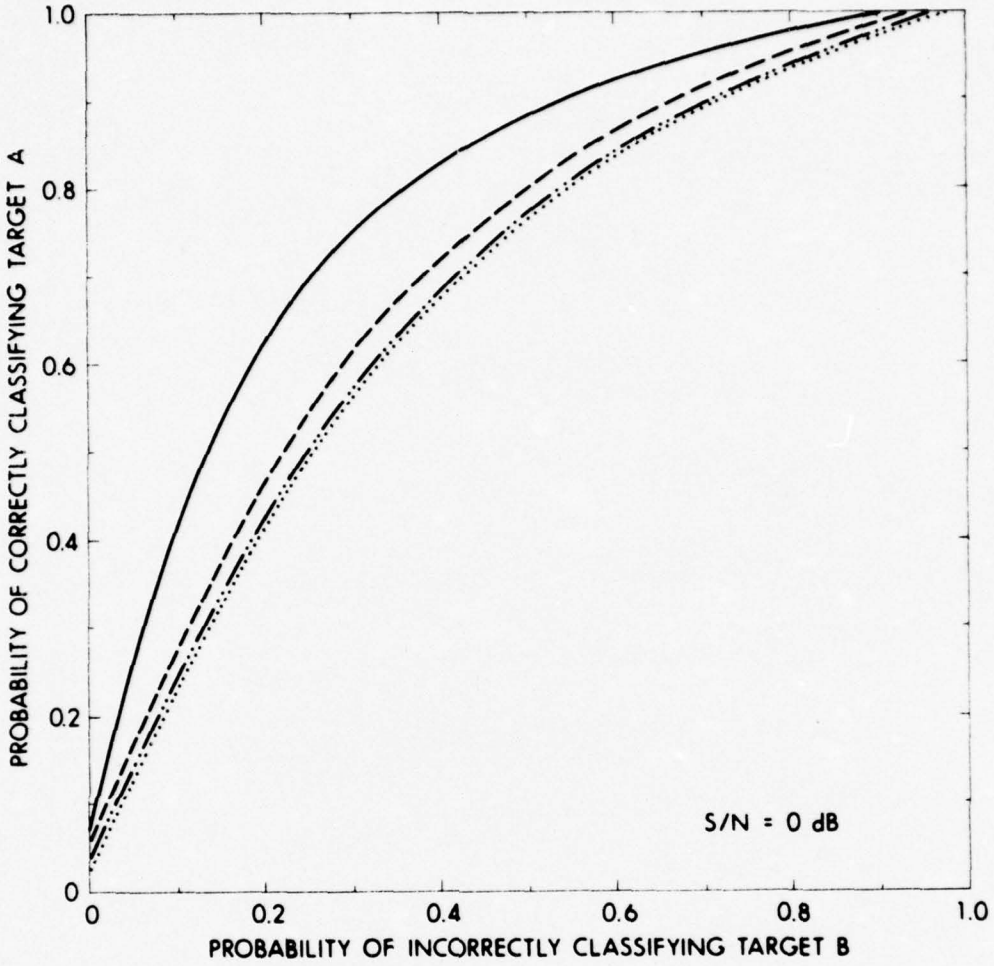

CODE FOR TARGET B

——— 7 in. diam SOLID ALUMINUM SPHERE
– – – – 5 in. diam SOLID ALUMINUM SPHERE
..... 5 in. diam STYROFOAM SPHERE
—··— 5 in. diam HOLLOW ALUMINUM SPHERE

FIGURE 4.8
RECEIVER OPERATING CHARACTERISTIC CURVES FOR SIMILAR TARGETS
TARGET A = 3 in. diam SOLID ALUMINUM SPHERE

TABLE 4.3

TARGET A = 3 IN. DIAM SOLID ALUMINUM SPHERE, S/N = 0 dB

Target B	7 in. diam Solid Aluminum Sphere	5 in. diam Solid Aluminum Sphere	5 in. diam Styrofoam Sphere	5 in. diam Hollow Aluminum Sphere
$\left\lvert\frac{r_A - r_B}{r_A}\right\rvert$	0.001	0.004	0.003	0.002
$\left\lvert\frac{d_A - d_B}{d_A}\right\rvert$	0.05	0.02	0.04	0.03
$\frac{D_T}{D_o}$	1.30	1.23	1.24	1.25
Area under ROC Curve	0.782	0.719	0.706	0.706

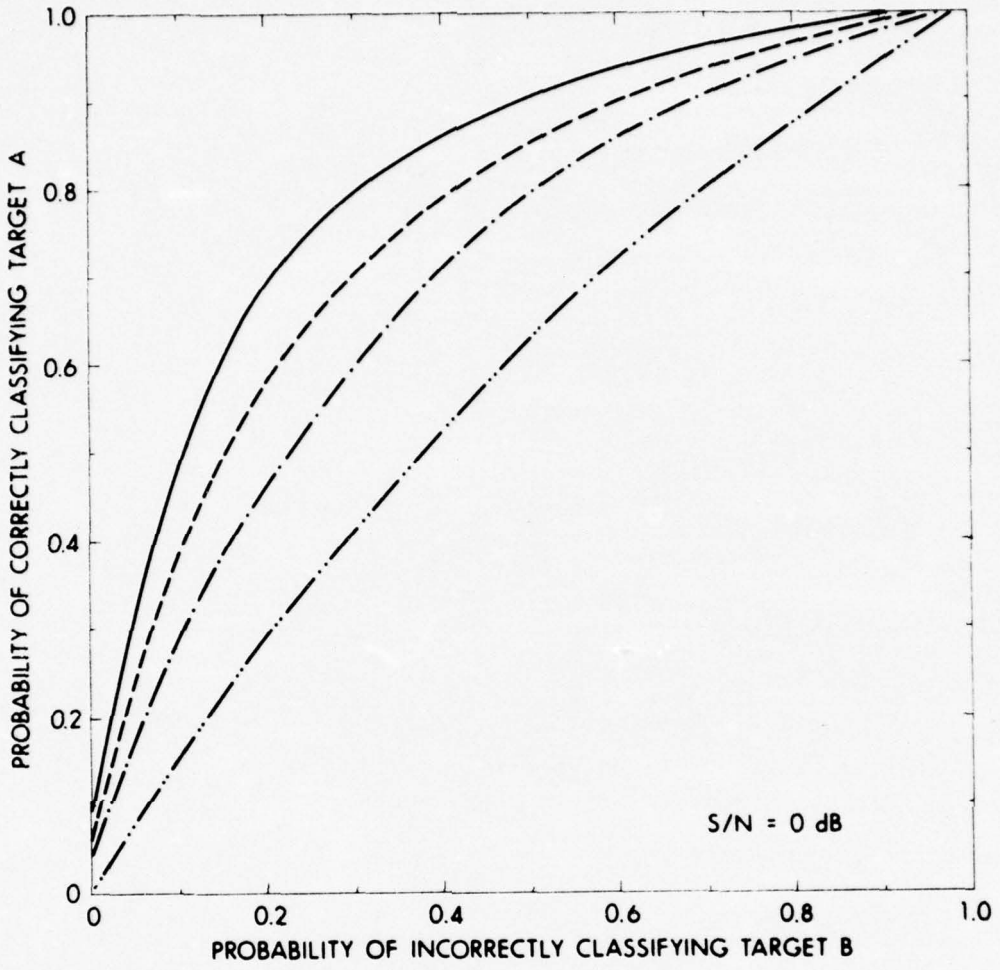

CODE FOR TARGET B

——— 7 in. diam SOLID ALUMINUM SPHERE
– – – – 5 in. diam SOLID ALUMINUM SPHERE
—·— 3 in. diam SOLID ALUMINUM SPHERE
—··— 5 in. diam HOLLOW ALUMINUM SPHERE

FIGURE 4.9
RECEIVER OPERATING CHARACTERISTIC CURVES FOR SIMILAR TARGETS
TARGET A = 5 in. diam STYROFOAM SPHERE

TABLE 4.4

TARGET A = 5 IN. DIAM STYROFOAM SPHERE, S/N = 0 dB

Target B	7 in. diam Solid Aluminum Sphere	5 in. diam Solid Aluminum Sphere	3 in. diam Solid Aluminum Sphere	5 in. diam Hollow Aluminum Sphere
$\left\|\frac{r_A - r_B}{r_A}\right\|$	0.001	0.004	0.003	0.002
$\left\|\frac{d_A - d_B}{d_A}\right\|$	0.02	0.04	0.04	0.004
$\frac{D_T}{D_o}$	1.43	1.30	1.24	1.08
Area under ROC Curve	0.816	0.763	0.706	0.581

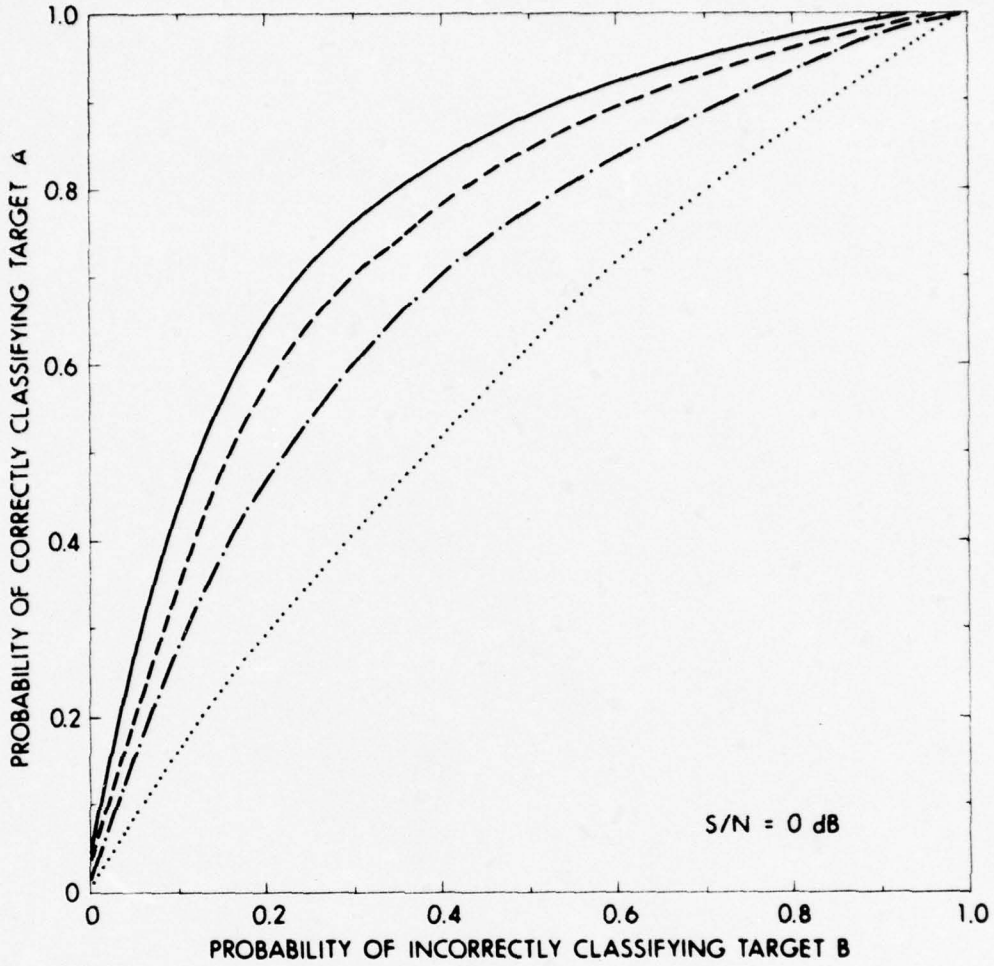

CODE FOR TARGET B

——— 7 in. diam SOLID ALUMINUM SPHERE
– – – – 5 in. diam SOLID ALUMINUM SPHERE
—·— 3 in. diam SOLID ALUMINUM SPHERE
····· 5 in. diam STYROFOAM SPHERE

FIGURE 4.10
RECEIVER OPERATING CHARACTERISTIC CURVES FOR SIMILAR TARGETS
TARGET A = 5 in. diam HOLLOW ALUMINUM SPHERE

TABLE 4.5

TARGET A = 5 IN. DIAM HOLLOW ALUMINUM SPHERE, S/N = 0 dB

Target B	7 in. diam Solid Aluminum Sphere	5 in. diam Solid Aluminum Sphere	3 in. diam Solid Aluminum Sphere	5 in. diam Styrofoam Sphere
$\left\lvert\frac{r_A - r_B}{r_A}\right\rvert$	0.004	0.003	0.002	0.002
$\left\lvert\frac{d_A - d_B}{d_B}\right\rvert$	0.07	0.05	0.03	0.004
$\frac{D_T}{D_o}$	1.38	1.32	1.25	1.08
Area under ROC Curve	0.789	0.773	0.706	0.581

In Tables 4.1 through 4.5, $|r_A - r_B|$ and $|d_A - d_B|$ are small compared to r_A and d_A respectively. Therefore, a threshold of 1 can be interpreted geometrically as a hyperplane which perpendicularly bisects the line that connects the centers of the two overlapping hyperspheres generated by the vectors $\vec{V}^A$ and $\vec{V}^B$.

The test functions computed from the vectors $\vec{V}^A$ and the test functions computed from the vectors $\vec{V}^B$ both have Gaussian distributions. The Gaussian distributions determine the shape of the ROC curves in Figs. 4.6 through 4.10.

All the computations described in this chapter and in later chapters were done on the CDC 3200 computer at the Applied Research Laboratories of The University of Texas at Austin. The flow diagram of the program used in the computation of the ROC curves is listed in Appendix B.

B. Target Classification for Various S/N Ratios

In this section, the performance of the likelihood ratio processor in classifying targets using the S/N ratio of the messages from the target classes as a variable parameter was measured. The transmission mode used was the sinusoidal pulse described in Chapter III. The rms of the amplitude of the noise to be added to the echoes from a target in order to lower the S/N ratio of the messages from the target class to a desired value was specified by Eq. (4.2). The knowledge of epoch was retained during the addition of the noise to the echoes so that the techniques discussed in Chapter IV, Section A, and the test function $\sum_{p,q=1}^{TW'_Q} a_{pq}^{W'_Q}\left[V_{1m}S_{1n}^B + V_{2m}S_{2n}^B - V_{1m}S_{1n}^A - V_{2m}S_{2n}^A\right]$ could be used in the classification of the targets.

The following three pairs of targets were used: the 7 in. diam and 5 in. diam solid aluminum spheres, the 5 in. diam and 3 in. diam solid aluminum spheres, and the 5 in. diam styrofoam sphere and the 5 in. diam hollow aluminum sphere (described in Chapter III). Four ROC curves for each target pair were computed, each curve corresponding to a different S/N ratio of the messages from each of the two target classes. The four values for the S/N ratio were 6 dB, 3.5 dB, 0 dB, and -6 dB. The ROC curves are plotted in Figs. 4.11 through 4.13.

The area under each ROC curve along with the values $\frac{|r_A - r_B|}{r_A}$, $\frac{|d_A - d_B|}{d_B}$, and $\frac{D_T}{D_o}$ are listed in Tables 4.6 through 4.8. $\frac{D_o}{D_T}$ multiplied by 100 gives the percent overlap of the hyperspheres generated by the vectors $\vec{V}^A$ and $\vec{V}^B$ in a $2TW'_Q$-dimensional vector space. For each target pair, the percent overlaps for the four S/N ratios are listed in Table 4.9.

C. Target Classification Using One Quadrature Component

In this section the ability of a likelihood ratio processor to classify messages of known epoch using only one quadrature component is measured. The two targets used were the 7 in. diam and 5 in. diam solid aluminum spheres. The waveform used in transmission was the sinusoidal pulse described in Chapter III. From Eq. (2.69), the equation for $\ell(\vec{V}_1)$ using only the in-phase components $\vec{S}_1^A$, $\vec{S}_1^B$, and $\vec{V}_1$ is

$$\ell(\vec{V}_1) = e^{-\frac{F^2}{W'^2_Q} \sum_{p,q=1}^{TW'_Q} a_{pq}^{W'_Q} \left[V_{1p} S_{1q}^A - V_{1p} S_{1q}^B - 1/2\, S_{1p}^A S_{1q}^A + 1/2\, S_{1p}^B S_{1q}^B \right]} . \quad (4.6)$$

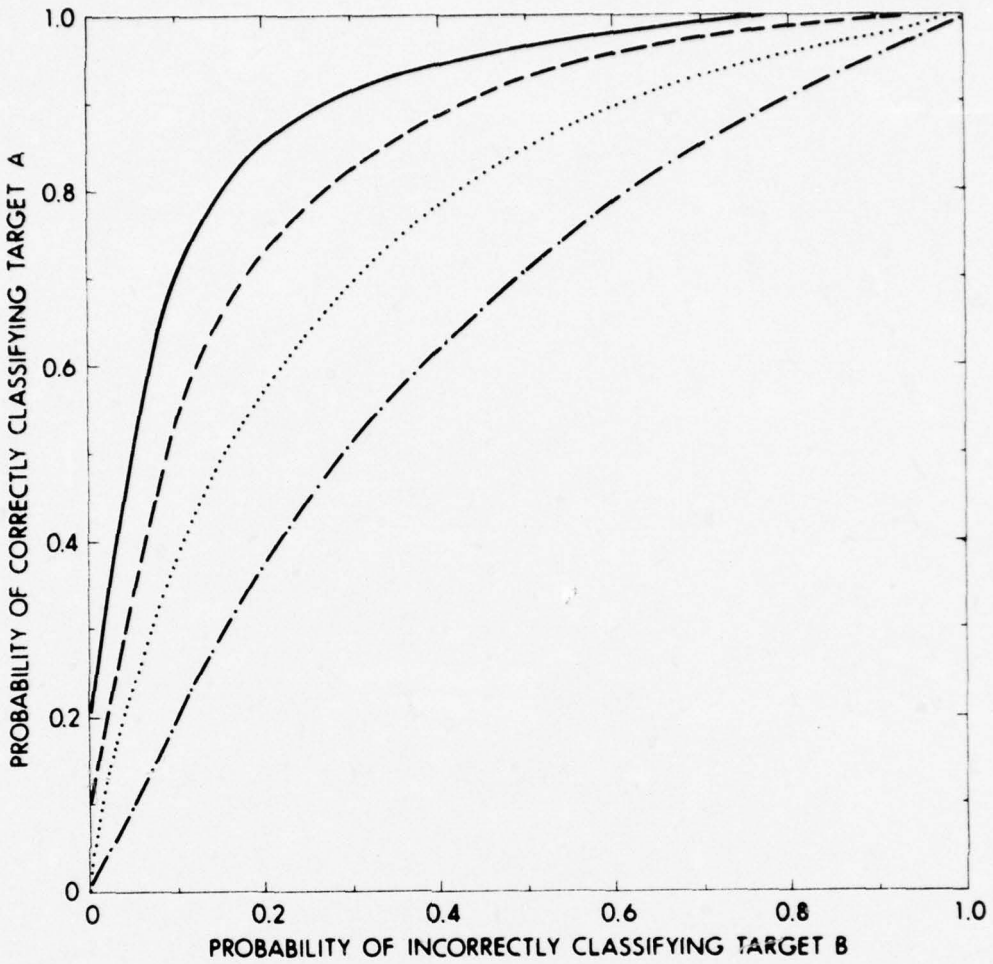

FIGURE 4.11
RECEIVER OPERATING CHARACTERISTIC CURVES FOR VARIOUS S/N RATIOS
TARGET A = 7 in. diam SOLID ALUMINUM SPHERE
TARGET B = 5 in. diam SOLID ALUMINUM SPHERE

TABLE 4.6

TARGET A = 7 IN. DIAM SOLID ALUMINUM SPHERE

TARGET B = 5 IN. DIAM SOLID ALUMINUM SPHERE

	S/N = 6 dB	S/N = 3.5 dB	S/N = 0 dB	S/N = -6 dB
$\left\|\frac{r_A - r_B}{r_A}\right\|$	0.03	0.02	0.009	0.004
$\left\|\frac{d_A - d_B}{d_A}\right\|$	0.09	0.08	0.06	0.04
$\frac{D_T}{D_o}$	1.65	1.46	1.29	1.13
Area under ROC Curve	0.899	0.844	0.760	0.644

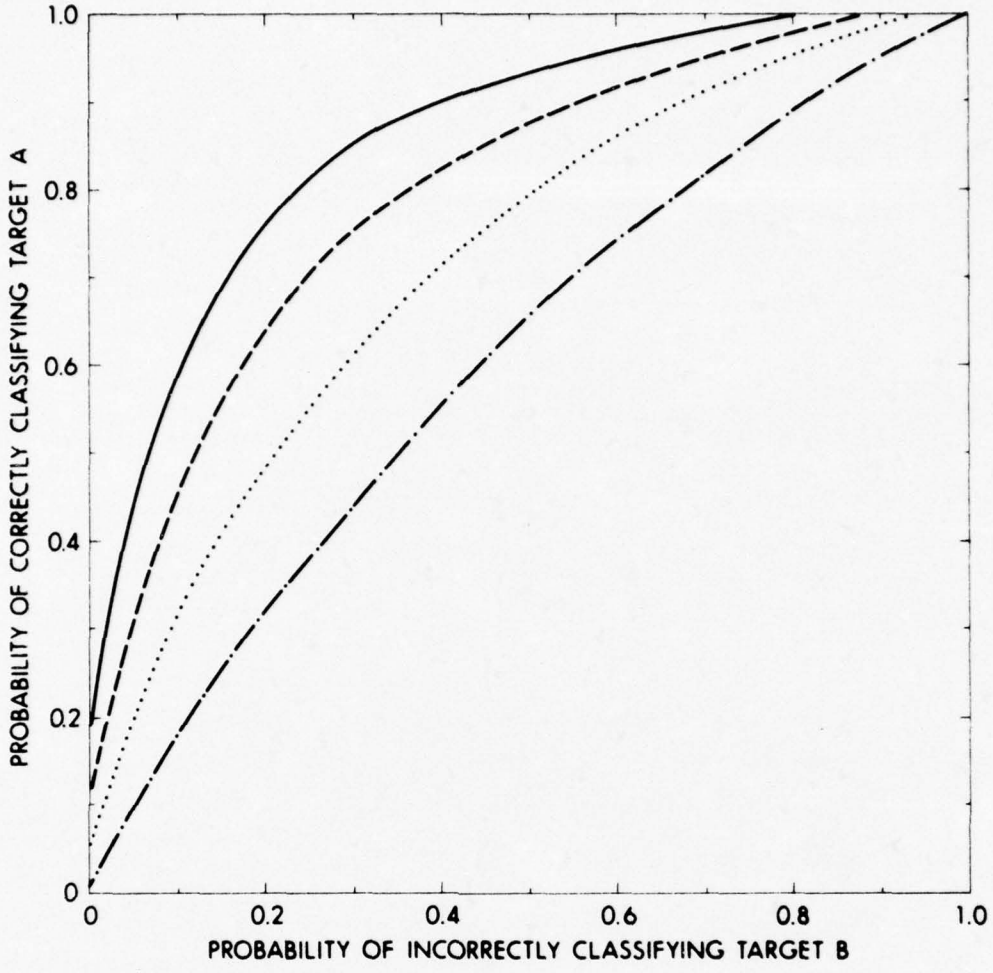

FIGURE 4.12
RECEIVER OPERATING CHARACTERISTIC CURVES FOR VARIOUS S/N RATIOS
TARGET A = 5 in. diam SOLID ALUMINUM SPHERE
TARGET B = 3 in. diam SOLID ALUMINUM SPHERE

TABLE 4.7

TARGET A = 5 IN. DIAM SOLID ALUMINUM SPHERE

TARGET B = 3 IN. DIAM SOLID ALUMINUM SPHERE

	S/N = 6 dB	S/N = 3.5 dB	S/N = 0 dB	S/N = -6 dB
$\left\|\frac{r_A - r_B}{r_A}\right\|$	0.02	0.01	0.008	0.003
$\left\|\frac{d_A - d_B}{d_A}\right\|$	0.007	0.02	0.03	0.03
$\frac{D_T}{D_o}$	1.42	1.31	1.20	1.09
Area under ROC Curve	0.872	0.809	0.719	0.613

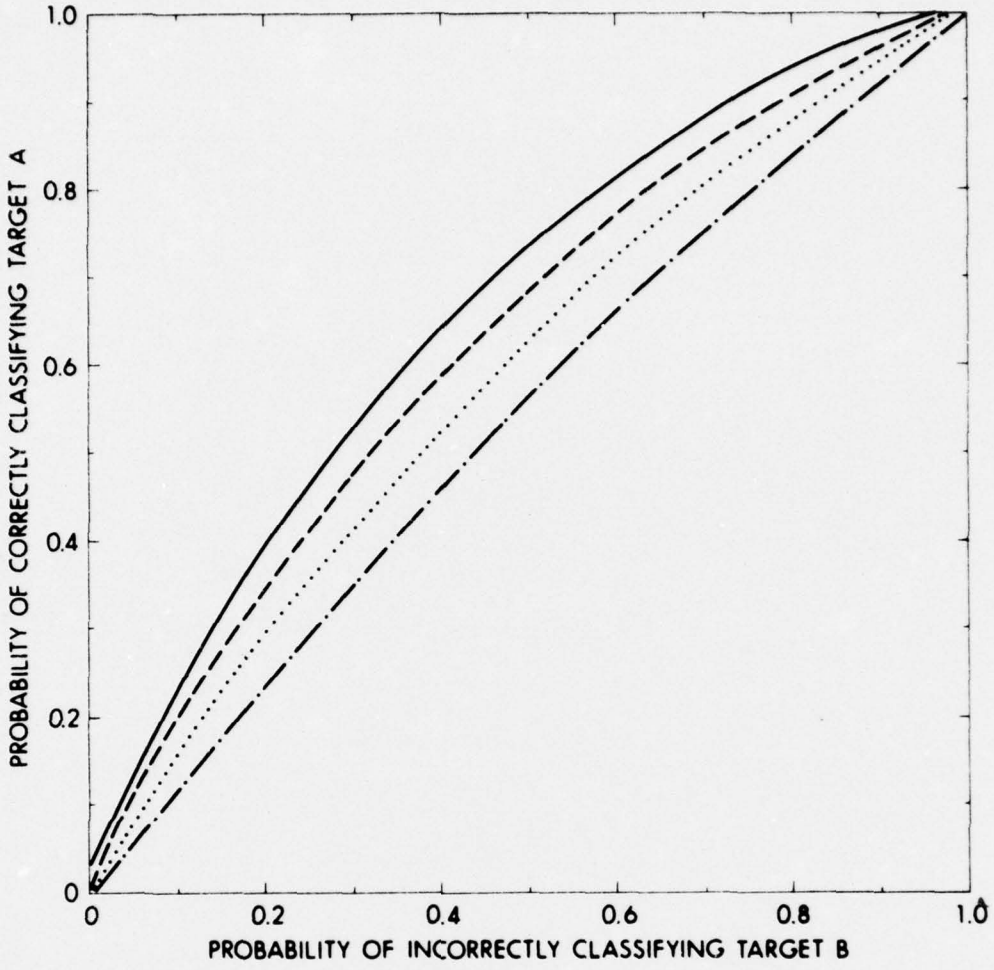

FIGURE 4.13
RECEIVER OPERATING CHARACTERISTIC CURVES FOR VARIOUS S/N RATIOS
TARGET A = 5 in. diam STYROFOAM SPHERE
TARGET B = 5 in. diam HOLLOW ALUMINUM SPHERE

TABLE 4.8

TARGET A = 5 IN. DIAM STYROFOAM SPHERE

TARGET B = 5 IN. DIAM HOLLOW ALUMINUM SPHERE

	S/N = 6 dB	S/N = 3.5 dB	S/N = 0 dB	S/N = -6 dB
$\left\|\frac{r_A - r_B}{r_A}\right\|$	0.007	0.003	0.002	0.002
$\left\|\frac{d_A - d_B}{d_A}\right\|$	0.007	0.002	0.004	0.01
$\frac{D_T}{D_o}$	1.17	1.12	1.08	1.04
Area under ROC Curve	0.651	0.620	0.581	0.535

TABLE 4.9

PERCENT OVERLAP OF HYPERSPHERES GENERATED BY $\vec{V}^A$ AND $\vec{V}^B$ FOR FOUR S/N RATIOS

	7 in. diam Solid Aluminum and 5 in. diam Solid Aluminum Spheres	5 in. diam Solid Aluminum and 3 in. diam Solid Aluminum Spheres	5 in. diam Styrofoam and 5 in. diam Hollow Aluminum Spheres
S/N=6 dB	61%	70%	86%
S/N=3.5 dB	69%	77%	89%
S/N=0 dB	78%	84%	92%
S/N=-6 dB	88%	91%	96%

The equation for $\ell(\vec{V}_2)$ using only the out-of-phase components $\vec{S}_2^A$, $\vec{S}_2^B$, and $\vec{V}_2$ is

$$\ell(\vec{V}_2) = e^{-\frac{F^2}{W_Q'^2} \sum_{p,q=1}^{TW_Q'} a_{pq}^{W_Q'} \left[V_{2p} S_{2q}^A - V_{2p} S_{2q}^B - 1/2\, S_{2p}^A S_{2q}^A + 1/2\, S_{2p}^B S_{2q}^B \right]} \quad . \quad (4.7)$$

From Eq. (2.69), Eq. (4.6), and Eq. (4.7), it follows that

$$\ell(\vec{V}) = \ell(\vec{V}_1)\ \ell(\vec{V}_2) \quad , \text{ or} \quad (4.8)$$

$$\log\left(\ell(\vec{V})\right) = \log\left(\ell(\vec{V}_1)\right) + \log\left(\ell(\vec{V}_2)\right) \quad . \quad (4.9)$$

If $\log\left(\ell(\vec{V}_1)\right)$ and $\log\left(\ell(\vec{V}_2)\right)$ are of opposite sign, the sign of $\log\left(\ell(\vec{V})\right)$ will be determined by the larger of the two numbers, $\left|\log\left(\ell(\vec{V}_1)\right)\right|$, or $\left|\log\left(\ell(\vec{V}_2)\right)\right|$.

In Fig. 4.14 the in-phase and the out-of-phase components of an echo from a 7 in. diam solid aluminum sphere and the in-phase and the out-of-phase components of an echo from a 5 in. diam solid aluminum sphere are plotted. In Fig. 4.14 the S/N ratio of the echo from the 7 in. diam solid aluminum sphere was 39.8 dB, and the S/N ratio of the echo from the 5 in. diam solid aluminum sphere was 38.8 dB. In Fig. 4.15 the in-phase and the out-of-phase components of a message from each of the two target classes are plotted. The S/N ratio of the messages was 6 dB. The ROC curves in Fig. 4.16 and in Fig. 4.17 were plotted using

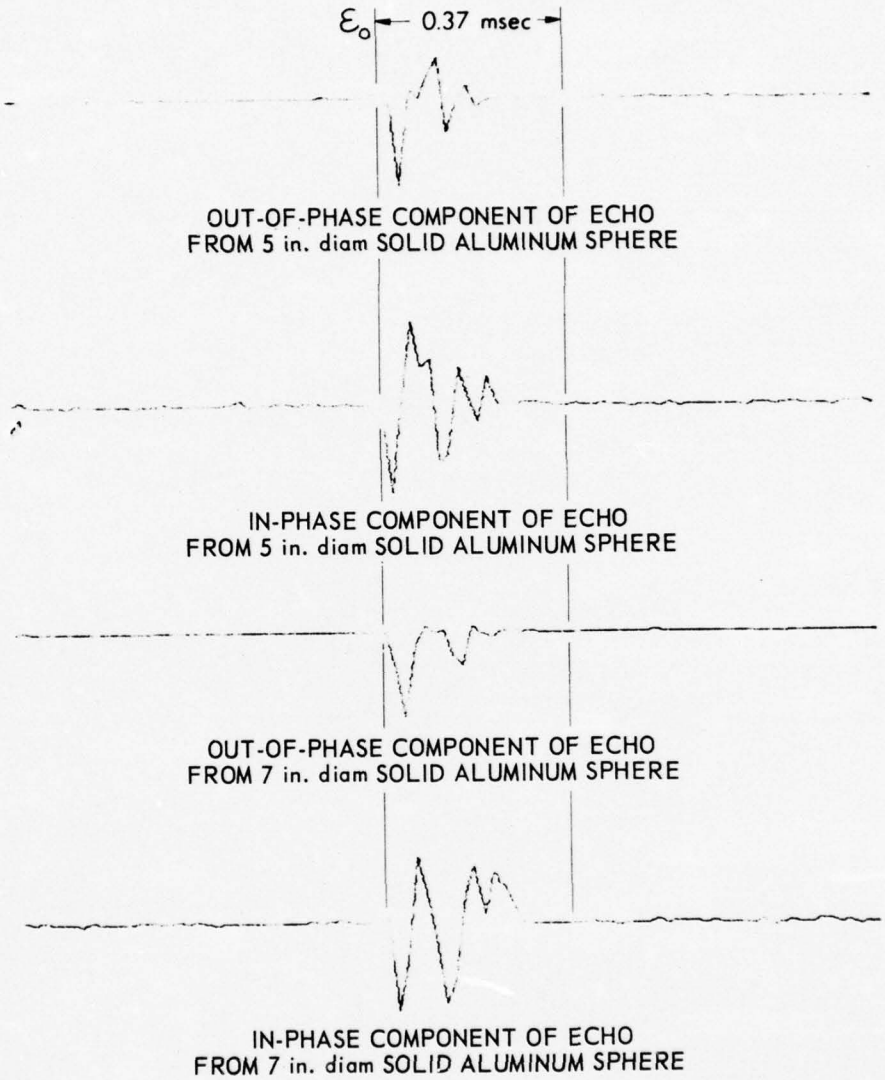

FIGURE 4.14
QUADRATURE COMPONENTS FOR SINUSOIDAL PULSE
PULSE LENGTH = 0.37 msec EPOCH = $\mathcal{E}_o$ Δt = 8/300 msec
f_o = 0 kHz W = 20 kHz PEAK |AMPLITUDE| = 0.5 in.

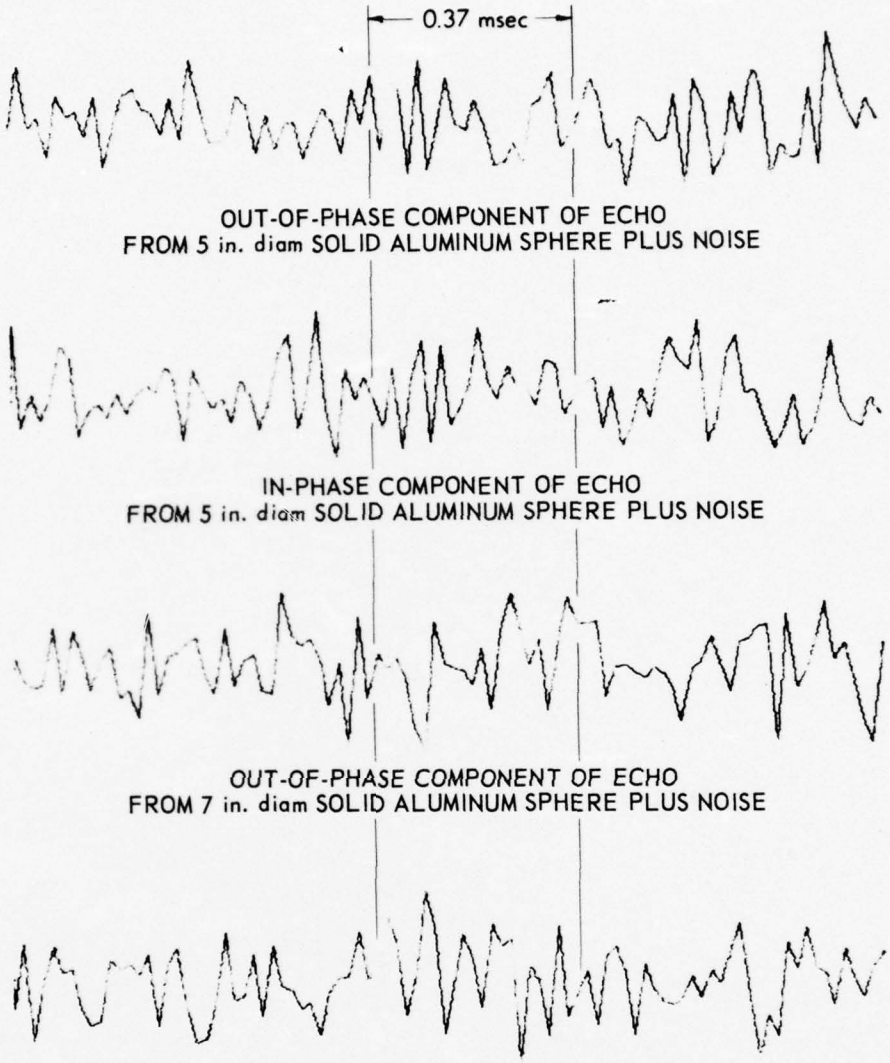

FIGURE 4.15

QUADRATURE COMPONENTS OF MESSAGES FOR A SINUSOIDAL PULSE

POSITION OF 0.37 msec TIME INTERVAL INDICATES LOCATION OF EMBEDDED COMPONENT
PULSE LENGTH = 0.37 msec Δt = 8/300 msec f_o = 0 kHz
W = 20 kHz S/N = 6 dB PEAK |AMPLITUDE| = 0.5 in.

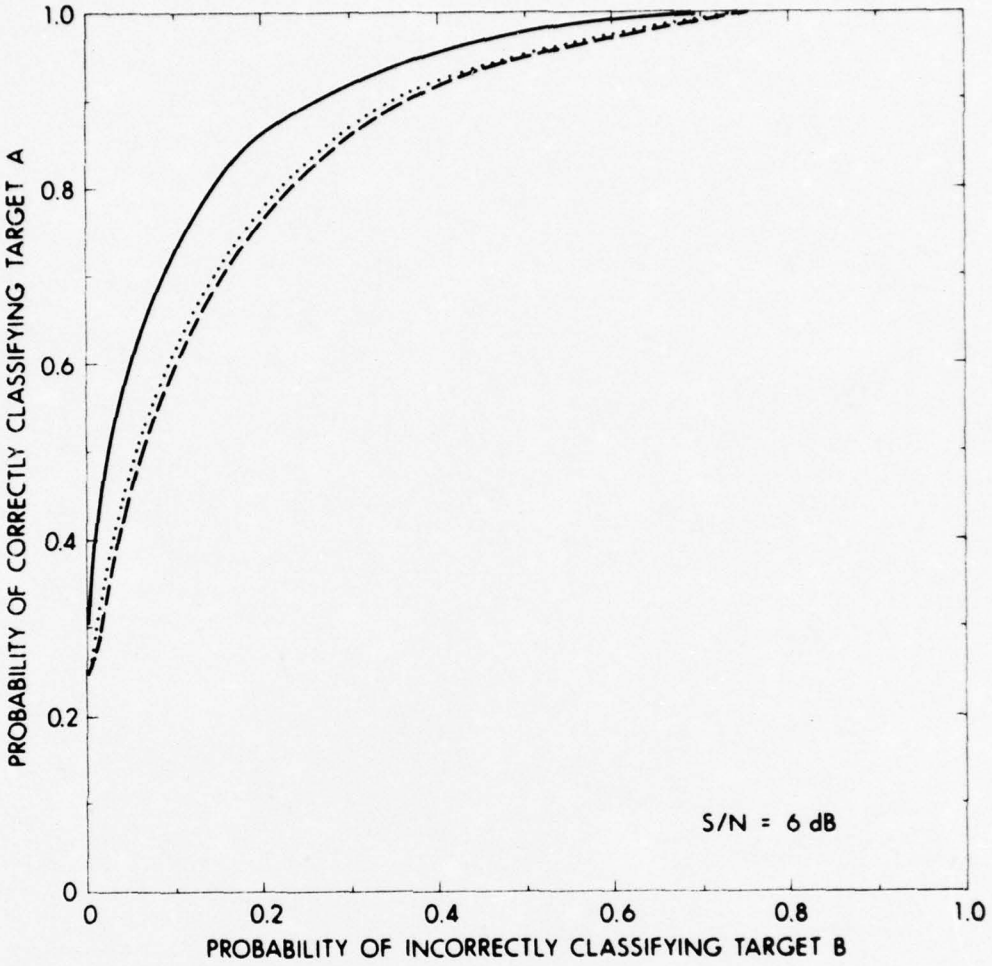

CODE FOR QUADRATURE COMPONENTS:

——— IN-PHASE PLUS OUT-OF-PHASE COMPONENTS
..... IN-PHASE COMPONENT
— — — — OUT-OF-PHASE COMPONENT

FIGURE 4.16
RECEIVER OPERATING CHARACTERISTIC CURVES
COMPUTED FROM ONE QUADRATURE COMPONENT
AND BOTH QUADRATURE COMPONENTS
TARGET A = 7 in. diam SOLID ALUMINUM SPHERE
TARGET B = 5 in. diam SOLID ALUMINUM SPHERE

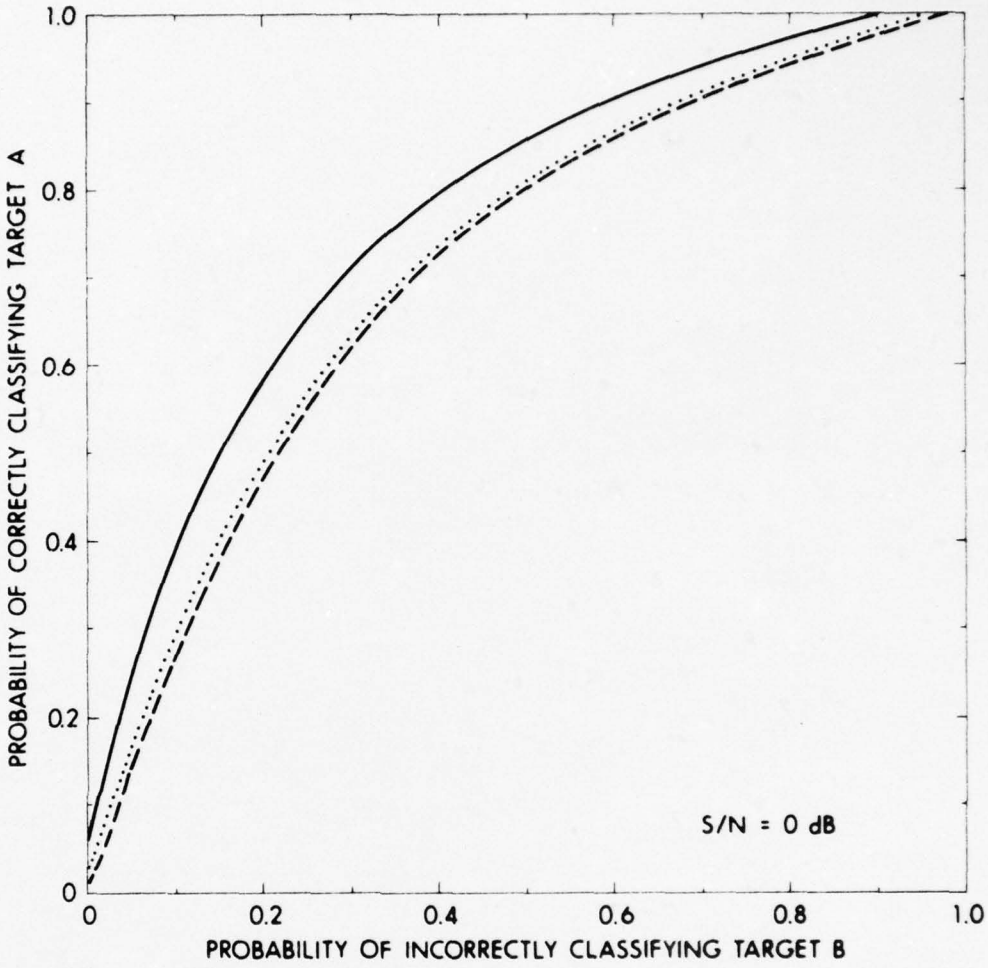

CODE FOR QUADRATURE COMPONENTS:

——— IN-PHASE PLUS OUT-OF-PHASE COMPONENTS
..... IN-PHASE COMPONENT
– – – – OUT-OF-PHASE COMPONENT

FIGURE 4.17
RECEIVER OPERATING CHARACTERISTIC CURVES
COMPUTED FROM ONE QUADRATURE COMPONENT
AND BOTH QUADRATURE COMPONENTS
TARGET A = 7 in. diam SOLID ALUMINUM SPHERE
TARGET B = 5 in. diam SOLID ALUMINUM SPHERE

AD-A032 018 TEXAS UNIV AT AUSTIN APPLIED RESEARCH LABS F/G 17/1
TARGET CLASSIFICATION USING LIKELIHOOD RATIOS AND QUADRATURE CO--ETC(U)
JUN 69 J F HOFFMAN N00024-69-C-1129
UNCLASSIFIED ARL-TM-69-11 NL

2 OF 2
AD
A032 018

END

DATE
FILMED
1-77

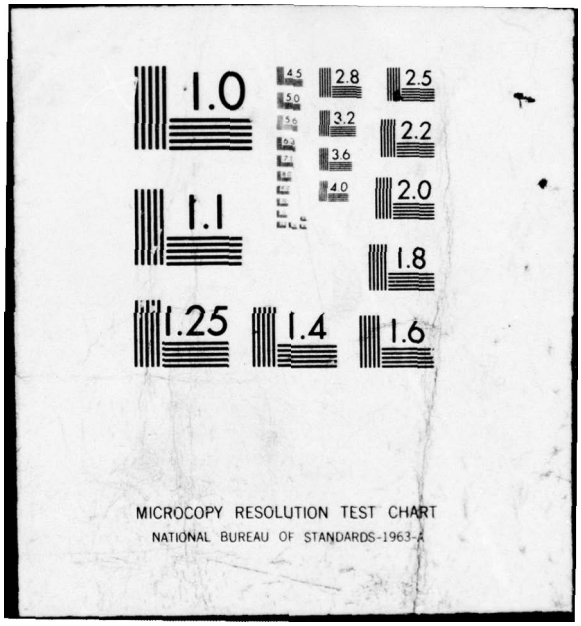
1.0
1.1
1.25
1.4
1.6
1.8
2.0
2.2
2.5
2.8
3.2
3.6
4.0
4.5
5.0
5.6
MICROCOPY RESOLUTION TEST CHART
NATIONAL BUREAU OF STANDARDS-1963-A

the test functions

$$\sum_{p,q=1}^{TW'_Q} a_{pq}^{W'_Q}\left[V_{1p}S_{1q}^{B} - V_{1p}S_{1q}^{A}\right] \quad ,$$

$$\sum_{p,q=1}^{TW'_Q} a_{pq}^{W'_Q}\left[V_{2p}S_{2q}^{B} - V_{2p}S_{2q}^{A}\right] \quad , \text{ and}$$

$$\sum_{p,q=1}^{TW'_Q} a_{pq}^{W'_Q}\left[V_{1p}S_{1q}^{B} + V_{2p}S_{2q}^{B} - V_{1p}S_{1q}^{A} - V_{2p}S_{2q}^{A}\right]$$

respectively and the techniques discussed in Chapter IV, Section A. The test functions are monotonically increasing functions of $\ell(\vec{V}_1)$, $\ell(\vec{V}_2)$, and $\ell(\vec{V})$ respectively. The average S/N ratio of the messages from each target class in Fig. 4.16 was 6 dB, and the average S/N ratio of the messages from each target class in Fig. 4.17 was 0 dB. The area under each ROC curve in Fig. 4.16 and Fig. 4.17 is listed in Table 4.10.

From Fig. 4.16 and Fig. 4.17, the test function that used the in-phase components gave better performance than the test function that used the out-of-phase components. No general statement can be made from this result since it is highly dependent on the transmission mode, epoch, and the target pair.

The best performance in classification was from the test function that used both quadrature components. This result was predicted in Eq. (4.9).

TABLE 4.10

AREA UNDER THE ROC CURVES IN FIG. 4.16 and FIG. 4.17

	In-phase and Out-of-phase Components	In-phase Components	Out-of-phase Components
S/N=6 dB	0.907	0.865	0.862
S/N=0 dB	0.754	0.718	0.695

D. Target Classification Using a Generalized Likelihood Ratio Processor

In this section the performance of the generalized likelihood ratio processor (Eq. (2.67)) is compared with the performance of the likelihood ratio processor (Eq. (2.69)) in the classification of targets. The two targets used were the 7 in. diam and 5 in. diam solid aluminum spheres. The average S/N ratio of the messages from each target class was 6 dB. The starting phase of the messages was varied in intervals of $\pi/2$ radians over a full cycle of the carrier. The number of values of epoch for each message was thereby increased from 1 to 4. The test function $\left(\lambda^{B^2} + \nu^{B^2}\right)^{1/2} - \left(\lambda^{A^2} + \nu^{A^2}\right)^{1/2}$, which is a monotonically increasing function of $\Lambda(\vec{V})$ described by Eq. (2.67) where $\lambda^B = \frac{F^2}{2W_Q'^2} \sum_{p,q=1}^{TW_Q'} a_{pq}^{W_Q'} \left[V_{1p} S_{1q}^B + V_{2p} S_{2q}^B \right]$ etc., was calculated for each value of epoch. Next, an average value for the test functions was computed for each message. In Fig. 4.18 an ROC curve was plotted using the average values for the test functions. A second ROC curve was computed for the same target pair and was plotted on the same graph. The second ROC curve was computed from messages of known epoch using the test function $\sum_{p,q=1}^{TW_Q'} a_{pq}^{W_Q'} \left[V_{1n} S_{1n}^B + V_{2n} S_{2n}^B - V_{1n} S_{1n}^A - V_{2n} S_{2n}^A \right]$, which is a monotonically increasing function of $\ell(\vec{V})$ described by Eq. (2.69).

The degradation in performance due to the loss of epoch can be estimated from a comparison of the two curves. For the likelihood ratio processor, the probability of correctly classifying target A

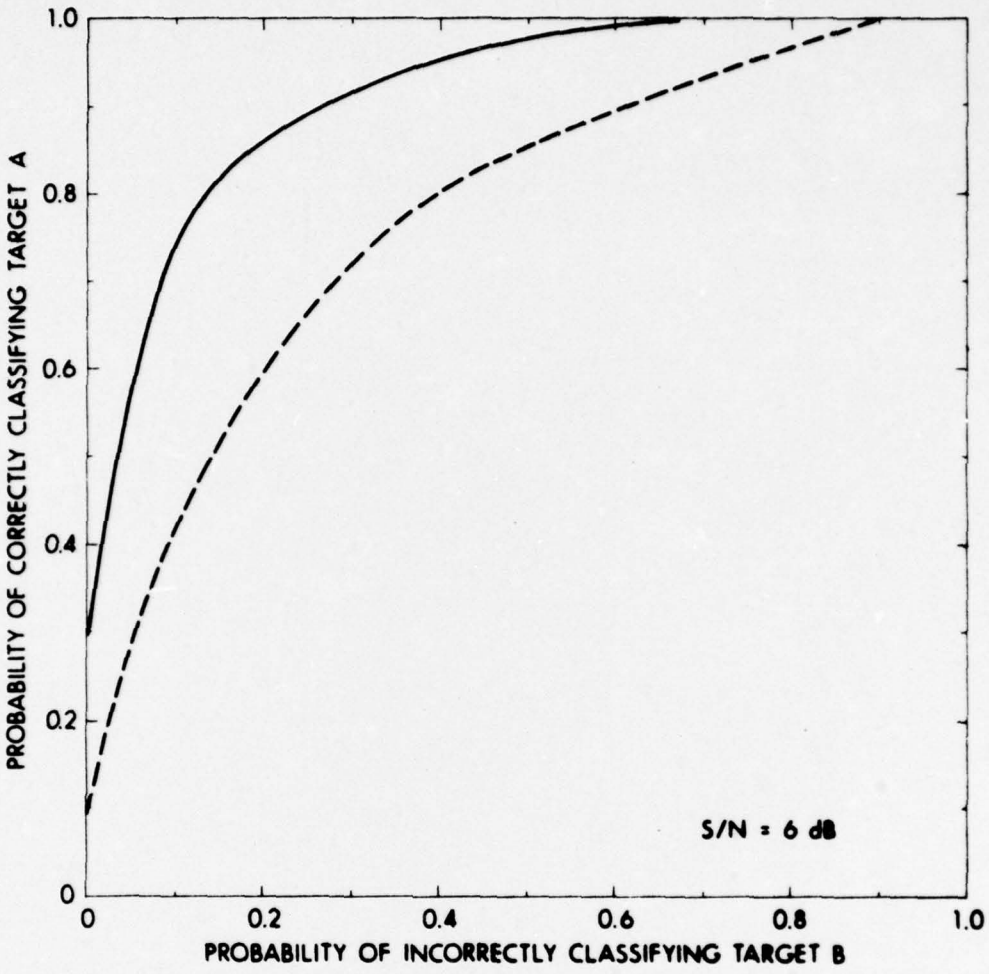

FIGURE 4.18
RECEIVER OPERATING CHARACTERISTIC CURVES FOR KNOWN EPOCH AND AVERAGE OF VARIED EPOCH
TARGET A = 7 in. diam SOLID ALUMINUM SPHERE
TARGET B = 5 in. diam SOLID ALUMINUM SPHERE

was 86% when the probability of incorrectly classifying target B was 20%, and for the generalized likelihood ratio processor, the probability of correctly classifying target A was 60% when the probability of incorrectly classifying target B was 20%. From Fig. 4.11 the degradation in the performance of classification because of loss of epoch of the messages is approximately equal to the degradation in the performance due to a 6 dB decrease in the S/N ratio of the messages.

CHAPTER V

TARGET CLASSIFICATION USING LINEAR FM TRANSMISSION

A. Classification of Similar Targets

1. Epoch

The investigation concerning the classification of targets using a linear FM transmission is presented in this chapter. A plot of the linear FM transmission is shown in Fig. 3.2. The echoes from the linear FM transmission were passed through a 5 msec gate. A plot of a gated echo from each of the 5 targets, the 7 in. diam, the 5 in. diam, and the 3 in. diam solid aluminum spheres, the 5 in. diam styrofoam sphere, and the 5 in. diam hollow aluminum sphere, is shown in Fig. 3.4.

The epoch for a gated echo was determined by the time, τ_o, at which $Z^F(\tau)$ had a maximum value, where $Z^F(\tau)$ is the correlation between a gated echo $\vec{V}$ and a transmitted signal $\vec{S}^T$. The epoch of an echo was defined to be ϵ_o, where $\epsilon_o = \tau_o$. The epoch for an echo from each target is indicated in Fig. 3.4.

The correlation between a gated echo $\vec{V}$ and a transmitted waveform $\vec{S}^T$ for $N_L + 1$ number of lags is described as follows:

$$Z^F(\tau) = \frac{1}{N_S} \sum_{\sigma=1}^{N_S} S_\sigma^T V_{\sigma+\tau} \quad , \tag{5.1}$$

and

$$\tau = 0, 1, 2, \ldots N_L, \; N_L \leq N_V - N_S \quad ,$$

where

N_S is the number of samples of $\vec{S}^T$,

N_V is the number of samples of $\vec{V}$,

$$S^T_\sigma = S^T\left(\frac{\sigma}{F}\right) \quad ,$$

$$V_{\sigma+\tau} = V\left(\frac{\sigma+\tau}{F}\right) \quad , \text{ and}$$

F is the sampling rate; i.e., 300 kHz.

The minimum number of lags which were sufficient to determine epoch was 160. The same transmitted waveform $\vec{S}^T$ was used in the determination of epoch for each echo. After the epoch for an echo was established, the echo was scaled so that its peak amplitude was equal to 1400. As stated in Chapter IV, the echoes from the sinusoidal pulse were also scaled so that the peak amplitude of each echo was 1400.

For the sinusoidal pulse and the elastic spheres, the portion of the echoes that was the result of reradiation of energy was approximately 0.2 msec in length. Since the pulse length of the linear FM transmission was 3 msec, the pulse length of the echoes from the linear FM transmission was estimated as 3.2 msec.

The energy contained in each echo from a target for the linear FM transmission was reliably measured by the peak amplitude of each echo. Table 5.1 was computed to show that the $\frac{\text{peak amplitude}}{\text{rms of amplitude}}$ of an echo was approximately constant from echo to echo for each

target. In Table 5.1 the following three quantities for each target are tabulated:

$$(1)\quad M = \frac{1}{N_E}\sum_{j=1}^{N_E}\left(\frac{P_A}{<{}_jV^2>^{1/2}}\right) \quad , \tag{5.2}$$

$$(2)\quad D = \left[\frac{1}{N_E}\sum_{j=1}^{N_E}\left(\frac{P_A}{<{}_jV^2>^{1/2}} - M\right)^2\right]^{1/2} \quad , \text{ and} \tag{5.3}$$

$$(3)\quad \frac{D}{M} \times 100 \quad ,$$

where

$P_A = 1400$ = peak amplitude of each echo from the target,

$<{}_jV^2>^{1/2}$ = rms of the amplitude of j^{th} echo from the target, and

N_E = number of echoes from the target.

The quantity D/M is small for each target.

2. Addition of Gaussian Noise to Echoes

Gaussian noise from the random noise generator was added to the echoes from each target in order to make the simulation of target classification more realistic and to increase the number of messages (echo-noise combinations) from each target class. The bandwidth of the Gaussian noise was 20 kHz with a center frequency of 65 kHz. The rms of the amplitude of the noise from the random noise generator was specified as follows:

$$<N^2>^{1/2} = \frac{P_A}{R_{SN}} \quad , \tag{5.4}$$

TABLE 5.1

M, D, AND $\frac{D}{M} \times 100$ FOR EACH TARGET

	7 in. diam Solid Aluminum Sphere	5 in. diam Solid Aluminum Sphere	3 in. diam Solid Aluminum Sphere	5 in. diam Styrofoam Sphere	5 in. diam Hollow Aluminum Sphere
M	2.16	2.03	2.34	2.05	2.03
D	0.13	0.08	0.17	0.16	0.12
$\frac{D}{M} \times 100$	6.0%	3.9%	7.3%	7.8%	5.9%

where

$< N^2 >^{1/2}$ = rms of the amplitude of the noise from the random noise generator,

$P_A = 1400$ = peak amplitude of each echo from the target, and

R_{SN} = desired S/N ratio of the echoes from the target.

The rms of the amplitude of the ambient noise and of the reverberation present in each echo was considered to be negligible compared to the peak amplitude of each echo. In Fig. 5.1 a message with a S/N ratio of -6 dB from each target class is plotted. In Fig. 5.1 the messages of pulse length 3.2 msec are located between the two vertical lines. A comparison of the plots in Fig. 3.4 and Fig. 5.1 shows that it is very difficult to classify visually the echoes that are embedded in Gaussian noise.

For the linear FM transmission the number of echoes available from each target varied from 16 to 18. After the addition of noise to the echoes, the number of messages from each target class varied from 128 to 144. No noise signal was duplicated throughout the procedure involving the addition of noise to the echoes.

In obtaining the quadrature components of the messages, the center frequency of the messages was redefined as $f_o' = 75$ kHz, and the bandwidth was redefined as $W' = 40$ kHz. A sampling parameter of $K = 1$ was used, which resulted in a sampling rate W_Q' of 75 kHz.

The likelihood ratio calculation described by Eq. (2.69) was simplified by approximating the matrix $\left(a_{ij}^{W_Q'}\right)$ as a diagonal matrix;

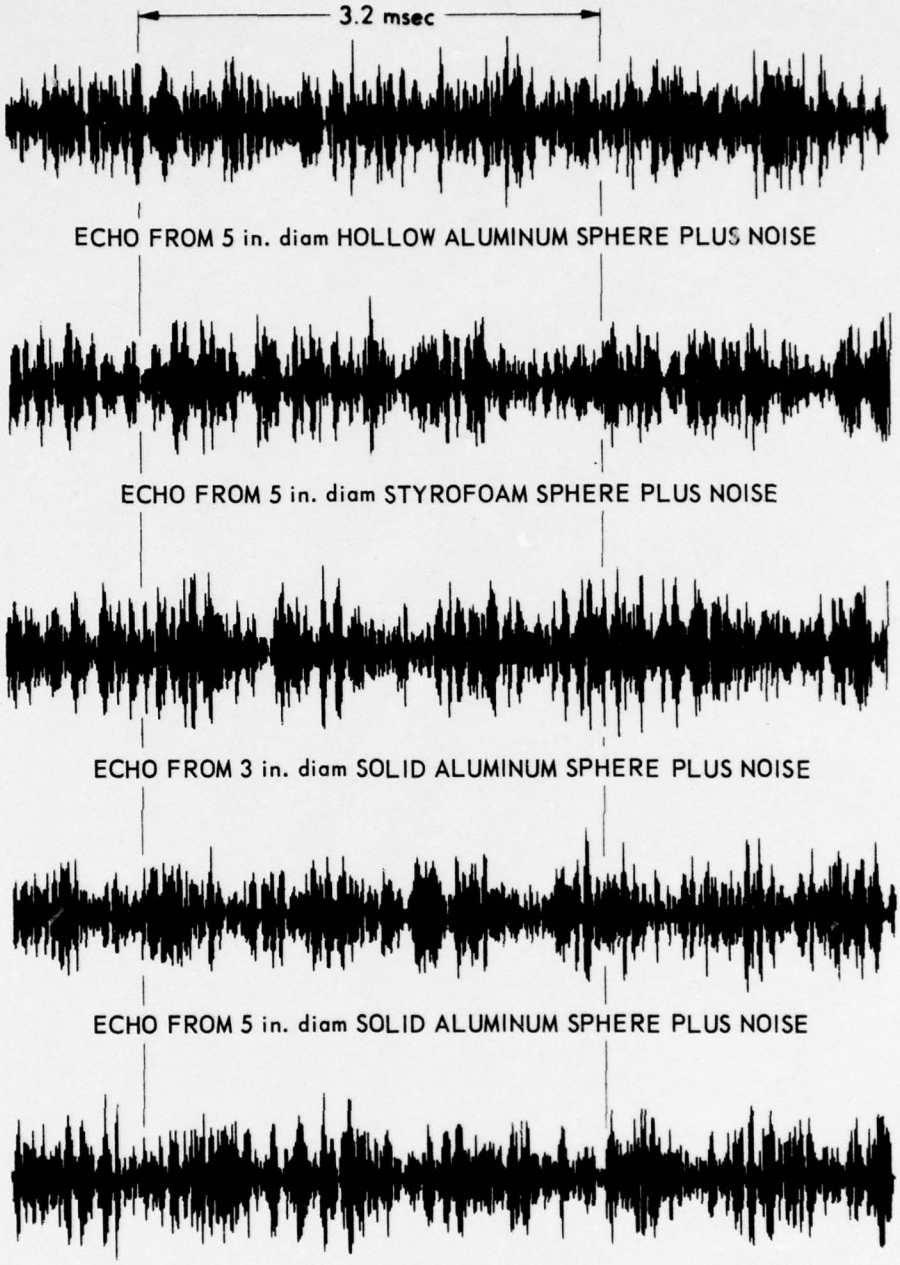

FIGURE 5.1

MESSAGES FOR LINEAR FM TRANSMISSION

POSITION OF 3.2 msec TIME INTERVAL INDICATES LOCATION OF EMBEDDED ECHO

PULSE LENGTH = 3.2 msec Δt = 1/300 msec f_o = 65 kHz

W = 20 kHz S/N = -6 dB PEAK |AMPLITUDE| = 0.5 in.

namely,

$$\left(a_{ij}^{W'_Q}\right) \approx \left(\frac{1}{< N^2 >}\,\delta_{ij}\right) \quad , \tag{5.5}$$

where

$$a_{ij}^{W'_Q} = a^{W'_Q}\left(\frac{i-j}{W'_Q}\right) \quad .$$

The approximation $\left(a_{ij}^{W'_Q}\right) = \left(\frac{1}{< N^2 >}\,\delta_{ij}\right)$ was necessary since the digital processing involving a matrix of the size TW'_Q by TW'_Q, where TW'_Q is 240, was not feasible. Justification for the use of a diagonal matrix was that an ROC curve computed using a diagonal matrix and messages for a sinusoidal pulse did not differ measurably from an ROC curve computed using a nondiagonal matrix and the same messages. The approximation $\left(a_{ij}^{W'_Q}\right) = \left(\frac{1}{< N^2 >}\,\delta_{ij}\right)$ was not needed in Chapter IV, since the size of the matrix required for the digital processing of the messages for the sinusoidal pulse did not present any computational difficulties.

Upon the substitution of Eq. (5.5) into Eq. (2.69), the likelihood ratio used in the classification of the messages for a linear FM transmission is described as follows:

$$\ell(\vec{V}) = e^{-\frac{F}{2W'_Q}\sum_{p=1}^{TW'_Q}\left(\frac{1}{< N^2 >}\right)\left[V_{1p}S_{1p}^{A} + V_{2p}S_{2p}^{A} - V_{1p}S_{1p}^{B} - V_{2p}S_{2p}^{B} - S_{1p}^{A}S_{1p}^{A} - S_{2p}^{A}S_{2p}^{A} + S_{1p}^{B}S_{1p}^{B} + S_{2p}^{B}S_{2p}^{B}\right]} \quad , \tag{5.6}$$

where

$$W'_Q = \frac{f'_o}{K} \ , \ S^A_{1p} = S^A_1\left(\frac{p}{W'_Q}\right) \text{, etc., and}$$

where TW'_Q is the number of samples of each quadrature component.

3. ROC Curves

Four ROC curves are plotted in Fig. 5.2 for the linear FM transmission. These curves were computed using the test function

$$\frac{1}{< N^2 >} \sum_{p=1}^{TW'_Q} \left[V_{1p} S^B_{1p} + V_{2p} S^B_{2p} - V_{1p} S^A_{1p} - V_{2p} S^A_{2p} \right] \quad .$$

This test function is a monotonically increasing function of $\ell(\vec{V})$, where $\ell(\vec{V})$ is described by Eq. (5.6). In Fig. 5.2, target A for each of the 4 ROC curves was the 7 in. diam solid aluminum sphere, and the average S/N ratio of the messages from each target class was -6 dB.

A comparison of the ROC curves in Fig. 5.2 with those in Fig. 4.6, which were computed for the sinusoidal pulse, reveals that the ROC curves for the different spheres, B, are in the same order. But each curve in Fig. 5.2 indicates a better performance in classification than the corresponding curve in Fig. 4.6, even though the average S/N ratio of the messages used in the computation of the ROC curves in Fig. 4.6 was 0 dB.

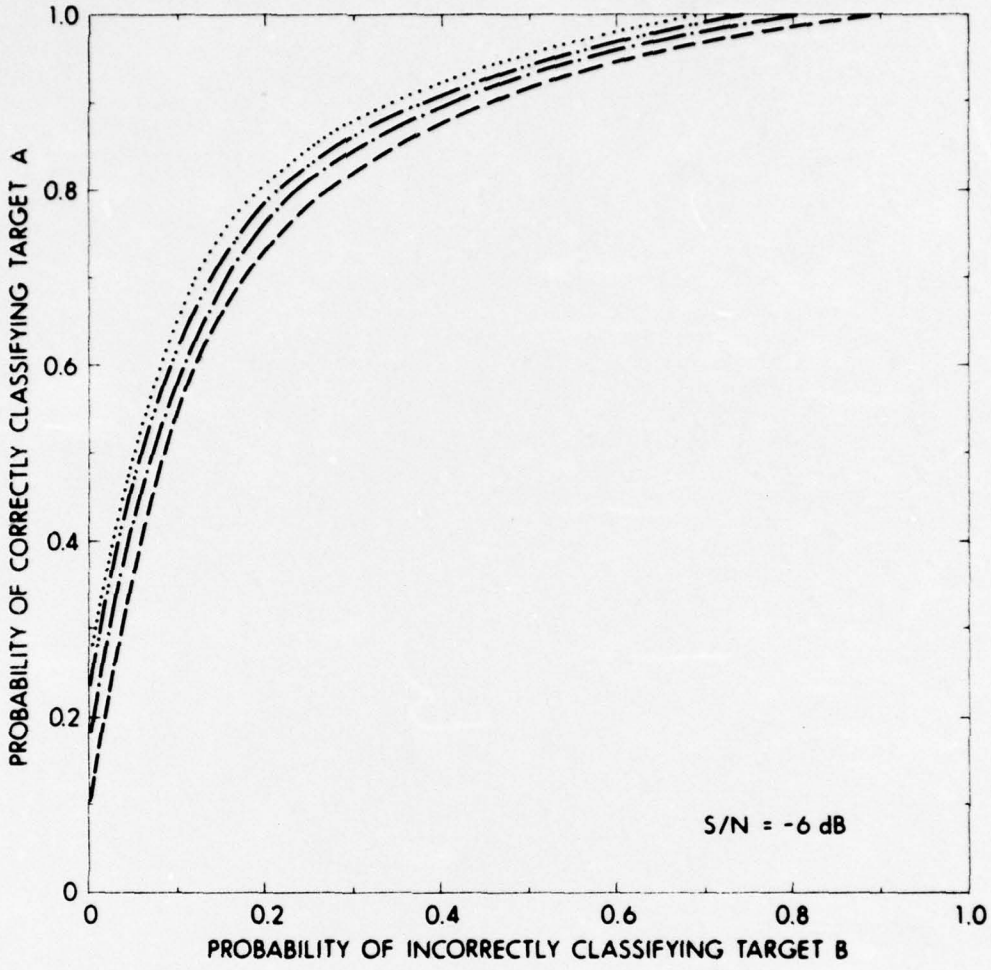

CODE FOR TARGET B

- 5 in. diam SOLID ALUMINUM SPHERE
- 3 in. diam SOLID ALUMINUM SPHERE
- 5 in. diam STYROFOAM SPHERE
- 5 in. diam HOLLOW ALUMINUM SPHERE

FIGURE 5.2
RECEIVER OPERATING CHARACTERISTIC CURVES FOR LINEAR FM TRANSMISSION
TARGET A = 7 in. diam SOLID ALUMINUM SPHERE

B. Conditions Necessary for Equivalent Performance in Classification Using Either of the Two Transmissions

The reason for the better results indicated by Fig. 5.2 is that an echo from the linear FM transmission contained more energy than an echo from the sinusoidal pulse. Since the energy in an echo is proportional to the pulse length of the echo times the peak amplitude squared and since every echo had the same peak amplitude, the greater energy of an echo from the linear FM transmission was the result of the longer pulse length of the linear FM transmission.

The reciprocal of the pulse length of the sinusoidal pulse was equal to the bandwidth of the linear FM transmission. Therefore, from simple energy considerations and by ignoring waveform, one would expect equivalent performances in classification if the following equality were satisfied:

$$\left(\frac{E}{<N^2>}\right)_{sp} = \left(\frac{E}{<N^2>}\right)_{FM} , \qquad (5.7)$$

where

E = energy in an echo,

$<N^2>$ = mean square of the amplitude of the added Gaussian noise,

sp denotes the sinusoidal pulse, and

FM denotes the linear FM transmission.

Since the energy in an echo is proportional to the pulse length of the echo times the peak amplitude squared, Eq. (5.7) can be written as

$$\left(\frac{TP_A^2}{<N^2>}\right)_{sp} = \left(\frac{TP_A^2}{<N^2>}\right)_{FM} , \qquad (5.8)$$

where

T = pulse length of an echo and

P_A = 1400 = peak amplitude of an echo.

Upon taking the square root of Eq. (5.8), the result is

$$\left(\frac{T^{1/2}P_A}{<N^2>^{1/2}}\right)_{sp} = \left(\frac{T^{1/2}P_A}{<N^2>^{1/2}}\right)_{FM} \quad . \tag{5.9}$$

After solving Eq. (5.9) for $\left(\frac{P_A}{<N^2>^{1/2}}\right)_{sp}$, the S/N ratio of the echo-noise combinations for the sinusoidal pulse, the result is

$$\left(\frac{P_A}{<N^2>^{1/2}}\right)_{sp} = \left(\frac{T_{FM}}{T_{sp}}\right)^{1/2}\left(\frac{P_A}{<N^2>^{1/2}}\right)_{FM} \quad , \text{ or, in dB,} \tag{5.10}$$

$$20 \log\left(\frac{P_A}{<N^2>^{1/2}}\right)_{sp} \text{ dB} = 10 \log\left(\frac{T_{FM}}{T_{sp}}\right)\text{dB} + 20 \log\left(\frac{P_A}{<N^2>^{1/2}}\right)_{FM} \text{ dB} \quad . \tag{5.11}$$

From Eq. (5.11), $20 \log\left(\frac{P_A}{<N^2>^{1/2}}\right)_{sp}$ dB is equal to 3.4 dB when $20 \log\left(\frac{P_A}{<N^2>^{1/2}}\right)_{FM}$ dB = -6 dB, T_{sp} = 0.37 msec, and T_{FM} = 3.2 msec.

In Fig. 5.3, 4 ROC curves were plotted for the sinusoidal pulse. The S/N ratio of the messages used in the computation of the ROC curves was 3.4 dB. The performances indicated by the ROC curves in Fig. 5.3 duplicated the performances indicated by the ROC curves in Fig. 5.2. The area under each ROC curve in Figs. 5.2 and 5.3 is listed in Table 5.2.

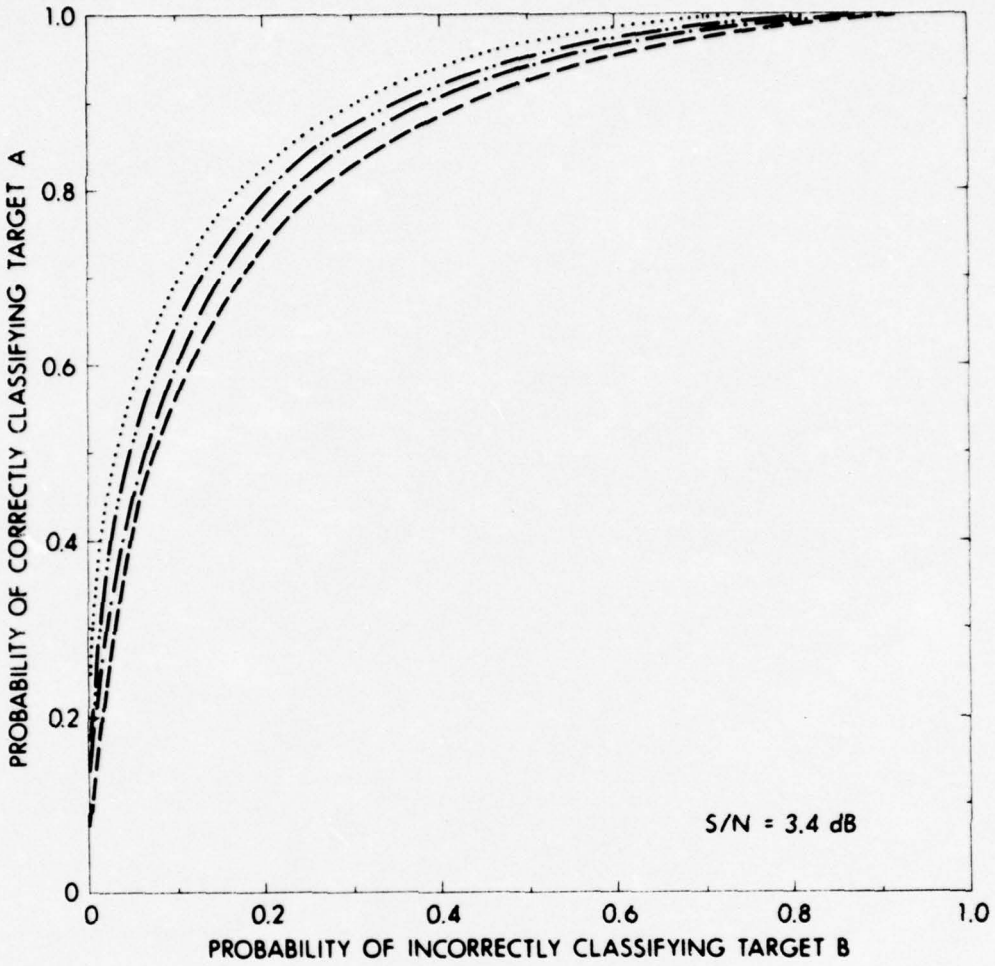

CODE FOR TARGET B

- – – – 5 in. diam SOLID ALUMINUM SPHERE
- —·— 3 in. diam SOLID ALUMINUM SPHERE
- ····· 5 in. diam STYROFOAM SPHERE
- —··— 5 in. diam HOLLOW ALUMINUM SPHERE

FIGURE 5.3
RECEIVER OPERATING CHARACTERISTIC CURVES FOR SINUSOIDAL PULSE TRANSMISSION
TARGET A = 7 in. diam SOLID ALUMINUM SPHERE

TABLE 5.2

AREA UNDER ROC CURVES IN FIGURES 5.2 AND 5.3

TARGET A = 7 IN. DIAM SOLID ALUMINUM SPHERE

Target B	5 in. diam Solid Aluminum Sphere	3 in. diam Solid Aluminum Sphere	5 in. diam Styrofoam Sphere	5 in. diam Hollow Aluminum Sphere
Figure 5.2	0.838	0.861	0.876	0.864
Figure 5.3	0.842	0.862	0.900	0.865

CHAPTER VI

CONCLUSIONS

The objective of this study was the quantitative determination of the applicability of a likelihood ratio processor in the classification of sonar returns from targets. The ability of a likelihood ratio processor to classify simple, similar targets was measured under highly controlled conditions. The 5 targets used were the 7 in. diam, 5 in. diam, and 3 in. diam solid aluminum spheres, the 5 in. diam styrofoam sphere, and the 5 in. diam hollow aluminum sphere, as described in Chapter III. The two transmissions used were:

(1) a sinusoidal pulse with a frequency of 70 kHz and a pulse length of 80 μsec, and

(2) a linear FM transmission of bandwidth 12.5 kHz with a center frequency of 63.75 kHz and a pulse length of 3 msec.

The echoes from the targets for both modes of transmission were scaled so that each echo had the same peak amplitude. The purpose of this scaling was to be able to base any future discrimination solely on the waveform of the echoes; namely, echo strength was not to be a factor in classification. For the echoes from the sinusoidal pulse, the epoch was determined by a threshold technique; for the echoes from the linear FM transmission, the epoch was determined by the time at which a correlation function obtained its maximum value.

In order to simulate a more realistic problem in target classification and to increase the number of messages (echo-noise combinations) from each target class, Gaussian noise from a random noise generator was added to the echoes. Upon the addition of noise to the echoes, the knowledge of epoch was retained. It was possible to select the S/N ratio of the messages by specifying the rms of the amplitude of the noise from the random noise generator. In classifying messages from two target classes, the performance of the likelihood ratio processor was measured by means of ROC curves. The number of messages used in computing an ROC curve was about 130 for each target class.

For the sinusoidal pulse, the likelihood ratio processor performed satisfactorily in classifying the messages for a majority of the target pairs when the S/N ratio of the messages was 0 dB or larger. A performance was considered satisfactory if the area under an ROC curve was 0.75 or greater, since the area under an ROC curve times 100 is equal to the expected percentage of correct decisions. For a S/N ratio of 0 dB, it was virtually impossible to classify or to detect visually the echoes embedded in noise.

An alternate method of measuring the ability to classify messages utilized a geometric representation of the messages from each target class in a multidimensional vector space. For a given target A and target B, the degree of overlap of the vector space containing the messages from target class A with the vector space containing the messages from target class B was indicative of the

performance of the likelihood ratio processor. Namely, the smaller the overlap, the larger was the area under the ROC curve.

For the sinusoidal pulse, the effects of variations in the S/N ratio of the messages on the performance of the likelihood ratio processor were measured. The S/N ratio of the messages was varied from 6 dB, 3.5 dB, 0 dB, to -6 dB. The S/N ratio was a sensitive parameter that affected the performance of the likelihood ratio processor. The larger the S/N ratio, the larger was the area under the ROC curve. As was expected, the degree of overlap of the vector spaces generated by the messages was also dependent on the S/N ratio. The larger the S/N ratio, the smaller was the overlap of the vector spaces.

For the sinusoidal pulse, the effect of a loss in epoch on the ability to classify the messages was measured. The loss in epoch occurred when the starting phase of the messages was varied in intervals of $\pi/2$ radians over a full cycle of the carrier. A test function that was a monotonically increasing function of a generalized likelihood ratio was calculated for each value of epoch, and for each message an average test function was computed. The loss in epoch had the same effect on the ability to classify the messages as a 6 dB drop in the S/N ratio of the messages. The degradation in performance was due to a loss in coherency between the messages and their respective reference signals.

For the sinusoidal pulse, it was possible to classify messages with a likelihood ratio processor that used only in-phase components or out-of-phase components. For target A equal to the

7 in. diam solid aluminum sphere and target B equal to the 5 in. diam solid aluminum sphere, the in-phase components resulted in better performance in classification than the out-of-phase components. But this result is limited, in that it is dependent on the arbitrary manner in which the quadrature components were defined. Better performance in classification was obtained with both quadrature components than with only one quadrature component, since the knowledge of both components gave the likelihood ratio processor additional information on which to base its classification.

The performance obtained with the likelihood ratio processor as indicated by ROC curves for the linear FM transmission when the S/N ratio of the messages was -6 dB was better than that obtained for the sinusoidal pulse when the S/N ratio of the messages was 0 dB. The reason for the better performance was that an echo from a linear FM transmission contained more energy than an echo from a sinusoidal pulse.

Since the reciprocal of the pulse length of the sinusoidal pulse was equal to the bandwidth of the linear FM, the two transmissions had equivalent capabilities in resolving the separate components of an echo. Therefore from simple energy considerations and ignoring waveform it was plausible that equivalent performances could be obtained with either of the two transmissions if the following equation were true:

$$\left(\frac{TP_A^2}{<N^2>}\right)_{sp} = \left(\frac{TP_A^2}{<N^2>}\right)_{FM} , \qquad (6.1)$$

where

T = pulse length of an echo,

$P_A = 1400$ = peak amplitude of an echo,

E is proportional to TP_A^2 where E is the energy in an echo,

$<N^2>$ = mean square of amplitude of noise from the random noise generator,

sp denotes a sinusoidal pulse, and

FM denotes a linear FM transmission.

The performances achieved with the linear FM transmission when the S/N ratio of the messages was -6 dB were also achieved with the sinusoidal pulse when the S/N ratio of the messages was 3.4 dB. The value 3.4 dB was obtained by solving Eq. (6.1) for $\left(\frac{P_A}{<N^2>^{1/2}}\right)_{sp}$, the S/N ratio of the messages for the sinusoidal pulse, when $\left(\frac{P_A}{<N^2>^{1/2}}\right)_{FM}$ was equal to -6 dB.

From Eq. (6.1) it was asserted that the performance of the likelihood ratio processor is dependent on the value of $\frac{E}{<N^2>}$; namely, the larger $\frac{E}{<N^2>}$ is, the better is the performance. The dependence of the performance on $\frac{E}{<N^2>}$ implies that a linear FM has more potential than a sinusoidal pulse for improvement in the performance of a likelihood ratio processor, since the energy in a sinusoidal pulse is restricted by the effects of cavitation.

APPENDIX A

RANDOM NOISE GENERATOR

The random noise generator used in obtaining samples of Gaussian noise was the type 1390-B random noise generator manufactured by General Radio Company. The type 1390-B random noise generator uses a gas discharge tube as its noise source. Samples of the amplitude of the output waveform are characterized by a Gaussian distribution.

Two of the pertinent specifications[28] on the type 1390-B random noise generator are:

(1) frequency range: 5 Hz to 5 MHz and

(2) spectrum-level uniformity: within ±3 dB from 20 Hz to 500 kHz.

---

[28] Operating Instructions, Type 1390-B Random Noise Generator, General Radio Company, West Concord, Mass., February 1964.

APPENDIX B

APPENDIX B
FLOW DIAGRAM OF COMPUTER PROGRAM USED IN CALCULATION OF ROC CURVE

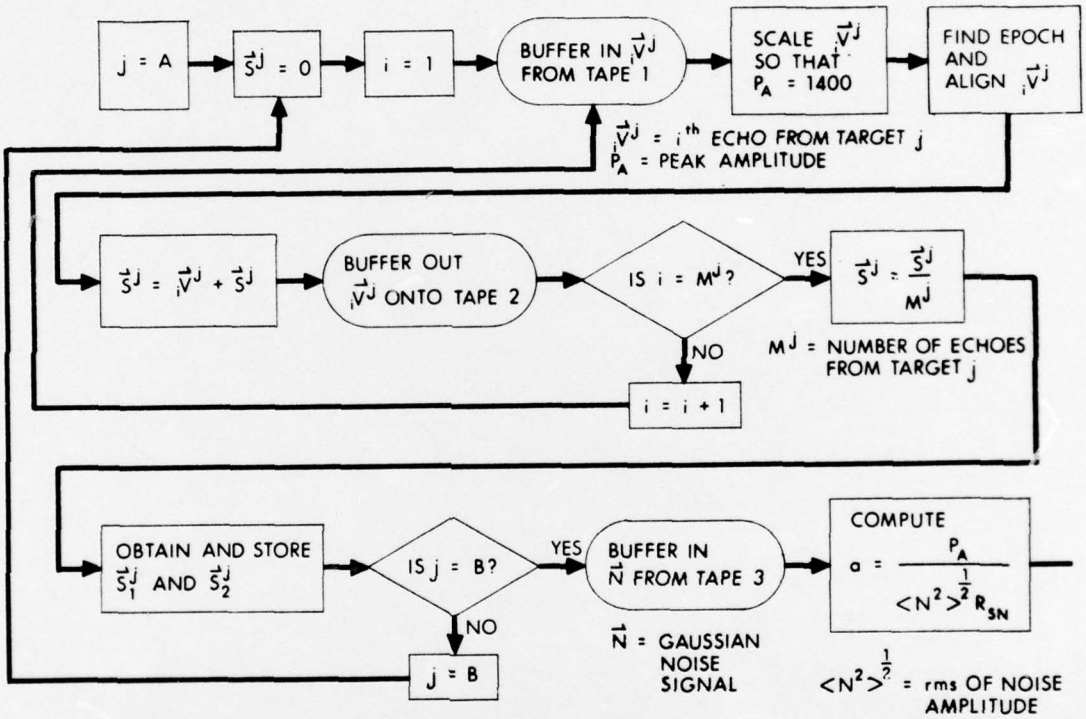

APPENDIX B CONTINUED

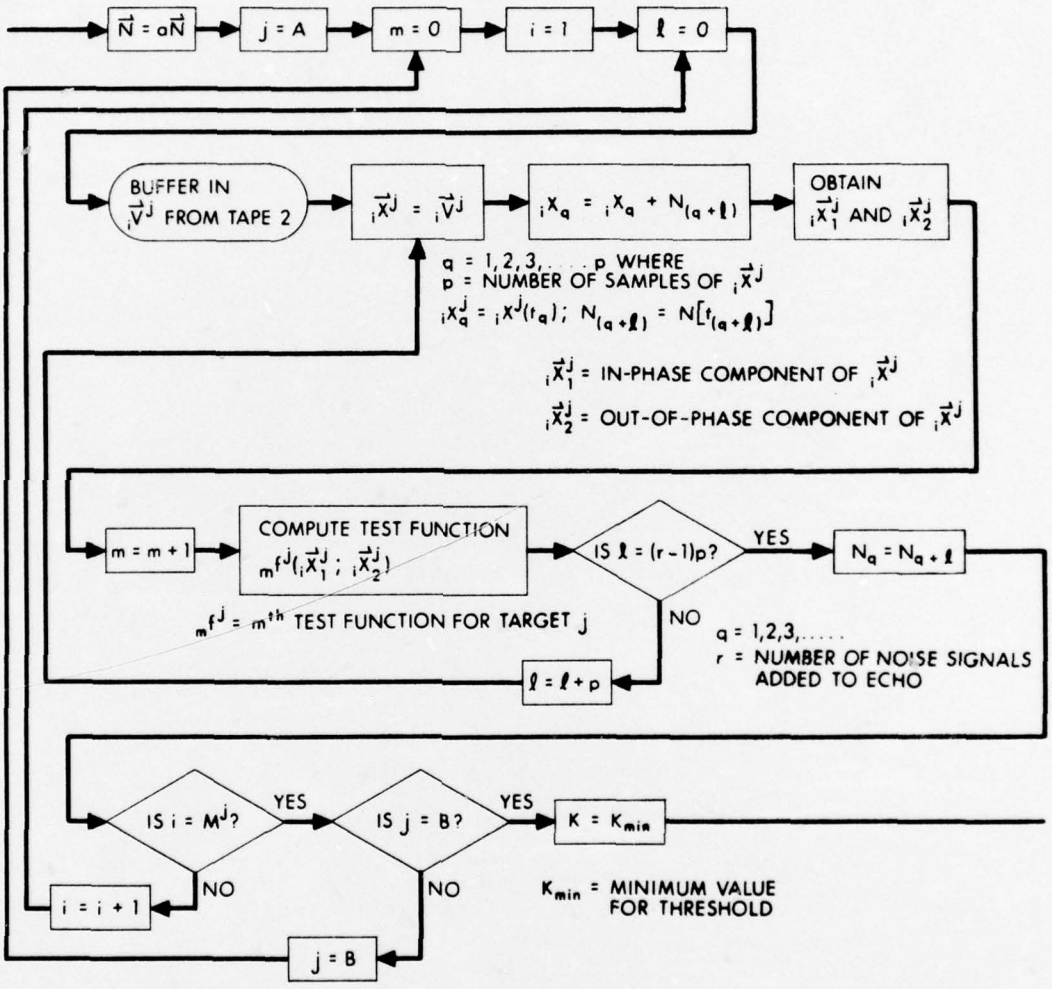

APPENDIX B CONTINUED

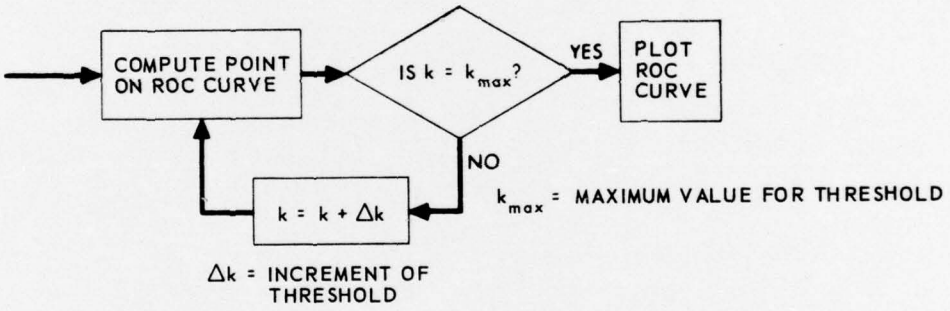

BIBLIOGRAPHY

Bendat, J. S., and A. G. Piersol. Measurement and Analysis of Random Data. New York: John Wiley and Sons, Inc., 1966.

Blackman, R. B., and J. W. Tukey. The Measurement of Power Spectra. New York: Dover Publications, Inc., 1958.

Dierks, K. Jerome, and R. Hickling. "Echoes from Hollow Aluminum Spheres in Water." Journal of the Acoustical Society of America 41, No. 2 (1967), pp. 380-393.

Grace, O. D., and S. P. Pitt. "Quadrature Sampling of High Frequency Waveforms." Letter to the Editor of the Journal of the Acoustical Society of America 44, No. 5 (1968), pp. 1453-1454.

Green, David M., and John A. Swets. Signal Detection Theory and Psychophysics. New York: John Wiley and Sons, Inc., 1966.

Hancock, J. C., and P. A. Wintz. Signal Detection Theory. New York: McGraw-Hill Book Company, 1966.

Hickling, Robert. "Analysis of Echoes from a Hollow Metallic Sphere in Water." Journal of the Acoustical Society of America 36, No. 6 (1964), pp. 1124-1137.

Hickling, Robert. "Analysis of Echoes from a Solid Elastic Sphere in Water." Journal of the Acoustical Society of America 34, No. 10 (1962), pp. 1582-1592.

Hickling, Robert, and N. M. Wang. "Scattering of Sound by a Rigid Movable Sphere." Journal of the Acoustical Society of America 39, No. 2 (1966), pp. 276-279.

Middleton, David. An Introduction to Statistical Communication Theory. New York: McGraw-Hill Book Company, 1960.

Middleton, David. Topics in Communication Theory. New York: McGraw-Hill Book Company, 1965.

Papoulis, Athanasious. "Limits on Band-limited Signals." Proceedings of the IEEE 55, No. 10 (1967), pp. 1677-1686.

Schooneveld, C. Van. "Some Remarks on Sampling Methods for a Band Pass Signal." Signal Processing, NATO Advanced Study Institute, Grenoble (1964), pp. 410-421.

Sebestyen, G. S. Decision-making Processes in Pattern Recognition. New York: The Macmillan Company, 1962.

June 1969

DISTRIBUTION LIST FOR
ARL-TM-69-11
CONTRACT N00024-69-C-1129
Project Serial No. SF 11121100, Task 08515

Copy No.	
1	Commander, Naval Ship Systems Command Department of the Navy Washington, D. C. 20360 Attn: SHIPS 00V1C
2	Commander, Naval Ship Systems Command Department of the Navy Washington, D. C. 20360 Attn: SHIPS 00V2
3	Commander, Naval Ship Systems Command Department of the Navy Washington, D. C. 20360 Att: PMS 385
4	Commander, Naval Ship Systems Command Department of the Navy Washington, D. C. 20360 Attn: PMS 386
5	Commander, Naval Ship Systems Command Department of the Navy Washington, D. C. 20360 Attn: PMS 387
6	Commander, Naval Ship Systems Command Department of the Navy Washington, D. C. 20360 Attn: Library
7	Chief of Naval Research Department of the Navy Washington, D. C. 20360 Attn: Code 466

June 1969

DISTRIBUTION LIST FOR
ARL-TM-69-11
CONTRACT N00024-69-C-1129 (CONT'D)

Copy No.

8 Commander
Naval Undersea Research and Development Center
San Diego Division
271 Catalina Boulevard
San Diego, California 92152
Attn: Code D606

9 Commander
Naval Undersea Research and Development Center
San Diego Division
271 Catalina Boulevard
San Diego, California 92152
Attn: Library

10 Commander
Naval Undersea Research and Development Center
San Diego Division
271 Catalina Boulevard
San Diego, California 92152
Attn: Bryson Pennoyer
Code D554

11 Commanding Officer
U. S. Fleet ASW School
San Diego, California 92147

12 Commanding Officer and Director
U. S. Navy Underwater Sound Laboratory
Fort Trumbull
New London, Connecticut 06320
Attn: Code 2242

13 Director
U. S. Naval Research Laboratory
Department of the Navy
Anacostia
Washington, D. C. 20390

June 1969

DISTRIBUTION LIST FOR
ARL-TM-69-11
CONTRACT N00024-69-C-1129 (CONT'D)

Copy No.

14 Commander
U. S. Naval Ordnance Laboratory
White Oak
Silver Spring, Maryland 20910

15 Commanding Officer
U. S. Naval Ship Research and Development
Laboratory
Panama City, Florida 32402

16 Commanding Officer
U. S. Naval Air Development Center
Johnsville
Warminster, Pennsylvania 18974

17 Commander
Naval Undersea Research and Development Center
3202 East Foothill Boulevard
Pasadena, California 91107

18 Naval Ship Research and Development Center
Department of the Navy
Washington, D. C. 20007
Attn: T. Kooij

19 Office of the Director of Defense
Research and Engineering
Room 3C128, The Pentagon
Washington, D. C. 20301

20 U. S. Naval Postgraduate School
Monterey, California 93940

21 Commander
Destroyer Development Group TWO
U. S. Atlantic Fleet
C/O Fleet Post Office
New York, New York 09501

June 1969

DISTRIBUTION LIST FOR
ARL-TM-69-11
CONTRACT N00024-69-C-1129 (CONT'D)

Copy No.	
22	Commander Submarine Development Group TWO Box 70, Naval Submarine Base New London Groton, Connecticut 06340
23	National Academy of Sciences 2101 Constitution Avenue, N.W. Washington, D. C. 20418 Attn: Committee on Undersea Warfare
24	Office of Naval Research Resident Representative The University of Texas at Austin 2507 Main Building Austin, Texas 78712
25	Signal Physics Division, ARL/UT
26	Computer Science Division, ARL/UT
27 - 31	J. F. Hoffman, ARL/UT
32	S. P. Pitt, ARL/UT
33	Library, ARL/UT
34 - 52	ARL Reserve, ARL/UT